Effects of Member Overstrength And Initial Residual Stresses On the Behaviour of 2D Steel Structure

---

A thesis submitted in partial fulfilment of the requirements for the
Degree of Master of Engineering in Civil and Natural Resources Engineering
in the University of Canterbury

By

Yen-Cheng (Arthur) Lu

University of Canterbury

2011

Supervised by:

Assoc. Prof. Gregory A. MacRae

Associated Professor, Department of Civil and Natural Resources Engineering,
University of Canterbury, New Zealand

Department of Civil and Natural Resources Engineering

University of Canterbury

Christchurch, New Zealand

2011

Abstract

Extended Direct Analysis (EDA), developed at the University of Canterbury, is an advance on the AISC Direct Analysis method for the analysis of frames subjected to static forces. *EDA* provides a faster, simple and more rational way to properly consider the second-order effects, initial residual stresses (IRS) and the initial imperfections for steel structures under one directional loading than conventional analysis methods.

This research applied the *EDA* method to quantify the effect of member overstrength on frame behaviour for a single storey frame. Also, the effects of *IRS*, which were included in the *EDA* static analysis, but which are not considered explicitly in non-linear seismic analysis, were evaluated in two ways. Firstly, they were considered for simple structures subject to increasing cyclic displacement in different directions. Secondly, incremental dynamic analysis with realistic ground motion was used to quantify the likely effect of *IRS* in earthquakes.

It was found that, contrary to traditional wisdom and practice, greater member strengths can result in lower frame strengths for frames under monotonic lateral loading. The structural lateral capacity of the overstrength case was reduced by 6% compared to the case using the dependable member strengths. Also, it resulted significantly different in member demands. Therefore, it is recommended that when either plastic analysis or *EDA* is used, that both upper and lower bounds on the likely member strength should be considered to determine the total frame strength and the member demands.

Results of push-pull analysis under displacement control showed that for *IRS* ratio, $\gamma <$ 0.5 and axial compressive force ratio, N^*/N_s, up to 0.5, *IRS* did affect the structural behaviour in the first half cycle. However, the behavior in the later cycles was not significantly affected. It also showed that the effect of initial residual stresses in the frame was less significant than for the column alone when the column was subjected to similar axial compressive force.

The incremental dynamic analysis results from both cantilever column and the three-storey steel frame showed that by increasing $\gamma = 0$ to 0.5, the effect of *IRS* on seismic responses, based on the 50% confidence level, was less than 3% for N^*/N_s, up to 0.5.

Acknowledgements

I would firstly like to specially thank my supervisor, Associate Professor Gregory MacRae. Thanks for all your support, guidance and encouragement through the entire research. I really appreciate all the time you have spent with me and the advice you have given me in both technical and other aspects.

Also, thanks to all the following people for your technical assistances:

- Dr Lip Teh, Dr Reidar Bjorhovde and Prof. Charles Clifton – providing useful references in initial residual stress distributions;
- Matthew Parkolap – for helping to create analysis model in OpenSEES and background on the current research on Direct Analysis;
- Dr Brendon Bradley – to help on performing the incremental dynamic analysis;
- Dr Vinod Sadashiva – information on SAC earthquake records and performing time-history analysis in OpenSEES;
- Prof. Ronald Ziemian – providing information on initial residual stress distributions and background of MASTAN2

Without your valuable and timely assistance, the project could not have been a success.

I also want to thank to these people: Simon Ma, Jose Golondrino, Antony Pearce, Antony Stubb and my past officemates for your friendship and fun during my study.

I wish to express my special and deepest thanks to my parents and all of the saints in the church life. Thank for your prayers, caring, love, supporting and encouragement during the past years.

Table of Contents

List of Figures

List of Tables

1 INTRODUCTION

1.1 BACKGROUND AND RESEARCH MOTIVATION

Steel frame structures are widely constructed around the world in many different countries. To ensure satisfactory performance, design methods are used. These methods consider many factors, including the structural strength, stiffness and stability. Design is generally conducted with aid of an analysis technique. It is important to ensure that the analysis techniques are used to approximate the frame behaviour adequately.

Traditionally and commonly in New Zealand, computer tools using simple first-order elastic analysis are being used. Due to the recent increase in computer processing power and the availability of more advanced software, material nonlinearity, geometric nonlinearity, initial imperfections and combinations of actions may now be considered. Table 1–1 presents three methods used in design for frames subject to static loads. These are the NZS3404 Appendix F method (NZS3404:1997) [1], the second-order inelastic analysis method used in computer programmes such as SAP2000 [10] and Mastan2 [11], and the newly introduced Extended Direct Analysis (*EDA*) method (Lu et al. 2008) [2, 3].

Table 1–1: Summary of Current Methods

Methods / Details	NZS3404 Appendix F	Second Order Inelastic analysis programmes	Extended Direct Analysis (EDA)
Type of Analysis	1st order elastic analysis	2nd order inelastic analysis	2nd order inelastic analysis
Geometric Nonlinearity	None	Frame coordinates change in models	Frame coordinates change in models
Initial Out-of-Plumbness	Additional notional loads	Additional notional loads/ Change in frame geometry	Additional notional loads
Initial Residual Stress	Column curves check each member individually	Column curves check each member individually	Stiffness reduction factor (SRF)
In-plane Check	Manually	Manually	Automatically

For the methods used in Appendix F of the New Zealand Steel Structures Standard (NZS3404:2007), and for those using second-order inelastic analysis, after the computer analysis has been conducted, a number of additional checks are still required as part of the design process. On the contrary, Extended Direct Analysis, which is an extension of

the AISC Direct Analysis method [4], requires no additional member in-plane checks, since initial imperfections (e.g. out-of-straightness and out-of-plumbness), initial residual stresses, member dependable strengths and section plasticity have also been considered.

The analysis/design methods described above generally use member dependable strengths and there are concerns that these methods may not be adequate for the design of structures under monotonic loading. It is because the member may be significantly stronger than the minimum (dependable) possible strength due to section variations, material yielding strength variation, strain hardening and floor slab effect.

The second concern is that of low-rise steel frames subject to wind loading, where the wind may come from different directions with different magnitudes, the response from cyclic loading may be more critical than from the monotonic analysis.

Also, in most analyses for earthquake design of steel frames, section initial residual stress effects and initial imperfections are seldom considered explicitly in the analysis possibly resulting in deterioration of structural performance.

1.2 RESEARCH OBJECTIVES

The objectives of this research are to address the concerns described above by seeking answers to the following questions:

i) Can the consideration of member overstrength, rather than the member dependable strength, result in significantly different element demands or a weaker overall structure strength?

ii) How likely is the response of steel frames with initial residual stresses affected by cyclic loadings, such as may occur from wind?

iii) Is the seismic response of steel frames likely to be detrimentally affected by member initial residual stresses?

iv) Based on the answers to the questions above, how should steel frames need to be analysed/designed?

1.3 THESIS OUTLINE

A general overview of the AISC Direct Analysis method and the methods in Table 1–1 are described in Chapter 2 together with information about member overstrength values and initial residual stress distributions. Chapter 3 described the computation analysis software used in the research.

Chapter 4 illustrates the effect of overstrength on the plastic response of the steel frames.

Chapter 5 describes how OpenSEES was used in the analysis and hot the initial residual stresses were considered.

Chapter 6 describes the member and frame models used for both the static and dynamic analysis. It is includes the dimensions of the model, mass and the member used.

Chapter 7 presents the effects of the initial residual stresses are included under both the monotonic and push-pull responses. The seismic responses of the frames considering the initial residual stresses in the seismic analysis are presented in Chapter 8.

Chapter 9 presents the conclusions of the research, discussion on the limitations and the recommendations for the future studies.

2 LITERATURE REVIEW

2.1 AISC DIRECT ANALYSIS

Studies on the *Direct Analysis Method* have been carried out in the USA by White and Clark (1997), Surovek-Maleck and White (2004), and Surovek et al. (2005) amongst others. Results of this work have been incorporated into the 2005 AISC specification for the design of steel structures. Key elements of the Direct Analysis Method are described below.

(a) Frame Out-of-Plumb Effects

The destabilizing effects of frame out-of-plumb can be included by modifying the geometry used in the analysis model. The AISC specification, Appendix 7 [4], assumes an out-of-plumbness in the structure of each storey height divided by 500. This is the maximum out-of-plumbness permitted by the specification. The AISC also permits an alternative, the use of notional loads as shown by Eq. 2-1, which in this case equals 0.002 times the factored gravity load effects on a given storey. Here, notional loads are artificial lateral forces that are applied to the structure at each framing level in the direction that adds to the destabilizing effects of the load combination being investigated.

The notional loads are applied to the structure to account for "destabilizing effects of geometric imperfections, non-ideal conditions (such as incidental patterned gravity load effects, temperature gradients across the structure, foundation settlement, uneven column shortening, and any other effects that could induce sway that is not explicitly considered in the analysis), inelasticity in structural members or combinations thereof (AISC, 2005). For cases when the ratio of second-order drift to first-order drift $\Delta_{2nd}/\Delta_{1st}$ does not exceed 1.5, the imperfection or equivalent notional load needs only be applied in the gravity-only load combinations and not in combination of with other lateral loads (AISC 2005, Appendix 7.3(2)).

$$N_i = 0.002Y_i \qquad \text{Eq. 2-1}$$

where

N_i = Notional lateral load applied at level *i*, *kN*

Y_i = Gravity load from LRFD load combination or 1.6 times the ASD load combination applied at level *i*.

(b) Partial Yielding, Residual Stress, and Member Out-of-Straightness Effects

Since partial yielding, accelerated by the presence of residual stresses, could potentially affect the stiffness of the frame, especially with members under high levels of axial force, these factors are considered in the analysis. The reduced flexural stiffness, EI_{eff}, is given by Eq. 2-2, with the factor τ_b defined in Eq. 2-3 (AISC 2005, Appendix 7.3(3)) [4]. The reduced axial stiffness, EA_{eff}, is given in Eq. 2-4 and it uses a 0.8 factor similar to that appearing in Eq. 2-2, although no τ_b factor is included. The parameter N_s in the equations below is the section axial force capacity.

$$EI_{eff} = 0.8\tau_b EI \qquad \text{Eq. 2-2}$$

$$\tau_b = \begin{cases} 1.0 & for \ \dfrac{N^*}{N_s} \le 0.5 \\ 4\dfrac{N^*}{N_s}\left(1-\dfrac{N^*}{N_s}\right) & for \ \dfrac{N^*}{N_s} > 0.5 \end{cases} \qquad \text{Eq. 2-3}$$

$$EA_{eff} = 0.8EA \qquad \text{Eq. 2-4}$$

These factors, including partial yielding, residual stresses, and out-of-straightness, along with the possibility of non-concentric axial loading and the requirement for a strength reduction factor ϕ (resistance factor in US notation) are represented in the design check for compression members, which is given by Eq. 2-5. Here, τ is the stiffness reduction factor (SRF) equal to EI_{eff}/EI and given in Eq. 2-6 and shown in Figure 2–1. The difference between the Euler buckling curve N_{Euler} and the AISC (2005) column design curve N_c may be used to obtain a τ which is defined as $(\lambda_{code}/\lambda_{Euler})^2$. It includes the effects of inelasticity with residual stresses and member out-of-straightness.

$$N^* < \phi N_c = \phi \frac{\pi^2 (EI)_{eff}}{L^2} = \phi\tau \frac{\pi^2 EI}{L^2} = \phi\tau N_{Euler} \qquad \text{Eq. 2-5}$$

$$\tau = \begin{cases} 1.0 & for \ \dfrac{N^*}{N_s} \le 0.39 \\ -2.389\left(\dfrac{N^*}{N_s}\ln\left(\dfrac{N^*}{N_s}\right)\right) & for \ \dfrac{N^*}{N_s} > 0.39 \end{cases} \qquad \text{Eq. 2-6}$$

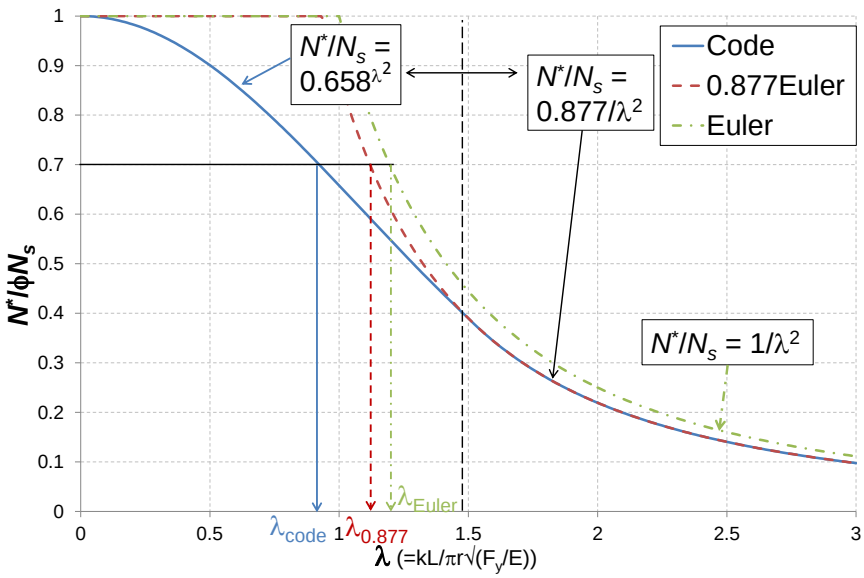

Figure 2–1: AISC steel column design curve

Because the AISC column curve uses the value of 0.877 to account for the impact of initial out-of-straightness on the behaviour of slender columns, this value could be used to obtain a stiffness reduction factor τ_a and can be derived directly by $(\lambda_{code}/\lambda_{0.877})^2$. It considers only the effects of partial yielding and residual stress, which is given by Eq. 2-7. This equation is different from Eq. 2-6 because it ignores the out-of-straightness effect.

$$\tau_a = \begin{cases} 1.0 & for \ \dfrac{N^*}{N_s} \le 0.39 \\ -2.724\left(\dfrac{N^*}{N_s}\ln\left(\dfrac{N^*}{N_s}\right)\right) & for \ \dfrac{N^*}{N_s} > 0.39 \end{cases} \qquad \text{Eq. 2-7}$$

Curves given by Eq. 2-3, 2-6 and 2-7 are shown in Figure 2–2. It should be noted that the τ curve considering out-of-straightness is similar to $0.877\tau_a$ indicating that the effect of out-of-straightness is roughly equivalent to reducing the column stiffness by 12%. It may be seen that the AISC recommendation of $0.8\tau_b$ is similar to the τ_a for high axial loads ($N^*/N_s > 0.7$), indicating that the out-of-straightness effect is not included here. This may be because geometrical imperfections are considered by the notional loads.

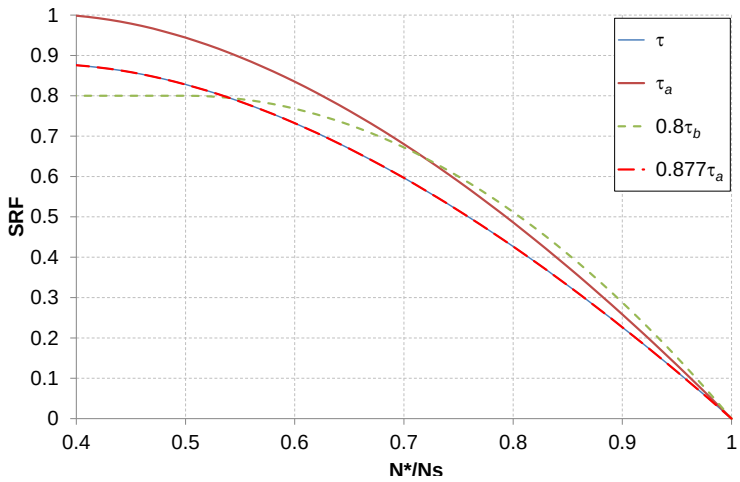

Figure 2–2: Comparison of stiffness reduction factors

Since that out-of-straightness usually does not impact the performance of stocky members (e.g., with $\lambda < 1.0$), hence, the 0.877 reductions may seem overly conservative for general application. The AISC specification uses the more simple equation thus giving a stiffness reduction factor of $0.8\tau_b$. In lieu of using $\tau_b < 1$ when $N^*/N_s > 0.5$, $\tau_b = 1$ is permitted (AISC Appendix 7.3(4)) providing that an additive notional load with a value of the 0.001 times the factored gravity load which is added to the notional load required in (a).

(c) Appropriate Consideration of Second-order Geometric Effects

The AISC specification requires that second-order effects be considered either through the use of moment amplification factors, which is limited to conditions when the ratio of second-order drift to first-order drift $\Delta_{2nd}/\Delta_{1st}$ does not exceed 1.5, or by use of rigorous geometric nonlinear analysis. In order to ensure that a second-order analysis method is accurate, AISC (2005) provides two benchmark problems, as given in Appendix A, requiring that the analysis solution is within 3% of the given theoretical solution when M_{max}/M_o and y_{max}/y_o are greater than 2.5.

2.2 EXTENDED DIRECT ANALYSIS (EDA)

2.2.1 Description of Extended Direct Analysis

Extended Direct Analysis (*EDA*) is an extension of AISC Direct Analysis (*DM*) and was developed from University of Canterbury [2]. EDA method is considered to be more sophisticated than conventional methods such as Appendix F method in the NZS3404

because EDA considers the critical factors all together in a more transparent way. In addition, this method can produce economical designs when compared with the standard code-based methods and can produce better estimation of frame behaviours that are sensitive to second-order effects [2, 3].

The main concept of EDA is that both the model and analysis are so realistic so that special checks do not need to be made for design. The important elements for EDA, as partially mentioned in Table 1–1, are described below:

- Initial residual stress, out-of-straightness and accidental erection are considered by means of a stiffness reduction factors (*SRF*) defined as the ratio of effective flexural stiffness, EI_{eff}, over elastic flexural stiffness, *EI*, are derived from the column curves given in NZS3404 as shown in Figure 2–3 (Lu et al., 2008[2]). They are function of the ratio of applied axial force, N^*, over the section axial capacity, N_s. Therefore, it needs to be updated when the axial force changes. The five curves, from α_b = -1 to 1, correspond to the five different initial residual stress categories of the column curves.

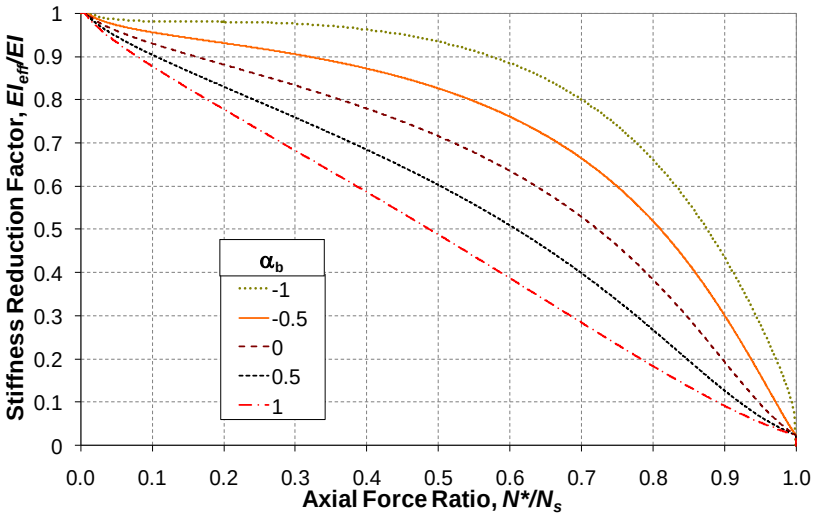

Figure 2–3: Stiffness reduction factor (*SRF*) for NZS3404 [2, 3]

- To account for destabilizing effects of geometric imperfections such as initial out-of-plumb, non-ideal conditions such as foundation settlement, incidental patterned gravity load effects, temperature gradients and uneven column shortening, notional loads are used. In *EDA*, these are same as the notional loads recommended in the US Direct Analysis approach (AISC, 2005). They are calculated by Eq. 2-1 and are

required to be applied independently in two directions as a lateral load in all load combinations and in addition to other lateral loads.

- To account for the statistical variations of material and sectional properties, strength reduction factor, ϕ, are used from the standards. Both material yield strength, F_y, and elastic modulus, E, are multiplied by ϕ to be the input values for the analysis as given by Eq. 2-9 and 2-10 below. This is consistent with the US Direct analysis approach.

$$E_{input} = \phi E \qquad \text{Eq. 2-9}$$

$$f_{y,input} = \phi f_y \qquad \text{Eq. 2-10}$$

- Second order effects such as global and local P-delta effects are considered directly by analysis programmes that are able to perform adequate second order analysis. A special provision given in ANSI/AISC 360-05 2005 Cluse C7.3, as mentioned in the previous section and also attached in Appendix A, provides benchmark problems to evaluate the accuracy of computer programmes to model second order effects.

2.2.2 Procedure of performing Extended Direct Analysis

EDA may be performed as follows with standard elastic computer programmes that adequately consider second-order effects and section plasticity:

a) Construct a computational model of the frame using the E_{input} and $f_{y,input}$ from Eq. 2-9 and Eq. 2-10.

b) Compute the notional forces and apply them in the critical direction;

c) Run an initial analysis with rigorous second-order inelastic software to obtain the axial forces for each member;

d) Calculate the plastic moment, M_p, considering the moment axial-force interaction and stiffness reduction factors for each member based on the member axial force level. The stiffness reduction factor, SRF, can be obtained by either of the following two methods:

   - Actual SRF values can be found directly from Figure 2–3 or table [2].
   - SRF values also may be approximated by Eq. 2-11 and Eq. 2-12.

$$SRF = 1 - \frac{\left|\frac{N^*}{N_s}\right|}{1 + c\left(1 - \left|\frac{N^*}{N_s}\right|\right)} \qquad \text{Eq. 2-11}$$

$$c = 1.5 * \exp\left(-1.8\alpha_b\right) - 0.35 \qquad \text{Eq. 2-12}$$

e) Multiply the stiffness reduction factor to the second moment of area, *I*, for each member.

f) Re-perform the second-order inelastic analysis until the forces in the frame members converge to be the same as those used to compute the *SRF*.

g) Check the design criteria such as bending moments, axial forces and the deflections of the frame. Also, if the frame collapses under the applied loads, then the design may not be satisfactory. On the other hand, if it does not collapse, then it is satisfactory for this limit state case. Each load case required to be checked separately.

The procedure described above can be carried out manually. It can also be performed automatically by analysis software [2, 3, 11, 12]. To achieve this, the computational software must incorporate the SRF values and consider moment axial-force interaction. Moreover, the applied loads should be applied in small increments and member stiffness and plastic moment are also updated at each load increment. Again, if the frames collapse, the design is no good. On the contrary, if it does not collapse, then the design is good.

2.3 CURRENT DESIGN METHODOLOGY

2.3.1 Member dependable strength (ϕR_u) in Limit States Design

In modern design of structures in New Zealand or around the world, Limit State (LS) design is the most widely used design approach for all types of structures. The approach requires that each structural design satisfies the two principal criteria which are the ultimate limit state (ULS) and the serviceability limit state (SLS) as stated in Section 2 of AS/NZS 1170.0:2002 [5]. The definitions of these two principal criteria given in Clauses 1.4 are:

- Serviceability Limit States are defined as the *"states that correspond to conditions beyond which specified service criteria for a structure or structural element are no longer met"* and,
- Ultimate Limit States are defined as the *"states associated with collapse or with other similar forms of structural failure*".

In the design of the steel structures by using the limit state theory, the dependable strengths, ϕR_u, of the member and connection are normally used. For example, Clause 3.3 in NZS3404 shows that the design capacity, ϕR_u, shall not be less than the design actions, S^*, for all members and connections where R_u is the nominal capacity of the sections or the connections and ϕ is the load reduction factor or load resistance factor, and S^* is from the combination of factored loads. The dependable strength may be considered to represent the minimum likely strength.

The load resistance factors (or load reduction factors), ϕ, used are to take account of the likely variations in material stress-strain characteristics, the cross-section properties, structural deterioration due to corrosion or fatigue and consequences of reaching the limit state. For the design of the steel structures in NZ, the $\phi = 0.9$ is generally used for the section capacity such as flexural or axial force capacity. A complete list of the ϕ are given in Table 3.3 in NZS3404:1997 for the sections and connections.

2.3.2 Member overstrength ($\phi_o R_u$) in a Capacity Design approach

In current seismic design practices, apart from the checks of the dependable strength criteria, it is also important to consider the overstrengths of the sections. It is especially important in the capacity design concept (Park and Paulay 1975) since it encourages ductile performance. For moment frame structures, it can be used to encourage specified mechanisms such as "beam-sway" mechanism which is generally more ductile than the "column-sway" or soft story mechanism as illustrated in Figure 2–4. As seen from the figures, the beam sway mechanism has plastic hinges in the beams and at the base of the ground story columns.

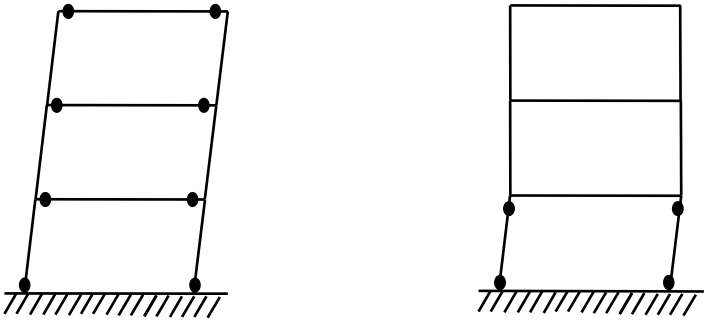

a) Beam-sway mechanism b) Column-sway mechanism

Figure 2–4: Structural deformation mechanisms for frame structures

The desired failure beam-sway mechanism is achieved by ensuring that the secondary members, such as columns, which are not expected to yield, can resist the maximum forces generated from the primary members such as beams without reaching their strengths. The maximum forces, or the overstrength capacity, $\phi_o R_u$, can be obtained by multiplying the overstrength factor and the member nominal capacity. This overstrength factor considers the effect of the material having higher yield strength than the nominal value, strain-hardening and the member size being larger than the nominally specified value and the slab effect.

Clause 12.2.8 in NZS3404, shown in Table 2–1 below, presents that overstrength factors should be used for different types of member and steel grades. There are different overstrength factors for the active links in the eccentrically braced frames. In this table, category 1 members are expected to sustain large amounts of inelastic action, while category 2 members are expected to sustain less, and category 3 members should remain elastic. Members from outside Australian and those of higher grade steels tend to have larger overstrength values then those shown in the table.

Table 2–1: Overstrength factors for normal members with Grade 300 steel produced in Australian and New Zealand

	Category 1 members	Category 2 members	Category 3 members
Strain hardening (ϕ_{os})	1.15	1.05	1.00
Material variation (ϕ_{om})	1.20	1.20	1.20
Overstrength Factor (ϕ_{oms})	1.25	1.15	1.10

In the current design practices, the overstrength demand, ϕ_{oms}, must be less than the dependable capacities, ϕR_u, shown in Eq. 2-13. Here the beam is the yielding element with a nominal strength, F_{beam}, and the column is designed not to yield. It has a nominal strength, F_{column}. It should be noted that dynamic magnification effects have not been included in this equation. For example, for a category 1 Australia Grade 300 steel member, from the above table, $\phi_{os} = 1.15$ and $\phi_{om} = 1.2$ and $\phi = 0.9$. The maximum force that the beam can produce is therefore $\phi_{os}\phi_{om}$ (= 1.15×1.2 = 1.38) times the nominal force. The overstrength used for design is $\phi_{oms} = \phi\phi_{os}\phi_{om}$ (= 0.9×1.38 = 1.242 ≈ 1.25) as given in Table 2–1.

$$\begin{array}{ccc} Demand & \leq & Capacity \\ \phi\phi_{om}\phi_{os}F_{beam} = \phi_{oms}F_{beam} = 1.25F_{beam} & \leq & \phi F_{column} = 0.9F_{column} \end{array} \qquad \text{Eq. 2-13}$$

2.4 DIRECT ANALYSIS FOR SEISMIC DESIGN

Recent studies have been conducted to expand the application and benefits of the Direct Analysis method (DM) in seismic frames (Okazaki, Parkolap and Fahnestock (2009) [6, 7]). The main objectives of the project are as follows. First, to clarify how the DM addresses seismic effects; secondly, to evaluate how the DM including plastic analysis, termed "direct elastic-plastic hinge analysis," addresses seismic effects; and lastly, to identify research need related to the interface of the DM and seismic design requirements.

Preliminary analyses were conducted using 3, 9 and 20-story special steel moment-resisting frames (*SMRFs*) which were extracted from the SAC project, and three different levels of seismicity were considered. The dimensions, layout, section sizes and weight of SMRFs were based on the pre-Northridge design models reported by Gupta and Krawinkler (1999) [8]. Both monotonic and cyclic analyses were conducted to evaluate and clarify how the DM addresses seismic effect. For monotonic behaviour, five different methods were used which are:

1. Second-order distributed plasticity analysis (*DPA*) - It was performed by using OpenSEEs which considered both initial imperfections and initial residual stresses;

2. Direct elastic-plastic hinge analysis (*DM-EP*) – It was by using SAP2000 [10]. Here 20% reduction of elastic stiffness was used;
3. Second-order analysis (*SOA*) with unreduced material elastic stiffness;
4. First-order analysis (*FOA*) with additional notional loads of 0.42% of the gravity loads and with unreduced material elastic stiffness.
5. Plastic analysis.

The initial residual stress distribution they were using is according to Galambos and Ketter (1959) [9]. While they applied the distribution directly into their analysis, they did not show whether those were related to any specific column curves.

The cyclic pushover analyses were conducted to examine the influence of the initial imperfection and initial residual stresses effects on the cyclic behaviour. Both analyses with and without these effects were performed and compared against each other. OpenSEES was used for cyclic analysis to perform the second-order plasticity analysis for this analysis.

The first preliminary conclusion, which they have made, based on the results obtained above is that the current version of the Direct Analysis method (DM) may not be adequate for seismic design of SMRFs because the amplification in force demands is underestimated. This can be expected because the *DM* involves an elastic analysis. During earthquake motions, significant yielding can occur and developments may be several times greater than the elastic displacements. This results in greater P-delta effects and greater amplification of the forces than those from the *DM*.

They also concluded that the initial residual stresses and imperfections, based on the results, might accelerate the collapse of frame when deformation concentrates in a number of stories. On the other hand, the initial residual stresses and imperfections generally have greater effect on the taller structures and less effect on the low-rise building.

2.5 INITIAL RESIDUAL STRESS DISTRIBUTION

The type of the initial residual stress (IRS) distribution is one of the important components in developing of the column curves. The magnitude and distribution of *IRS* in a section not only depend on the types manufacturing process such as hot-rolled, welded or cold-formed, they are also influenced by the types of cross section, thickness of the section, cooling conditions, rolling temperature, straightening method and steel properties (Beedle et al., 1960). Figure 2–5, taken from Figure 3.3 of *Guide to Stability Design Criteria for Metal Structures* [20], illustrates the *IRS* distribution in different cross-section. For a hot-rolled section, it is generally expected that for tension to form at centre of web and edge of flange because those place always cool fast whereas the web-flange junction, due to slow cooling process, contain tensile initial residual stresses.

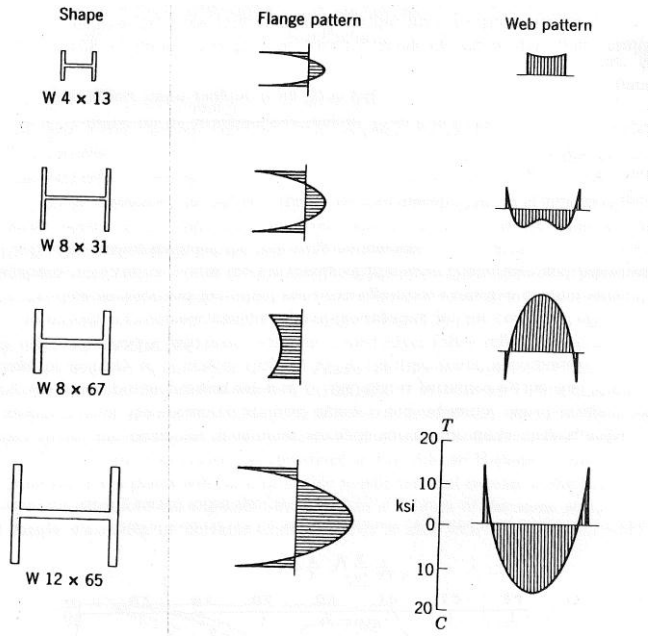

Figure 2–5: Typical initial residual stress distribution in hot-rolled I shapes[20]

As it is time-consuming and impractical to incorporate the real initial residual stress distribution directly into an analysis, the column curves, such as SSRC (Bjorhovde, 1972) and ECCS (Beer and Schultz, 1970; Jacquet, 1970; Sfintesco, 1970) as shown in Figure 2–6 a) and b) respectively, are used generally in design processes. Both of the column curves were developed based on the multiple column curve concept (Bjorhovde, 1972) that each curve represents a certain type of similar initial residual stress distribution. The methods for obtain column curves for different *IRS* are available. For example, Bornscheuer (1981) and Bjorhovde[22] (1972).

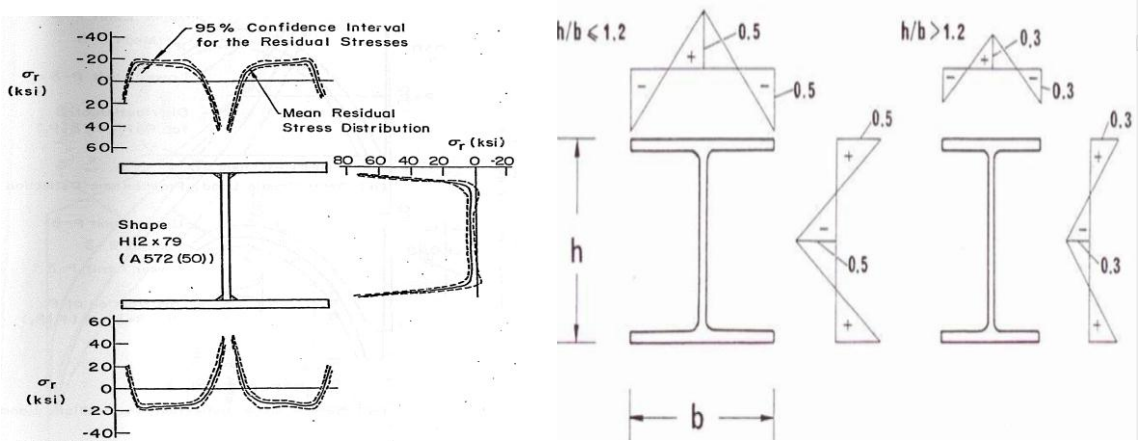

a) *IRS* pattern of H12x79 (Bjorhovde)[22] b) ECCS pattern for a hot-rolled I-section [14]

Figure 2–6: Typical *IRS* patterns general used in the researches

The two methods presented in the Ph.D. thesis of Bjorhovde (1972) are:

- Deterministic multiple column curves were developed based on the experimental data of 112 columns with different *IRS* distributions and an assumption of the maximum initial out-of-straightness of 1/1000 of the column length. From those experimental results, Bjorhovde observed that there were three distinct subgroups. For each subgroup, an average curve, according to statistical analysis, was given. The resulting three curves are known as the SSRC column curves.
- Probabilistic analysis of column strength, based on a computational method, was conducted to compare with results from deterministic method. These curves were developed by statistical method to account for the uncertainties in each of the parameters of developing the column curves.

The five Australian/New Zealand column curves also use multiple column curves. The column curves are semi-empirical, in that the analytical prediction which included a number of imperfections, such as initial out-of-straightness (L/1000) or accidental eccentric loadings, as well as the range of the initial residual stresses found in reality, are adjusted to agree with experimental results (Davids et al., 1985; Key et al., 1988; Rasmussen et al., 1989; HERA R4- 80, 1994). Hence, the initial residual stress distribution associated with each column curve type is not explicitly addressed.

3 COMPUTATIONAL SOFTWARE

The analytical programmes used in this project are MASTAN2 [11] and OpenSEEs [13]. Both of these are open source, freely available and can be downloaded from the websites. In this project, MASTAN2 is used to perform analysis for the first part of the project to consider the monotonic response of frames under combined effect of overstrength and initial residual stresses. OpenSEEs is used for the second part of the research which requires performing more advanced analyses such as inelastic time-history analysis.

3.1 MASTAN2

3.1.1 Descriptions of MASTAN2

MASTAN2 is developed by Prof. Ronald Ziemian and Prof. William McGuire as shown in Figure 3–1. This programme is developed based on MATLAB© platform which is a numerical computing and data analysis software. It it has sophisticated graphical interface for users and provides varieties of pre-processing, analysis and post-processing options. MASTAN2 has been purposely limited in a number of pre- and post- processing options to minimize the time for a user to become proficient.

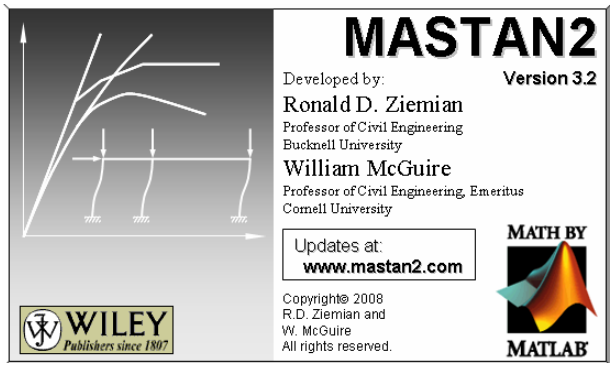

Figure 3–1: MASTAN2 copyright and developers' information [11]

Pre-processing options are definitions of frame geometries, support conditions, section and material properties and loading conditions including temperature effects and initial settlements. For the analysis, MASTAN2 is able to perform the 1st or 2nd order elastic or inelastic analysis of 2- or 3-dimensions frame and truss structures subjected to static loads. There are also some special options, which perform functions such as the elastic or inelastic critical load analysis and natural period computation. Post-processing includes

interpretation of results through diagrams, printed output and plotting of response curves. The analysis routines of MASTAN2 are based on the numerical and theoretical formulations presented in Matrix Structural Analysis, 2nd Edition [11].

MASTAN2 is able to perform Direct Analysis (DM) and Extended Direct Analysis (*EDA*) automatically. The values of stiffness reduction factor (*SRF*) for different column curves can be incorporated into MASTAN2 so that SRF values can be found for different member axial load ratios [2].

However, MASTAN2 has some limitations which are explained in the following:

a) It does not perform multiple cycle large displacement inelastic analysis nor does it allow analysis for records.
b) The reduced stress situation does not change as flexural load is applied and released, as it would be in a fibre model.
c) Only elastic-plastic hinges are considered.
d) The current version of MASTAN2 is only able to specify one initial residual stress category for all the members in frame. However, there is a possibility that there are members with different initial residual stress categories since the EDA method have five different SRF curves instead of only one such as DM in US. Therefore, it requires to ensure that all the members have the same initial residual stress category or the code may need to be modified.

Another feature of Mastan2 is the option for the user to develop specific analysis routines. As MASTAN2 is written in the modular format, it enables user to write and implement alternative or additional analysis routines to meet the specific project requirements.

3.1.2 Analysis Routines and Models in MASTAN2

3.1.2.1 Methods of solving nonlinear equilibrium equations

The 2nd-order inelastic analysis in MASTAN2 is performed by incremental single-step approaches where the total forces are applied in increments and the stiffness matrix is updated at each increment of applied load to account for both the material and geometric nonlinearities. The advantage of this single step approaches are the simplicity and efficiency since only one or two analyses are performed in each increment. However, due

to the fact that the two solution methods are based on load control integrator, it can only capture the structural behaviour up to the maximum capacity strength.

Two solution types are provided in the 2nd-order inelastic analysis of MASTAN2 to solve the nonlinear equilibrium equations. The first approach is called Simple Step, that is the Euler method, and the other is predicator-corrector (PC) or 2nd-order Runge-Kutta method. The PC method is more accurate than the Simple Step method. This is because the stiffness matrix for PC method is computed from the tangent stiffness at the start of the increment, K_1, and the stiffness using the deformed geometry and corresponding element forces at some point within the increment, K_2. On the other head, Simple Step only uses K_1. The formula of both methods are given in Eq. 3-1 and 3-2. Figure 3–2 (a) and (b), taken from *Matrix Structural Analysis* [11], illustrate the influence of the size of the load steps and different efficiency between these two methods and the incremental iterative approach, which is the work control method.

$$\overline{[K_{Simple\ Step}]} = [K_1] \qquad \text{Eq. 3-1}$$

$$\overline{[K_{Predictor-Corrector}]} = \alpha_1[K_1] + \alpha_2[K_2] \qquad \text{Eq. 3-2}$$

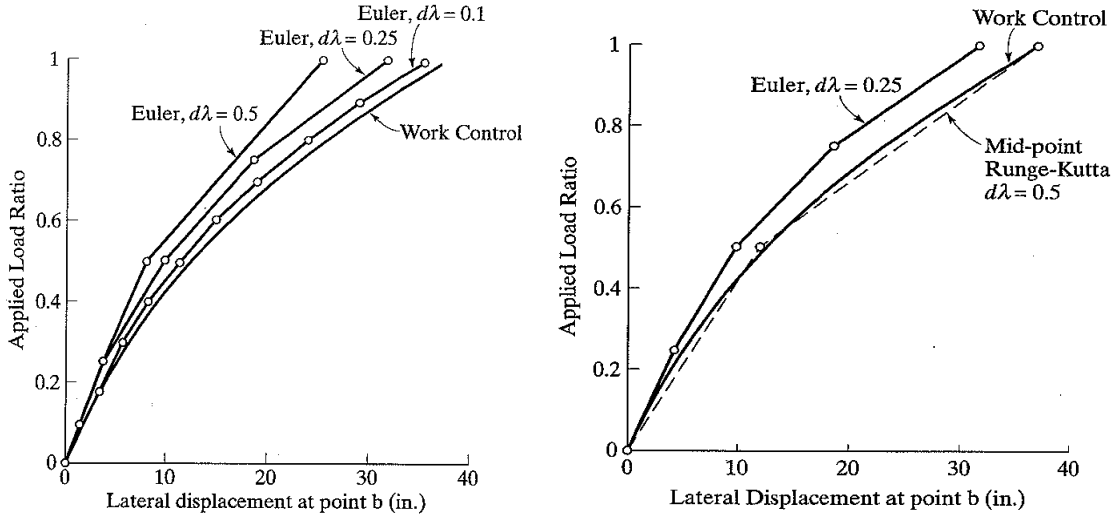

a) Comparison of step size b) Comparison of solution type

Figure 3–2: Comparisons of step sizes and solution types[11]

3.1.2.2 Modelling of the sectional and material properties

The concentrated plasticity (*CP*) approach is used for the inelastic analysis. It assumes that the plastic hinges would only form at the ends of elements or at the nodes. In contrast to the spread-of-plasticity model that will be described in the later section, it ignores the process of the partial yielding across the sections and along the length of elements. Therefore, the hinges are formed at a certain point once the section reaches the section plastic capacity. The perfect elastic-plastic relationship used for modelling material behaviour in MASTAN2 ignores the strain-hardening of steel.

The yield surface model [12] is applied to account for the axial force-moment interactions in both major and minor axes. For simplicity and easiness with regard to computer application, a widely used equation as shown in Eq. 3-3 is applied for the light to medium I-shaped sections. The internal forces, the combination of axial force, N^*, and the bending moments, M^*_z and M^*_y, in each nodal point are checked at the end of each load increment. According to the equation, the plastic hinge would be formed at a specified node if the value from the combination of N^* and M^* is equal to or greater than one. On the contrary, the section remains in the elastic region if the value is less than one. It should be noted that this yield surface method only considers the internal axial forces and moments. The shear force and torsion effects are neglected.

$$p^2 + m_z^2 + m_y^2 + 3.5p^2 m_z^2 + 3.0p^2 m_y^2 + 4.5m_z^2 m_y^2 = 1.0 \qquad \text{Eq. 3-3}$$

where

$p = N^*/N_y$; $m_z = M^*_z/M_{zp}$; $m_y = M^*_y/M_{yp}$,

N^* = Axial force at the current load increment,

N_y = Compressive axial force capacity of the specified member,

M^*_z = Strong-axis bending moment at the current load increment,

M_{zp} = Plastic bending moment capacity of strong-axis,

M^*_y = Weak-axis bending moment at the current load increment,

M_{yp} = Plastic bending moment capacity of weak-axis

3.2 OPENSEES

3.2.1 Description of OpenSEES

Open System for Earthquake Engineering Simulation (OpenSEES) [13], which was developed by F. McKenna and G. L. Fenves with many other contributors at the NSF sponsored Pacific Earthquake Engineering (PEER) centre (Mazzoni et al., 2006), is an open source and object-oriented software framework for finite element analysis. It can perform many types of analysis, such as linear or nonlinear static pushover, reverse-cyclic analyses, or inelastic time-history analysis with uniform or multi-supported excitations for both structural and geotechnical systems.

OpenSEES, including its interface, interpreter, source codes and commands, is based on the Tcl/Tk scripting language. Each finite element analysis is performed on the four main abstractions in OpenSEES as shown in Figure 3–3 below. ModelBuilder is the object where the models are constructed and added to the domain that is responsible for storing the objects. The analysis object moves the state of model from t to t plus Δt and the recorder records user-defined parameters during the analysis. In OpenSEES, users are required to develop the model in the modelBuilder section, and to define how the analysis is performed and how the parameters are to be recorded in the format of Tcl commands.

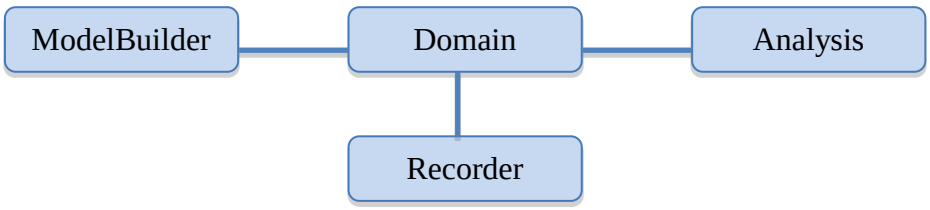

Figure 3–3: Main abstractions in OpenSEES

Compared to other commercial softwares, OpenSEES is probably more difficult to use because users themselves need to be familiar with the Tcl/Tk commands before using it and they need to develop the models on a non-graphical user-interface platform. Also, to avoid errors, users must understand how the software works. However, OpenSEES still has the following features that make it convenient for the researchers:

- the inter-changeability of components and the ability to integrate new and existing components into the framework without the need to change the current codes;

- as an open source software, the source codes are visible to all the users;
- it is a powerful program because OpenSEES contains a comprehensive library of material, section, element and analysis commands that allows users to produce simulations easily;
- it has the ability to allow users to create and change parts of the program by themselves such as hysteretic rules;
- OpenSEES has been available for over 10 years and is still in the process of continuing being developed and improved by many researchers. As the results, the number of available commands is still increasing;
- additional tools are available such as BuildingTcl and OpenSEES navigator to assist users to create the models and view the results graphically;
- models can be specified in a number of levels such as stress-strain relationship for material models, relationship of force-displacement or moment-curvature for sections and types of elements.

3.2.2 Descriptions of the models in the ModelBuilder

The current vision of the OpenSEES management committee is to provide a great number of material, section and element models. The material models are mainly categorised into steel/reinforcing-steel, concrete, standard uni-axial materials such as elastic and elastic-plastic materials and other uni-axial material including the models for modelling soil-structure interaction. The available section objects include elastic, uni-axial, fibre, plate and isolator2spring sections. For the element types, there are truss, zero-length beam-column, bearing, quadrilateral, brick, contact elements, and some special types. Since there are many different types of models, only those being used in this research are briefly described in the following sections.

3.2.2.1 Steel02 Material "Giuffre-Menegotto-Pinto" Model

Steel02 – Giuffre-Menegotto Pinto model with isotropic strain hardening is one of the inbuilt material models developed by Filippou [15] in OpenSEES for steel. The material command allows users to modify the behaviour of the steel hysteresis loop in four ways. The first is the value of the post-yielded stiffness that is controlled by the strain-harden ratio. This is the ratio between post-yield tangent stiffness and initial elastic tangent

stiffness. Second is the type of transition from the elastic to plastic region, such as smooth or sharp transitions. The next is the isotropic hardening responses under the cyclic motion where the stresses of the steel may increase or decrease after each cycle of loading. The last modification is the incorporation of initial residual stresses due to the manufacturing process in the section [16].

3.2.2.2 Fibre with quadrilateral section

Fibre section is used to incorporate the initial residual stress distributions into the steel sections. This section command automatically generates quadrilateral sections according to the user-specified points. These may then be subdivided into numbers of smaller fibre elements as shown in Figure 3–4(a). Figure 3–4(b) illustrates the discretization of an I-section consisting of several quadrilateral fibre sections. Each fibre section can be assigned to its own specific material property.

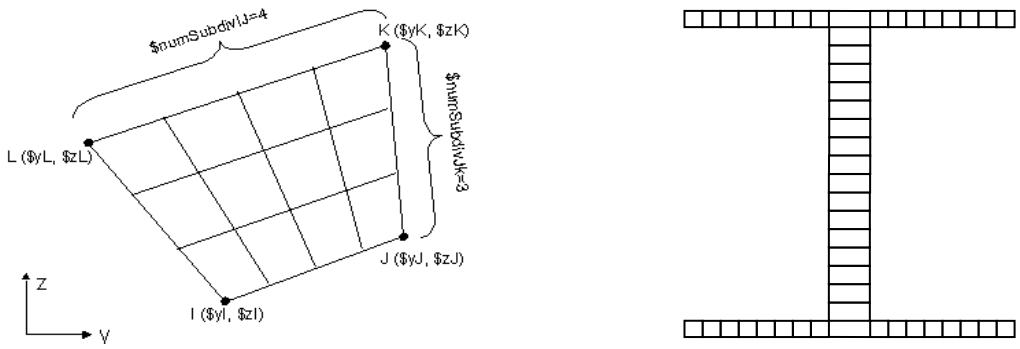

a) Fibre elements over a cross-sectional area b) Cross-sectional view of an I-section

Figure 3–4: Discretization of the elements and sections

3.2.2.3 Force-based nonlinear beam-column element

The nonlinear beam-column element is based on either iterative or non-iterative force formulation and automatically considers the spread of plasticity along the element. The integration method is based on the Gauss-Lobatto quadratural rule [18] where the integration points are located at the element ends. It denotes that the section models previously defined are assigned to the integration points and the response of the element is based on the responses at each integration point.

3.2.2.4 Corotational geometric transformation

The corotational geometric transformation code in OpenSEES was developed to transform from the local coordination system of stiffness and resisting force of the members to the global coordination system. The speciality of the corotational geometric transformation is that it can be used for large-displacement small-strain behaviour [19]. However, a deficiency of the current corotational transformation is that it can only consider the point loads and it does not deal with any element loads such as uniform distribution loads.

3.2.3 Spread-of-plasticity analysis

Spread-of-plasticity (*SoP*), or distributed plasticity (*DP*) analysis approaches, which are used in the OpenSEES, allow yielding to gradually develop through the cross-sectional area of the member and along the member length. It is achieved by implementing the fiber section with nonlinear beam-column elements to the models. This type of analysis approach is considered to be more advanced, rational and realistic than the concentrated plasticity hinge approach for predicting the frame behaviour because it captures the responses of reductions in member stiffness prior to full plastification of the sections as illustrated in Figure 3–5.

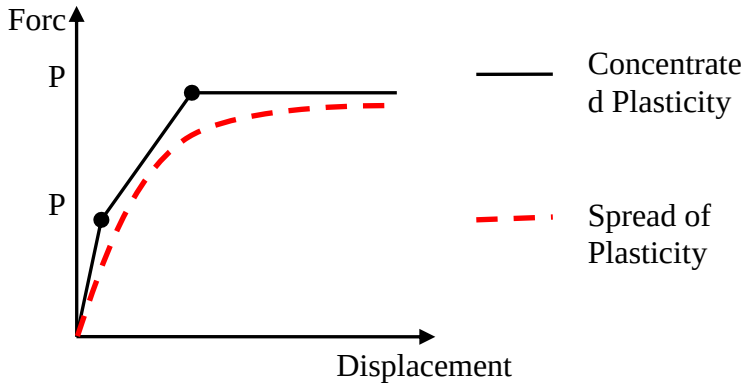

Figure 3–5: Responses of load-displacement from the two plasticity models [12]

Figure 3–5 shows the differences in load-displacement responses between the two analysis approaches for a simple frame [12]. The *SoP* produces a smooth curvy transition from the elastic response to the ultimate strength since it is able to capture the gradual change of the stiffness within the sections. On the contrary, the concentrated plasticity approach gives an abrupt response which the stiffness only changes at the points where the hinges form as indicated by the two dots in the figure. Moreover, the ultimate

strength from the *SoP* approach, in general, is smaller than the strength from the concentrated plasticity method. This is because the second order effect is stronger for the *SoP* approach than the concentrated plasticity approach due to the larger deformations in the early stage of the analysis due to the gradual reductions of the stiffness.

3.2.4 Accounted effects by using above configurations

By applying the combination of the fibre discretization of the cross section and the spread-of-plasticity approach, i.e. using the force-base nonlinear beam-column element, the interaction between the axial force and the bending moment of the element can be accounted for. Also, with the usage of the above stress-strain relationship, the kinematic and isotropic hardening, as well as the Bauschinger effect of the material can be considered.

It should be noted that the above configurations only account for the small deformations in the element. However, the large displacement geometry can be considered by the corotational geometric transformation.

3.2.5 Descriptions of analysis commands

Each analysis in OpenSEES consists of the following seven commands [13]:

- Constraints – determine how the constraint equations are enforced in the analysis.
- Numberer – the way to number the degrees-of-freedom in the system equation.
- System – construct the solving objects to store and solve the system of equation
- Test – establish the convergence test to ensure the convergence can be achieved at the an end of iteration step.
- Algorithm – determine the sequence of steps taken to solve the non-linear equation.
- Integrator – determine the meaning of the terms in the system equation and the incremental step for the next time step, and specify the tangent matrix and residual vector at any iteration.
- Analysis – define the type of analysis to be performed

OpenSEES provides more than one option, as listed in Table 3–1, for each analysis commands. It gives freedom and allows analysts to choose the most appropriate computation procedures for their analyses.

Table 3–1: List of options for analysis commands in OpenSEES

Commend	Available Options						
Constraints	Plain		Transformation		Lagrange Multipliers		Penalty
Numberer	Plain		RCM		AMD		
System	Band General	Band SPD	Profile SPD	UmfPack	Sparse SPD	Sparse General	
Test	Norm Unbalance	Rel. Norm Unbalance	Norm Displacement Increment	Rel. Energy Increment	Energy Increment	Rel. Norm Displacement Increment	
Algorithm	Linear	Newton	Modified Newton	Newtown with Line Search	Krylov Newton	Broyden	BFGS
Integrator	Load Control	ArcLength Control	Min. Unbalanced Disp. Norm	Displacem ent Control	Central Difference	Hilber-Hughes-Taylor	Newmark
Analysis	Static		Transient		Variable Transient		

3.3 COMPARISON OF MASTAN2 AND OPENSEES

A simple monotonic second-order elastic analysis was performed to evaluate how different the computation routine between these two software is. The configurations and the loading conditions are given in Appendix B. Both software subdivide the column into 8 sub-elements. The analysis was performed in 1000 load steps with the load increment of 1/1000 of applied loads. The axial and lateral loads were analysed together.

Table 3–2 presents the actual values of horizontal and vertical displacements at the top of the column and the bending moment at the bottom from MASTAN2 and OpenSEES. Both computational programmes produced similar structural responses as the differences of the displacements and the moment between these two programmes were very small (less than 3%).

Table 3–2: Column responses from MASTAN2 and OpenSEES

Software	Horizontal displacement at Top (mm)	Vertical displacement at Top (mm)	Bending Moment at Bottom (kNm)
Mastan2	19.6	-2.648	418.6
OpenSEES	19.85	-2.688	419.2
Difference (%)	1.26	1.51	0.143

3.4 SUMMARY OF ANALYSIS SOFTWARE

The two programmes used in this research were MASTAN2 and OpenSEES as described in Chapter 3. For monotonic analysis i.e. pushover analysis, both programmes used the load control method to determine the ultimate structural capacity. The total applied loadings were performed in small load step size and the deformed structural geometry was updated after each load step to account for the *P*-delta effect. As given in Table 3–2, similar structural responses were obtained from both software.

For cyclic loadings, OpenSEES used displacement control integrator to conduct the push-pull analysis. By using the displacement control method, the reduction in structural capacity beyond yielding of structure could be captured. The inelastic time-history analysis (ITHA) was performed to evaluate the seismic behaviour of steel frames. Similar to load control method, *P*-delta effect was considered by updating the current structural state at the end of each time step. On the contrary, MASTAN2 performed load control method only and was unable to perform analysis subjected to seismic loading since it cannot incorporate earthquake records.

The method of considering initial residual stresses (*IRS*) in the section for MASTAN2 is by using the stiffness reduction factor (*SRF*) whereas OpenSEES considers the effect of *IRS* by incorporating it directly into the sectional model.

4 EFFECT OF OVERSTRENGTH

This chapter illustrates the effect of overstrength on the plastic response of the frames by comparing the two different overstrength cases with the benchmark case. The descriptions of the analysis method and the configurations of the frame including the section and material properties are given first followed by the descriptions of the three analytical cases for evaluation. The results and summary of the findings are presented at the end of this chapter.

4.1 FRAME MODELLING AND ANALYSIS

4.1.1 Basic frame descriptions

A single-storey frame shown in Figure 4–1 was specially designed and selected in this study to evaluate the effect of material overstrength to the frame performance. This selected structural form can be envisaged as a simple commercial structure that consists of a one bay frame with a 3m overhanging roof on the left hand side. A vertical prop or a leaning column with pinned connection at both ends was constructed to support the overhanging roof allowing the cladding to be placed. A distinct point of this structural layout is the fixity of the one-bay frame. Unlike the conventional layouts where both supports have the same type of fixities, this analytical model uses a fixed support to the central column but a pinned support to the right column.

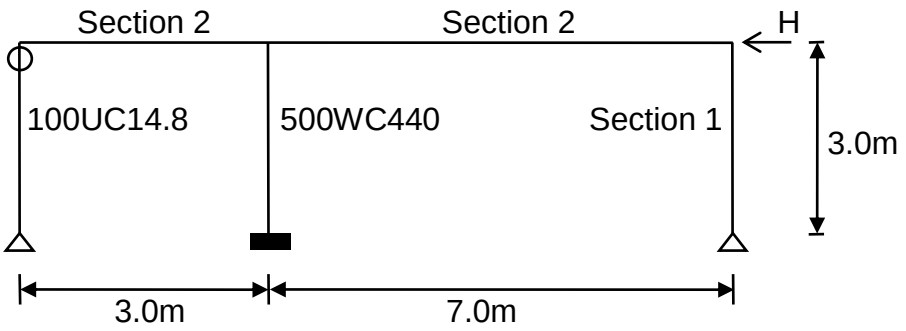

Figure 4–1: Configuration of selected analytical model

All sections selected are compact sections according to the NZS3404:2007. Hence, they are able to reach their plastic flexural capacities. As the analyses were considered in two-dimension only, all the members are fully braced out-of-plane. Table 4–1 presents the general properties of the sections used are given in where Z_x is the elastic section

modulus and S_x is the plastic section modulus according to the definition in the NZ/Australia steel codes. I_x is the second moment of area and A_g is the section area. The nominal yielding strength, f_y, is 300MPa and Young's modulus, E, is 200GPa. All the sections considered in this study are hot-rolled and have the initial residual stress category of $\alpha_b = 0$.

Table 4–1: Section properties

SECTION	A_g (mm^2)	I_x ($\times 10^6$ mm^4)	Z_x ($\times 10^3$ mm^3)	S_x ($\times 10^3$ mm^3)
500WC440	56000	2150	8980	10400
100UC14.8	1890	3.18	65.6	74.4
Section 1	109800	2090	12900	14900
Section 2	66800	6050	16100	18700

Table 4–2 gives the dependable section plastic flexural capacity, ϕM_p, and axial compression capacity force, ϕN_c. These were computed as the strength reduction factor, ϕ, times the nominal section capacities. Here, the strength reduction factor, ϕ, is 0.90. The beam sectional flexural strengths were designated to be greater than for the columns. Therefore, the plastic hinges are expected likely to form only in the columns. The steel material is also assumed to behave in perfect elastic-plastic manner since strain-hardening is not considered in all the analyses.

Table 4–2: Dependable section capacities

SECTION	ϕM_p (kNm)	ϕN_c (kN)
500WC440	2808	15120
100UC14.8	17.71	347
Modified S1	3248	24487
Modified S2	5049	18036

4.1.2 Analytical methodology and configuration

The analysis method used is the Extended Direct Analysis method [2, 3] as described in Chapter 2, and all the analyses are performed by MASTAN2. Rather than using the traditional plastic analysis, EDA was used because it includes the initial residual stresses effect on the member stiffness and considers the other different nonlinearities automatically as discussed previously. Moreover, EDA can easily incorporate the

reduction factors or the overstrength factors by simply multiplying the factors to the material yielding strength or the elastic modulus and use these as the input values.

The analysis results are obtained based on the following configurations:

- Second-order inelastic analysis were performed for a standard hot-rolled section (NZ Et alpha=0.0);
- Ten sub-elements are assigned to each member;
- Incremental size is 0.001 such that each load step is 1/1000 of the applied loadings;
- System equations are solved by the Predictor-Corrector method.

4.1.3 Loading conditions

It should be noted that the model described above was only subjected to a lateral force whereas the gravity load was neglected. The reason for neglecting the gravity force is that the gravity force has the tendency to alter the frame responses. It was found that the model was able to resist an upper maximum lateral force as well as a lower lateral force while the gravity loadings remain the same. However, when the lateral force with the value between these upper and lower values was applied, the frame collapsed.

The cause of the two lateral force values may be due to the size of the load increment. As mentioned previously, the size of each load increment depended on the magnitude of the applied load since the incremental size is calculated by 0.001 times the applied loads. In this case, the upper limit would have larger load incremental size for the lateral force than the lower limit when the gravity loads are the same.

4.2 EVALUATION METHODOLOGY

Three cases were considered as shown in Table 4–3. They are:

1) Case 1: The minimum material strength, defined as the dependable strength, was used as the benchmark case in this study. This case is identical to that described above for EDA; hence, $E_{input} = \phi E$ and $f_{y,input} = \phi f_y$.

2) Case 2: This is the first overstrength case which considered a lower bound estimate on the likely E, which could occur at the same times as a high material strength.

Therefore, the yielding strength, $f_{y,input}$, is $(1.25/0.9)\phi f_y = 1.39 \times \phi f_y$. The Young's modulus, E_{input}, was ϕE.

3) Case 3: In this overstrength case, it is assumed that the section strength is ϕ_o times the nominal value. The $f_{y,input}$ is therefore $(1.25/0.9)\phi f_y = 1.39 \times \phi f_y$ which is the same as Case 2. The E_{input} was E in this case. In contrast to Case 2, this is a greater estimate of E which may be due to a high strength with same section size or due to section size variation.

Table 4–3: Summary of material properties for each case

Case No.	Case Title	E_{input} (GPa)	$f_{y,input}$ (MPa)
1	Dependable Strength	180	270
2	Overstrength 1	180	375
3	Overstrength 2	200	375

Note that the overstrength factor used here is 1.25. According to Table 12.2.8(1) NZS3404, the values of overstrength considering strain hardening and material variation may be as large as 1.50 for members subject to large inelastic demands. The value of 1.25 represents the likely overstrength of a compact member manufactured in Australian or NZ which is subjected to moderate inelastic deformation. In general, approximately 20% of the strength increase occurs due to material strength variation and about 5% is due to strain hardening [1].

4.3 FRAME RESPONSES

Figure 4–2 specifies the labels for the position of peak moment at the member ends. In the convention used, positive displacements and forces are toward the left and upward.

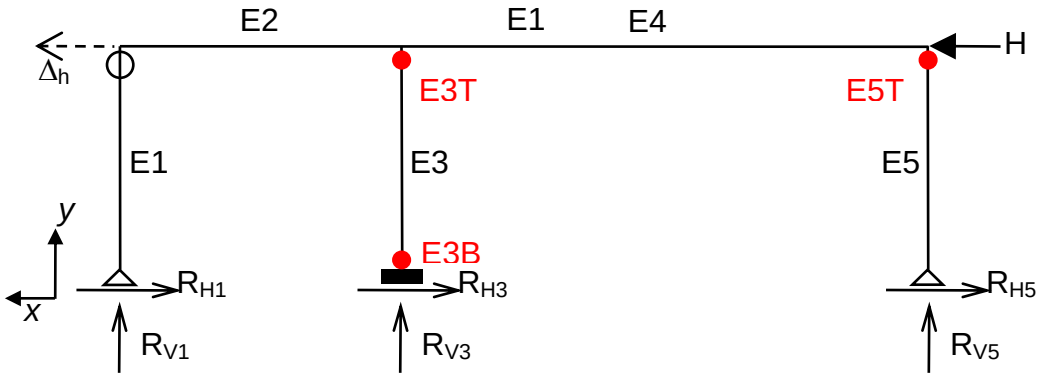

Figure 4–2: Labelling of hinges, forces and elements in the Frame

4.3.1 Frame behaviour

For the dependable strength case, Case 1, a column sway mechanism occurs after three hinges have formed in the columns and the frame becomes unstable. From Figure 4–3, it may be seen that the first hinge occurred at point E3B as shown in Figure 4–2. It is in the central column (E3) which is restrained at the top and bottom. However, it has more fixity at the bottom so that the moment is larger here than at the top. The second hinge is at E3T and the last hinge, which caused a mechanism, is at E5T. The maximum applied lateral force is 3189kN when the mechanism occurred.

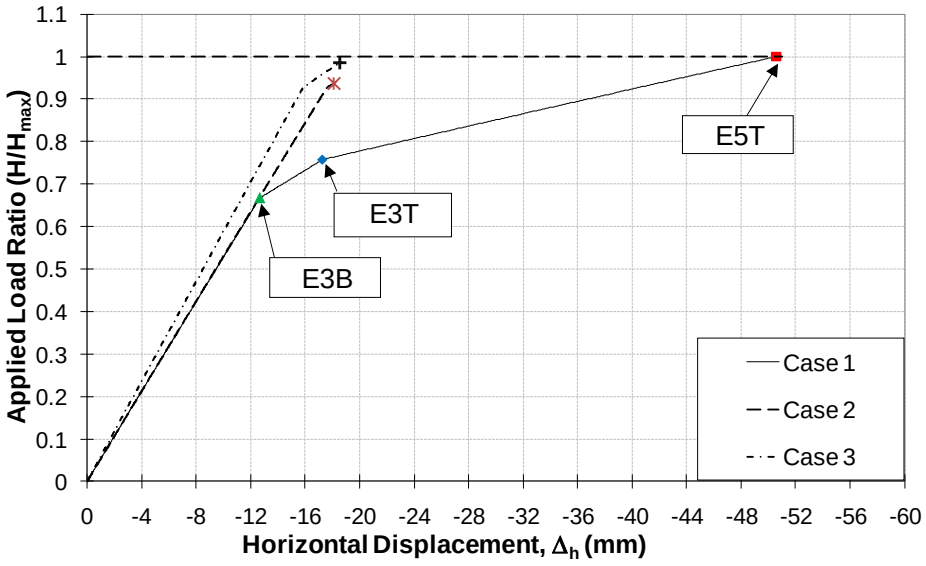

Figure 4–3: Diagram of lateral force – displacement responses

The collapse mechanism of Case 2, Overstrength 1, is formed due to the buckling of the left hand column, E1. For Case 2, unlike Case 1, only the first hinge, which is located at E3B, was able to form before the frame collapsed. In addition, the hinge formed at a

higher applied force as indicated by the changing of gradient of line in Figure 4–3. It can also be seen from Figure 4–3 that the strength of Case 2 is weaker than Case 1 since the frame can only resist a maximum applied lateral force of 2994.5kN (6.1% lower than Case 1).

The frame behaviour for Case 3, overstrength 2, is similar to Case 2. Case 3 also failed when the left hand column buckled. A plastic hinge was also formed at E3B approximately at the same force of Case 2. According to Figure 4–3, Case 3 is more stiff than Case 1 and 2 since the slope of line of Case 3 is steeper. Case 3 is stronger than Case 2 since it can resist a higher lateral applied force of 3147.5kN which is about 1.3% lower than Case 1.

Table 4–4 compares the horizontal and vertical support reactions. The values in the table are computed by using the ratio of the result of the case considered divided by the result of Case 1 and minus 1. Here, it was found that the largest increases in demand occurred in horizontal reaction of central support, R_{H3}, and vertical reaction of left-hand (LH) support, R_{V1}. The maximum increase was 34%.

Table 4–4: Support Reaction Forces

Case No	H	R_{H1}	R_{H3}	R_{H5}	R_{V1}	R_{V3}	R_{V5}
Case 1	0%	0%	0%	0%	0%	0%	0%
Case 2	-6%	-10%	29%	-55%	22%	-81%	-38%
Case 3	-1.3%	-3%	34%	-50%	29%	-76%	-32%

4.3.2 Reasons for lower strength of frame with greater element strength

Failure of the left hand column occurred in Case 2 and 3 due to the yielding occurring late. There was, therefore, no reduction to the force applied to the column. Unlike Case 1, the axial compression force increased at an approximately steady rate until the formation of the second hinge. Then the axial force demand in the column was decreasing. This was due to the moments/forces in the frame being redistributed as illustrated in Figure 4–4. It caused a reduction of moment in the left hand beam. Hence, the axial force in E1 was also reduced. Figure 4–5 shows that the behaviour after the second hinge (E3T) formation is a key in changing the frame behaviour.

On the contrary, there is no reduction of the axial force in the left hand column for Cases 2 and 3 since the second hinge does not form in the system and there is only minor moment redistribution in the system due to the formation of the first hinge.

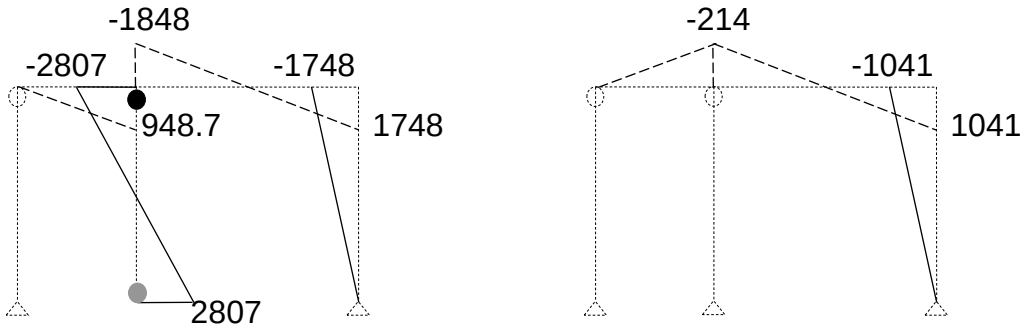

a) At moment of second hinge formation

b) Moment distribution for additional lateral force after second hinge formation

Figure 4–4: Illustration of the distributing of the bending moment after the formation of the second hinge in Case 1

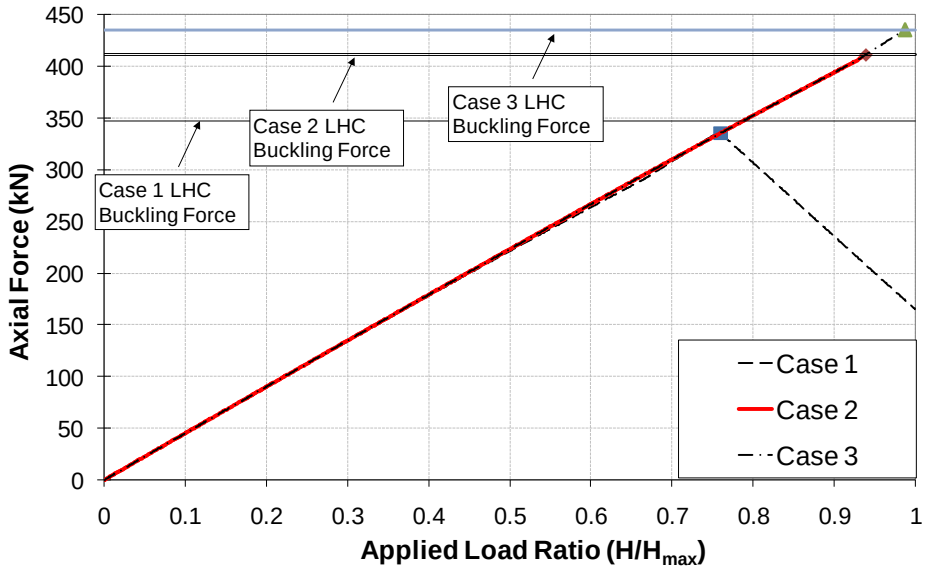

Figure 4–5: Axial Forces in Left Hand Column (E1)

The differences between Case 2 and 3 are caused by the different elastic modulus, *E*. The first difference is the stiffness of the frame. The Case 3 frame is stiffer than the Case 2 as shown by the slope of the line. The other difference is that the analysis of Case 2 is terminated earlier than Case 3 since the axial compression buckling capacity of the left

hand column for Case 2 is less than that for Case 3. The horizontal lines in Figure 4–5 show that the axial buckling capacities for Case 2 and Case 3 are 411.3kN and 435.4kN respectively.

4.4 SUMMARY OF OVERSTRENGTH EFFECT

The effect of overstrength was investigated in this study. It was found that:

1) Member demands may increase significantly when the likely maximum material strength is considered in the analysis. This will also have an impact on connection and foundation design.

2) The likely minimum frame lateral strength does not always occur when the frame has the minimum material/section strengths.

3) It was recommended that two sets of analysis be undertaken for design. One should consider the dependable strength and stiffness. The other should consider the overstrength.

5 INITIAL RESIDUAL STRESS RATIOS AND COLUMN CURVES

The main purpose of this chapter is to determine the column curves associated with a particular section of initial residual stresses (IRS) ratios. As part of this, a number of computer programme verification and sensitivity studies were conducted to ensure the precision and accuracy of the results from OpenSEES.

5.1 ANALYSIS MODEL CONFIGURATIONS

This section describes the analysis settings of the models in OpenSEES whereas the background information of some of the settings has been given in Chapter 3. The configurations described here are the initial residual stress ratios with the column curves, initial residual stress distribution model and the implementation of the distribution into sections, material property and element model. The configurations stated in this section are also used for the remaining analyses of the evaluation of cyclic response. All of the codes for OpenSEES are given in Appendix C.

5.1.1 Initial residual stress distribution model

In OpenSEES models, the initial residual stress value, σ_r, is defined as γf_y where γ is the initial residual stress ratio defined specially for this research. The approximated values of the *IRS* ratios are determined in the later section of this chapter.

5.1.1.1 Residual stress pattern 1 (Control case) – linear model (ECCS)

The initial residual stress (IRS) distribution used is linear model as shown in Figure 5–1 below. Note that the negative sign denotes that the section is in compression stress initially. This distribution has the maximum compressive *IRS*, - σ_r, in the edge of the flanges and centre of the web. On the contrary, the joints of the web and flanges have the maximum tensional residual stress, σ_r. The initial residual stresses vary linearly with constant gradient from maximum compression *IRS* at the edge of flanges or centre of web to the maximum tensional *IRS* at the joints of web and flange.

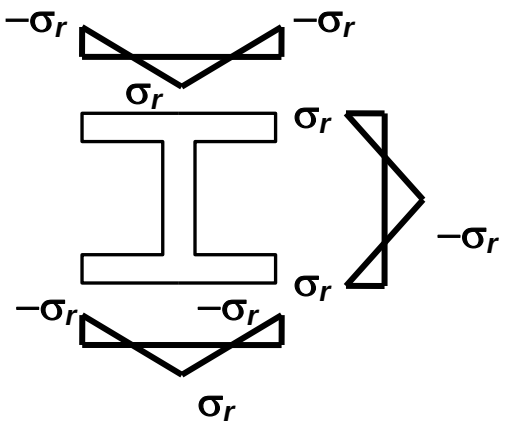

Figure 5–1: Linear initial residual stress distribution model (ECCS)

5.1.1.2 Residual stress pattern 2 – constant pattern

Apart from the linear model used in the control case, an additional constant initial residual stress distribution, as shown in Figure 5–2, was also investigated as a reference pattern to compare with the control case. This pattern is specifically defined for this research. This pattern is considered to be a more critical initial residual stress distribution for a hot-rolled I section. For this pattern, each quarter of the flanges from the free ends is in uniform maximum compression, -σ. On the other hand, the rest of the flanges is in uniform maximum tension stress, σ. For the web, one quarter of the web from the interfaces of the web and the flange is in maximum tension stress and the rest of the web is in maximum compression.

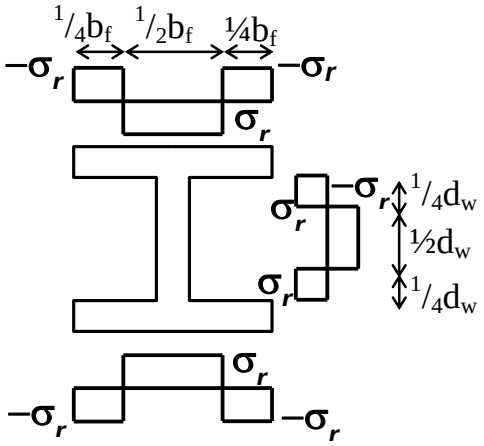

Figure 5–2: Constant initial residual stress pattern

5.1.2 Implementation of residual stress distribution

5.1.2.1 Residual stress pattern 1 (Control case) – linear model

A fibre section with quadrilateral elements is applied in OpenSEES to model the I-section with initial residual stresses. The OpenSEES code is given in Appendix C1. Each I-section is constituted with (6*i* + 3) fibre elements in total as shown in Figure 5–3 for *i* = 8. Each clear width of each flange outstand contains *i* fibre elements; there are (2*i* + 1) elements in the clear depth of the web. Note that the clear width or depth denotes the length from the edge of the element to the nearest face of the web or between the inner faces of the flange as shown in the figure. The last two fibre elements are for the top and bottom joints of the web and flange.

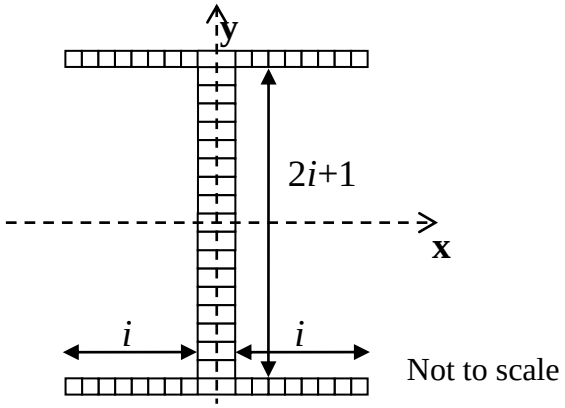

Figure 5–3: Section fibre discretization for the control case

Each fibre has its unique *IRS* value based on the provided *IRS* distribution. Eq. 5-1 and 5-2 present the equations used in OpenSEES to compute the values of *IRS* for each fibre in the flanges and web respectively. The b_f in Eq. 5-1 is the width of the flange and *d* in Eq. 5-2 is the depth of the section. The *x* in both equations is the distance from the sectional axes (the vertical axis for flange and horizontal axis for web as shown by the dashed lines in the figure above) to the centre of each fibre element. The web-flange joints and the centre of the web are simply assigned with the maximum tensional residual stress. It also should be noted that the *IRS* pattern of the web is applied to the length between the two centres of the web-flange joints.

Flange: $$\sigma_{r,i} = -\frac{2\sigma_r |x|}{b_f / 2} + \sigma_r$$ Eq. 5-1

Web: $$\sigma_{r,i} = \frac{2\sigma_r |y|}{(d - t_f)/2} - \sigma_r$$ Eq. 5-2

5.1.2.2 Residual stress pattern 2 – constant pattern

The difference between the constant case and the control case in the fibre discretization of the cross section is that there is no fibre for the flange and web joint for the constant case. For the constant case, each half of the flange contains *i* fibres as shown in Figure 5–4 and there is a total of 2*i* fibres in the clear width of the web. Hence, there are 6*i* fibres in each cross-sectional area. The figure illustrates a fibre discretization for a cross section with *i* = 8. In this case, the four elements counting from each free end of the four flanges are in full maximum compressive initial residual stress (IRS) and the rest 8 fibres are in maximum tension *IRS*. For the web, the four elements counting from both interfaces of the web and flange have the same *IRS*, which is in maximum tension, and the rest of the fibres are in same maximum compressive *IRS*. The OpenSEES code is given in Appendix C2.

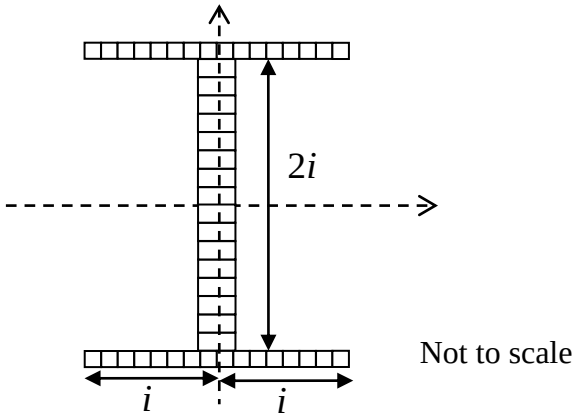

Figure 5–4: Section fibre discretization for the constant case

5.1.3 Material stress-strain relationship

Steel stress-strain relationship used in this study is established by "Giuffre-Menegotto-Pinto (GMP) Model with Isotropic Strain Hardening" as previously described in Chapter 3.2.2.1. Table 5–1 gives the settings of the commands and Figure 5–5 illustrates the full

cyclic response of the stress-strain relationship of the material. It was plotted up to the strain value of 0.02mm/mm based on the given settings and was similar for greater strains. The response shown in the figure does not include the effect of initial residual stresses. The material properties used are 300MPa for material yielding strength, f_y, and 200GPa for elastic modulus, E.

Table 5–1: Setting for parameters of GMP steel model

Strain-Hardening Ratio (b)	0.0
R0	20
cR1	0.925
cR2	0.15
Isotropic Hardening 1 (a1)	0.0
Isotropic Hardening 2 (a2)	1.0
Isotropic Hardening 3 (a3)	0.0
Isotropic Hardening 4 (a4)	1.0

This material configuration has the following key behaviour:

- No strain hardening is included;
- Smoothly transition from the elastic to plastic behaviour;
- No increase or reduction in strength due to cyclic loading.

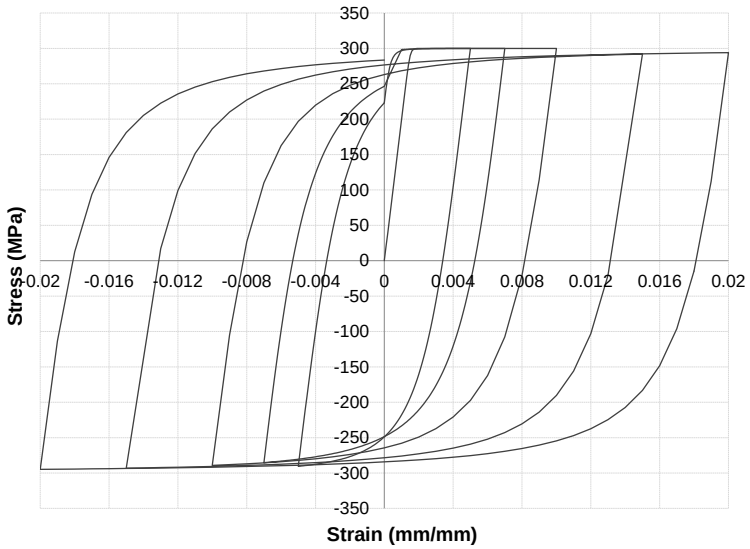

Figure 5–5: Material stress-strain relationship used for OpenSEES

5.1.4 Element model configuration

The element type used is the "Force-based nonlinearBeamColumn" element. The detailed descriptions of the command are given in Chapter 3.2.2.3. For this study, each column and beam is subdivided into eight nonlinearBeamColumn elements and each element contains 5 integration points.

5.1.5 Section size used for all analyses of Chapter 5

The section used in this study is 310UC137. The section property is given in Table 5–2. Here, d is the depth of section; bf is the width of flange; t_f is the thickness of the flange; t_w is the thickness of the web; A_g is the cross sectional area and I_x is the second moment of area about the major axis. Note that the area calculated here is based on the idealized shape where the area of fillet weld is ignored. Hence, both the area and the second moment of area given in the table are slightly less than the values provided by OneSteel [17] which is 17500 mm^2 and 329×10^6 mm^4 respectively.

Table 5–2: Idealised section property for 310UC137

Section	d (mm)	b_f (mm)	t_f (mm)	t_w (mm)	A_g (mm^2)	I_x (mm^4)
310UC137	321	309	21.7	13.8	17241	325.5×10^6

5.2 PRELIMINARY ANALYSIS OF OPENSEES

In this section, OpenSEES was verified by using the analysis results with the closed form solutions of the cantilever column from the ANSI/AISC 360-05 2005 Clause C7.3, as shown in Figure AA–1. Moreover, some sensitivity studies were conducted to investigate the effect of the key modelling parameters such as number of elements, number of fibre discretizations and the number of integration points, and to ensure the consistency of the results.

Table 5–3 and Table 5–4 summarise the analysis settings and the configurations of the elements used for the control case. Each analysis is carried out in 1000 steps with the load incremental ratio (IS) of 0.001 times the applied loads which give a total applied ratio of one. It should be noted that the axial force is initially applied before the cyclic deformations are imposed.

Table 5–3: Configurations of the analysis for the control case

Command	Method
Geometric Transformation	Corotational
Constraints	Transformation
Numberer	RCM
System	Band General
Test	NormDispIncr 1.0e-8 30 0
Algorithm	ModifiedNewton
Analysis	Static

Table 5–4: Configurations of the elements for the control case

Type	Number used
Sub-Element (*SE*)	8
Discretiztion (*i*)	8
Integration Points (*IP*)	5
Sub-Division *(SD)*	5

5.2.1 Verification of OpenSEES

The column properties of the model (310UC137 as given in Table 5–2) for the verification of OpenSEES are that the height of the column, L, is 4.8m and the applied horizontal force, H, and the axial compressive force, N^*, are 50kN ($\approx 0.0018N_{euler}$) and 4600kN ($\approx 0.165N_{euler}$) respectively. Here, N_{euler} is the Euler buckling load which is computed as $\pi^2 EI/L^2$. With this configuration, the M_{max}/M_o and y_{max}/y_o according to the closed form solutions are 2.58 (M_o = 240kNm) and 2.91(y_o = 28.3mm) respectively.

It should be noted that the closed form solutions of the benchmark problems only consider the second order effect and do not consider section plasticity. On the other hand, the second order elastic analysis should be performed in OpenSEES to produce the results that can be compared with the closed form solutions. To achieve this, instead of constructing a new model that can perform the second order elastic analysis, a simple method is by using a very large material yield stress. It ensures that the column, under the applied forces, is remaining in the elastic region. In this verification process, a f_y = 9000MPa is used.

From the results shown in Table 5–5, they show that the values by OpenSEES are slightly less than the values by the closed form solution but higher than the values from MASTAN2. However, the differences between the OpenSEES and the closed form solution for the overturning moment at the base and the lateral displacement at top of the column are less than 2% and 1% respectively. Because AISC (2005) requires that the difference from the analysed and closed form solutions to be less than 3%; therefore, it can be concluded that OpenSEES is able to capture the second order effect properly.

Table 5–5: Results of verification of OpenSEES

Analysis Methods	Lateral displacement, y_{max} (mm)	Diff. (%)	Base Moment, M_{max} (kNm)	Diff. (%)
OpenSEES	**81.5373**	**-**	**614.710**	**-**
Closed Form Solution	82.4927	1.172	619.467	0.774
Mastan2	79.3000	2.744	604.700	1.628

5.2.2 Sensitivity studies

The model setting used for the sensitivity studies for OpenSEES had the following parameters:

- Column height, L = 2400mm;
- Applied axial compressive force, N = 3200kN ($\approx 0.61N_s$);
- Applied horizontal force, H = 105kN.

Here, the sensitivity study was conducted with the second order inelastic analysis. This is different to the verification of the OpenSEES which was conducted by using elastic analysis. The elastic lateral yielded displacement at the top of the column, $\delta_{elastic}$, computing by Eq. 5-3, is 7.615 mm and the first order elastic base moment, $M_{base,elastic}$ = HL = 252kNm. For the control case, the lateral displacement and the base moment are 9.60mm and 283.6kNm.

$$\delta_{elastic} = \frac{HL^3}{3EI} + \frac{HL}{GA} \qquad \text{Eq. 5-3}$$

where

G = Shear modulus of elasticity (≈ 80GPa)

5.2.2.1 Load incremental ratio

Three different load incremental ratios of 0.002, 0.005 and the control case, 0.001, were examined. Here the load incremental ratio is defined as the load step size over an applied force. Table 5–6 presents the results of the lateral displacement at the top of the column and the overturning moment at the base for the three load incremental ratios. It clearly shows that there is no difference between the control case and the other two cases for both criteria. Therefore, it can be concluded that the load incremental ratio of 0.001 can produce consistent results.

Table 5–6: Effect of load incremental ratio

Load Incremental Size (IS)	Lateral displacement (mm)	Diff. (%)	Base Moment (kNm)	Diff. (%)
0.001 (control)	**9.960**	**-**	**283.626**	**-**
0.002	9.960	0.000	283.626	0.000
0.0005	9.960	0.000	283.626	0.000

5.2.2.2 Number of member sub-elements

Seven different numbers of sub-elements (SE) with 2 to 16 sub-elements were compared. The results and comparisons between the current and succeeding values for the lateral displacement at the top of the column and the base moment are shown in Table 5–7. The results show that both displacements and moments increase when the number of the sub-element increases. However, the rate of the change decreases with an increase of the sub-elements. Comparing the other cases with the control case, the results from the cases having less than 8 sub-elements are smaller than the values of the control case. On the contrary, for the cases having sub-elements greater than 8, the values are slightly larger or they are considered to be more precise. However, the differences between these cases and the control case are yet less than 0.5%. Therefore, it can still be concluded that the accurate result can still be achieved with 8 sub-elements.

Table 5–7: Effect of number of sub-elements

Number of Elements (SE)	Lateral Displacement (mm)	Diff. (%)	Base Moment (kNm)	Diff. (%)
8 (control)	**9.960**	**-**	**283.626**	**-**
2	9.806	1.548	283.134	0.173
4	9.915	0.445	283.485	0.050
6	9.942	0.176	283.570	0.020
10	9.969	0.094	283.656	0.011
12	9.975	0.150	283.674	0.017
14	9.978	0.186	283.686	0.021
16	9.981	0.211	283.693	0.024

5.2.2.3 Section fibre discretization size

The effect of fibre discretization is minor according to the results given in Table 5–8. From the results, the values, both the lateral displacements and the base moments, tend to decrease with an increasing number of the fibre. Comparing the control case and other cases, the difference for the lateral displacement and the base moment is less than 0.02%. Hence, i = 8 can produce consistent results. Note that the table only gives 3 significant figures. However, the differences given below were calculated with the full values (5 significant figures).

Table 5–8: Effect of size of fibre discretization

Number of Discretizations (i)	Lateral Displacement (mm)	Diff. (%)	Base Moment (kNm)	Diff. (%)
8 (control)	**9.960**	**-**	**283.626**	**-**
4	9.961	0.011	283.630	0.001
6	9.960	0.003	283.627	0.000
10	9.960	0.001	283.626	0.000
12	9.960	0.002	283.626	0.000
14	9.960	0.003	283.625	0.000
16	9.959	0.003	283.625	0.000

5.2.2.4 Element integration points

Table 5–9 presents the results of the displacement and base moment for 2, 5 (control case) and 10 integration points (IP). In this case, the analysis with IP = 2 was not able to reach the full applied loads (with the applied load ratio = 0.997 instead of 1). This case

also gave the greatest displacement and moment. On the contrary, the control case and *IP* = 10 were able to reach the full applied loads. The differences between the control case and *IP* = 10 are less than 0.01% for both displacement and moment. The results indicate that the analysis must have at least 5 integration points in an element to be able to give proper results. It also shows that 5 integration points are able to give consistent solutions.

Table 5–9: Results for effect of number of integration points

Number of Integration Point (IP)	Lateral Displacement (mm)	Diff. (%)	Base Moment (kNm)	Diff. (%)
5 (control)	**9.960**	**-**	**283.626**	**-**
2	11.085	11.296	286.359	0.964
10	9.960	0.003	283.625	0.000

5.2.2.5 Number of fibre element subdivisions

The three values that are being compared for the number of the subdivisions in a fibre element are 4, 25 and 100. It means that there are 2, 5 and 10 sub-elements in each *i-j* and *j-k* directions as shown in Figure 3–4(a). It should be noted that all the subdivisions in a fibre element have the same material property.

The results, as shown in Table 5–10, are similar to the element integration points. For the case with *SD* = 4, the analysis was not able to reach the full applied loads which the analysis terminated at the applied load ratio = 0.997. It also results in a higher lateral displacement and base moment. The comparison between the remaining two cases and *SD* = 4 indicates that it is best to use 5 or more sub-divisions to generate satisfactory results. Another observation that can be made is that the lateral displacements and the base moments became smaller with increasing number of subdivisions.

As it clearly shows in the table, the difference between the control case and *SD* = 100 is less than 0.1% for both criteria. Hence, 5 elements along each *i-j* and *j-k* direction are sufficient to achieve good results.

Table 5–10: Comparison for the number of sub-divisions

Number of Sub-Divisions (SD)	Lateral Displacement (mm)	Diff. (%)	Base Moment (kNm)	Diff. (%)
5 (control)	**9.960**	**-**	**283.626**	**-**
4	11.196	12.412	286.713	1.088
100	9.957	0.028	283.617	0.003

5.2.2.6 Effect of different combinations of the analysis options

In this section, the effect of the different combinations of the analysis commends was inspected. The studied analysis commends studied and the results of the comparisons between all the different combinations are presented in Tables AB–1 and AB–2 in Appendix B. There are a total of 17 cases were conducted and compared with the control case as given in Table 5–3. These 17 cases are in combinations of the two constraints, which are plain and transformation, three systems, BandSPD, BandGeneral and UmfPack and three algorithms which are the linear, Newton and ModifiedNewton. The results show that only those combinations using the linear algorithm give slightly less conservative (smaller) results. All other combinations have the same results as the control case. The differences between the combinations of using the linear algorithms and the control case are 0.00013% and 0.0012% for the lateral displacement at the top and the overturning moment at the base respectively.

5.3 DESCRIPTION OF ANALYSIS MODEL

The simply supported column is shown in Figure 5–6. This column has a pinned connection at the bottom and a roller support at the top, which allows vertical movement.

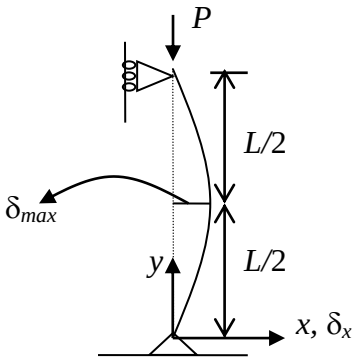

Figure 5–6: Illustration of vertical column with initial out-of-straightness

An initial out-of-straightness is applied to the column. From Figure 5–6, the maximum out-of-straightness, δ_{max}, is located at the mid-length of the column. It is assumed that the column has an initial deflection shape that can be described by a half sine wave. For calculation simplicity, the shape of the initial out-of-straightness along the length at each node can be computed by Eq. 5-4 below. Here, *y* is the height of the node measured from the bottom of the column and *L* is the length of the column. The column section used in the remaining analyses of this chapter is 310UC137 unless a different section is specified.

$$\delta_x(y) = \delta_{\max} \sin\left(\frac{y}{L}\pi\right) \qquad \text{Eq. 5 – 4}$$

5.4 OBTAINING INITIAL RESIDUAL STRESS (IRS) RATIOS

5.4.1 Analysis cases

Three initial out-of-straightness values were studied. They are:

a) $\delta_{max} = L/300000$ – A small out-of-straightness value was used. It is expected that the results from this case would be similar to the first case ($\delta_{max} = 0$);

b) $\delta_{max} = L/1500$ – It is the initial out-of-straightness value that was recommended by SSRC (1985) for the development of design curves for steel columns. It is also the value used to develop the AISC column curves[20];

c) $\delta_{max} = L/1000$ – This is the maximum permissible out-of-straightness value. The development of both SSRC and ECCS multiple column curves was based on this initial out-of-straightness value[20, 25].

d) $\delta_{max} = 0$ – a straight column with no initial out-of-straightness. Only performed for the control case, the linear *IRS* pattern.

In this research, the column curves compared are the Australia/New Zealand column curves which are based on the SSRC curves [1, 23, 25]. For both initial residual stress (IRS) patterns, five initial residual stress ratios were considered. They are γ = 0.0, 0.3, 0.5, 0.7 and 0.9. For other ratios, they could be approximated by linear interpolation. The lengths of the column studied were from 2m to 30m.

5.4.2 Method for obtaining critical forces of column with no initial deflection

In general, OpenSEES is able to capture the buckling loads automatically if an initial out-of-straightness is applied to the column. This is because the analysis is able to terminate when the buckling force is reached. On the contrary, if there is no initial out-of-straightness such as the first case, the analysis can only be terminated until the maximum sectional compressive strength is reached. However, some irregularities occur during this loading at the critical frame.

The way to obtain the buckling force for a perfectly straight column is to approximate it visually from the curve of the applied axial force versus the deflection at the central column. The buckling force seems to be the smallest force that causes a relative large deflection at the central of the column. For example, the axial force-lateral displacement curve, as shown in Figure 5–7, is for the column having the initial residual stress ratio of 0.0 and the column length of 14m. For this case, only one force, 3320kN, can cause a relatively large deflection at centre of the column. Also, this force is very close to the Euler buckling force which is 3278.12kN (difference is about 1.28%). Therefore, this force is considered to be the buckling force for this specific column length and the *IRS*.

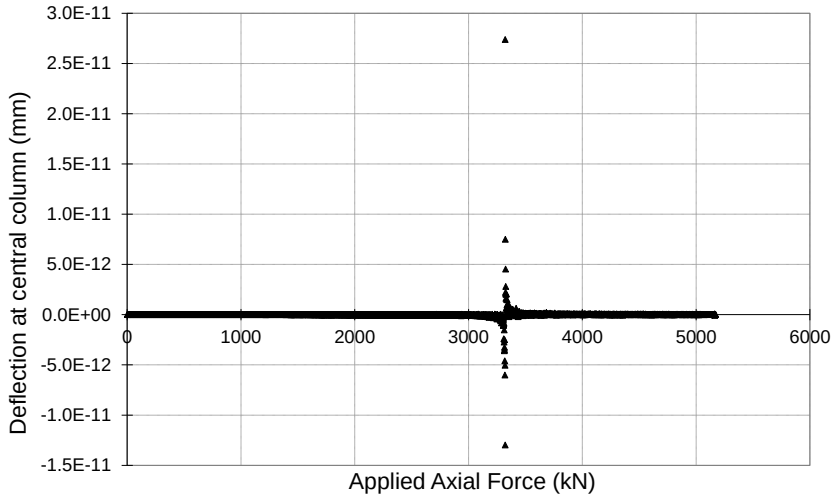

Figure 5–7: Curve of the applied axial force versus the displacement

5.4.3 Comparisons of the magnitudes of the initial out-of-straightness

Figure 5–8 (linear *IRS* pattern) and Figure 5–9 (constant *IRS* pattern**)** present the comparison of the effect of the initial out-of-straightness values for the five initial residual stress ratios. It should be noted that the lengths of the column are converted to

the slenderness ratios by using Eq. 5-5[1] where r is the radius of gyration of the about the axis considered and k_f is the form factor. For the section used in this comparison, 310UC137, the radius of gyration about the strong axis is 137mm and the form factor is 1 since the section used is assumed to be the hot-rolled section[1]. In addition, the maximum axial compressive forces, N^*, are also normalised with the maximum sectional compressive strength, N_s.

$$\lambda_n = \frac{L}{r}\sqrt{k_f}\sqrt{\frac{f_y}{250}} \qquad \text{Eq. 5 – 5}$$

Figure 5–8 shows that the compressive axial forces generally decrease as the initial out-of-straightness increases. For the linear *IRS* pattern in Figure 5–1, the most affected range is the slenderness ratios of less than 200. When the slenderness ratio is above 200, the magnitudes of the effect of the initial out-of-straightness become insignificant. Comparing the results from the five initial residual stress ratios, it can be seen that the degree of effectiveness of the initial out-of-straightness is reduced with increasing initial residual stress ratio. The first case, $\delta_{max} = 0$, and the second case, $\delta_{max} = L/300000$, are almost identical for $\gamma = 0.0$ to 0.5. For $\gamma = 0.7$ and 0.9, the results of $\delta_{max} = L/300000$ are slightly larger than the results of $\delta_{max} = 0.0$. The differences are most likely due to the uncertainties of determining the buckling forces from the figures of the first case. However, the differences between these two cases are small enough to be neglected. Therefore, the results from the second case be used to represent the first case.

For the constant *IRS* pattern in Figure 5–2, the column curves are shown in Figure 5–9. These have the same behaviour as those by the linear *IRS* model in that the buckling forces decrease with the value of the initial out-of-straightness increase. However, a sudden reduction in forces was observed for $\gamma = 0.5$ at $\lambda_n \approx 75$ and $\gamma = 0.7$ at $\lambda_n \approx 100$. Moreover, for $\gamma = 0.9$, $\delta_{max} = L/300000$ has the lowest strengths for λ_n between approximately 80 and 175. This is because the initial residual stresses are constant. Hence, there is a higher chance for a sudden change in the column strength. Another observation that can be seen is that the difference between the $\delta_{max} = L/1500$ and $\delta_{max} = L/1000$ is smaller for the constant case than the difference from linear model.

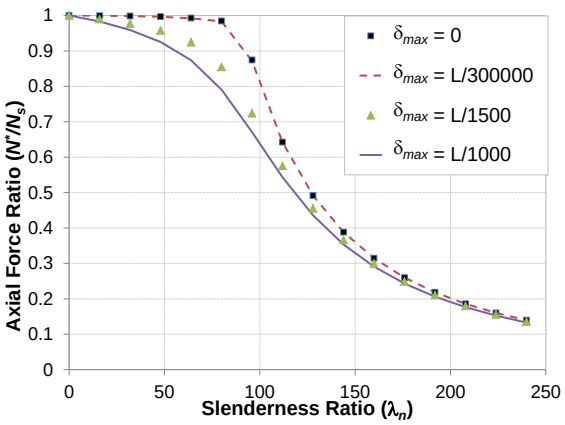

a) γ = 0.0

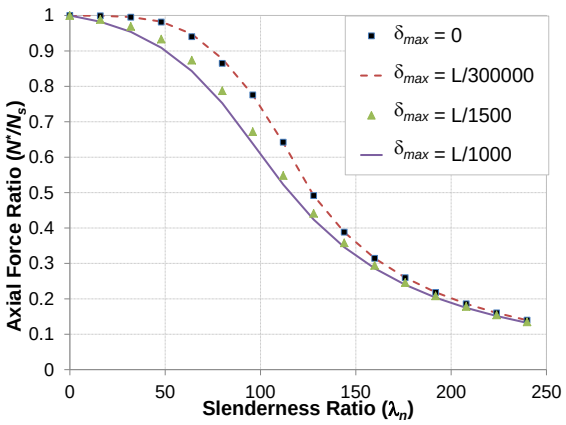

b) γ = 0.3

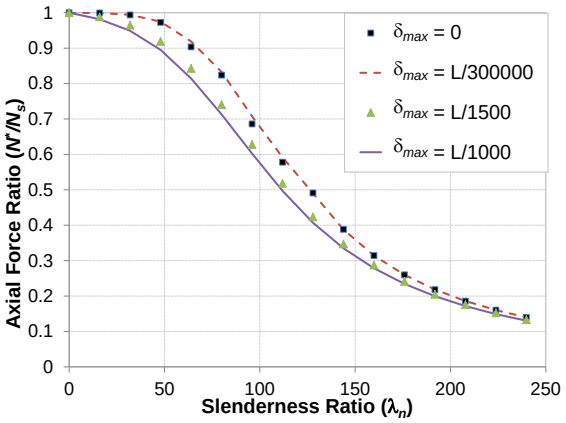

c) γ = 0.5

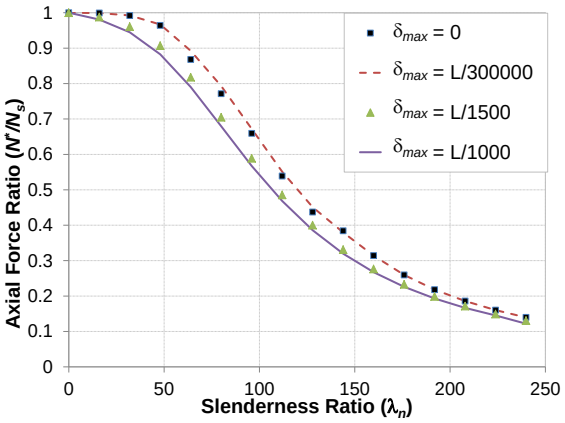

d) γ = 0.7

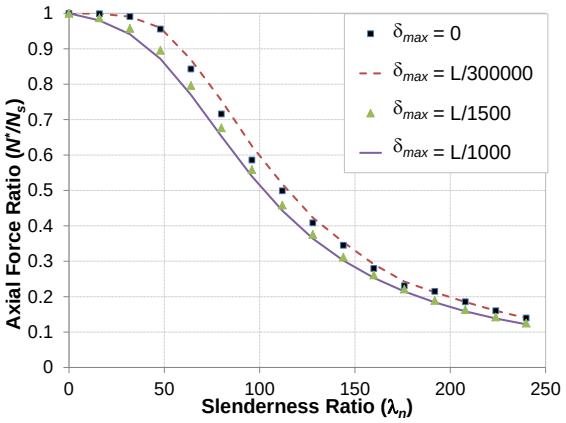

e) γ = 0.9

Figure 5–8: Comparisons of magnitude of initial out-of-straightness for linear *IRS* pattern

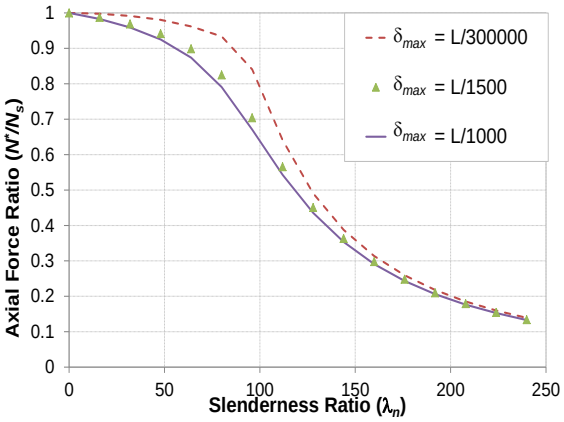

a) γ = 0.0

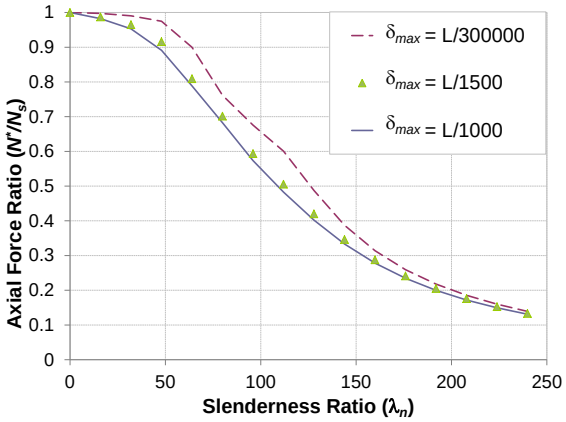

b) γ = 0.3

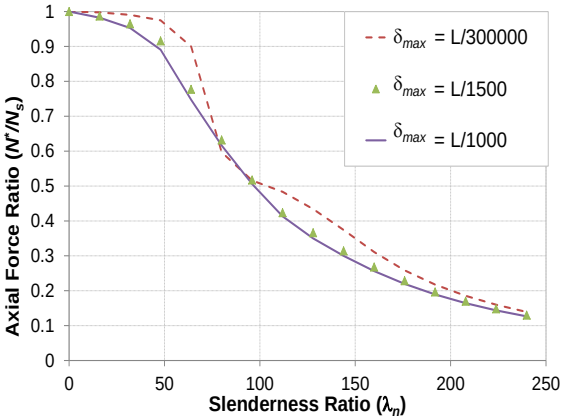

c) γ = 0.5

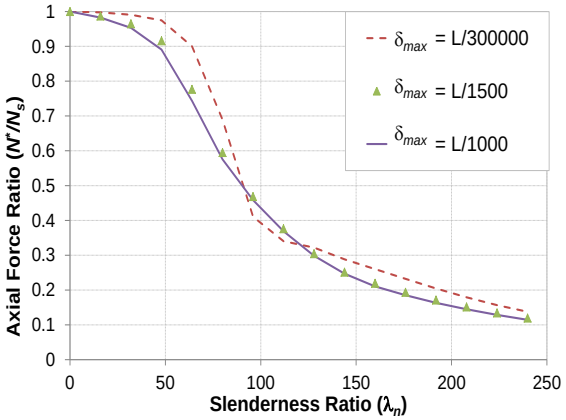

d) γ = 0.7

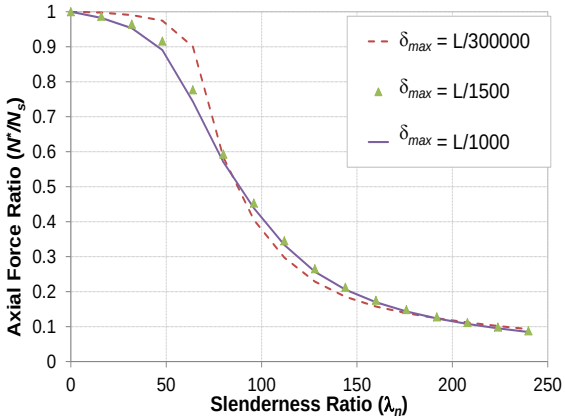

e) γ = 0.9

Figure 5–9: Comparisons of magnitude of initial out-of-straightness for constant *IRS* pattern

5.4.4 Matching with the column curves

5.4.4.1 Linear *IRS* pattern (control case)

Figure 5–10 to Figure 5–13 show the column curves from NZS3404[1] and the critical buckling forces, the Euler buckling capacity. These results are also expressed in the slenderness ratios, λ_n from Eq. 5-4 and the axial force ratios which have described in the previous section.

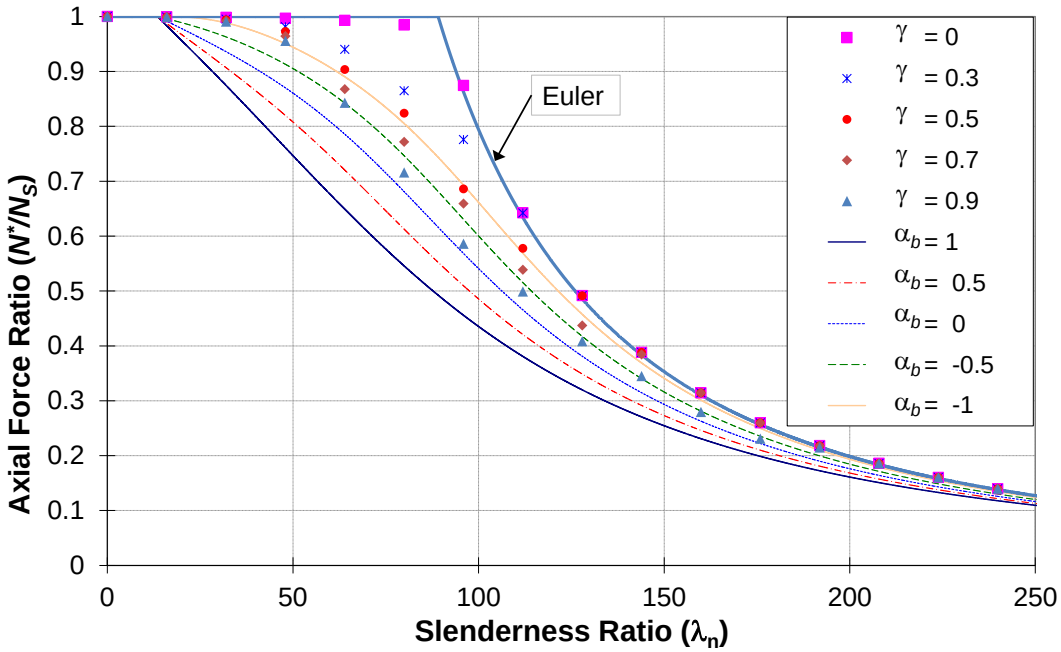

Figure 5–10: Column curves for linear *IRS*, $\delta_{max} = 0$

Figure 5–10 shows that the case of $\gamma = 0.0$ is identical to the Euler curve. For the other four cases, the buckling forces would be equal to the values of the Euler loads after the slenderness ratios are higher than approximately 110, 125, 145 and 190 for $\gamma = 0.3$, 0.5, 0.7 and 0.9 respectively. For $\alpha_b = -1$, until $\lambda_n \geq 145$, it lies between $\gamma = 0.5$ and 0.7 but it tends to be closer to $\gamma = 0.5$. For $\alpha_b = -0.5$, it lies between $\gamma = 0.7$ and 0.9 until $\lambda_n \geq 130$. It then lies on the curve of $\gamma = 0.9$ for λ between 130 and 190. For $\alpha_b = 0$, the closest point that can be identified is on the line of $\gamma = 0.9$ at $\lambda_n = 112$. For both $\alpha_b = 0.5$ and 1, no initial residual stress ratio can be assigned.

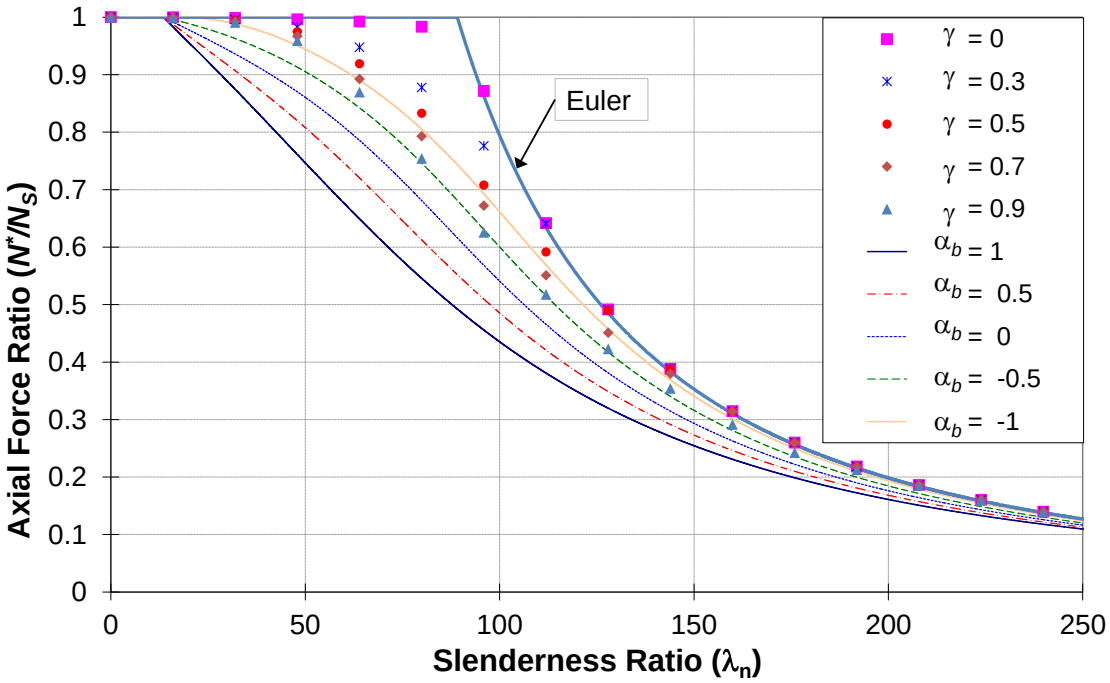

Figure 5–11: Column curves for linear *IRS*, $\delta_{max} = L/300000$

As mentioned in the previous section, the results of the second case, $\delta_{max} = L/300000$, and the first case, $\delta_{max} = 0$, are very similar except for $\gamma = 0.7$ and 0.9 where the results of $\delta_{max} = L/300000$ are slightly larger than the results of $\delta_{max} = 0.0$. Therefore, in the second case as shown in Figure 5–11, the column curve of $\alpha_b = -1$ now lies between $\gamma = 0.6$ and 0.7. Moreover, there are a few points where both the column curve of $\alpha_b = -1$ and the curve of $\gamma = 0.7$ have the same axial force ratios such as at $\lambda_n = 112$. It is most likely, for $\alpha_b = -0.5$, to be matched with $\gamma = 0.9$. Since the results of $\gamma = 0.9$, for $\lambda \geq 95$, are all laid on the column curve of $\alpha_b = -0.5$. For $\alpha_b = 0$ to 1, there is no initial residual ratio that could match them.

Based on the first and second cases, the initial residual stress ratios can only be assigned to column curves of $\alpha_b = -1$ and -0.5 which are approximately 0.6 for $\alpha_b = -1$ and 0.8 for $\alpha_b = -0.5$.

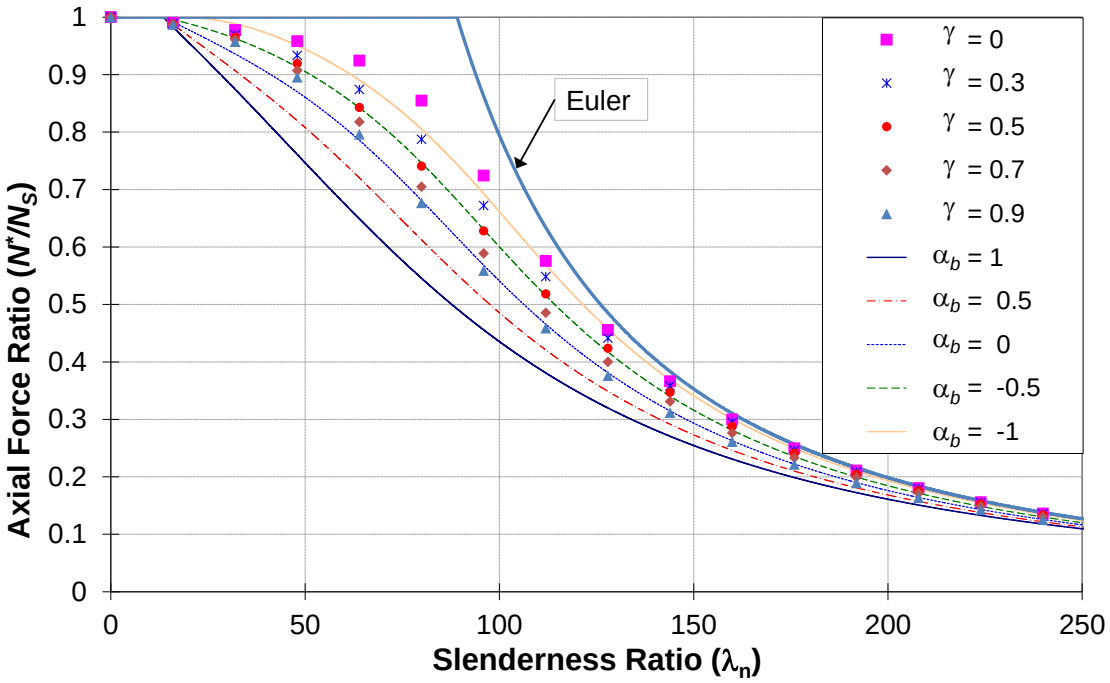

Figure 5–12: Column curves for linear *IRS*, $\delta_{max} = L/1500$

According to the observations from the previous section, the axial force ratios of the third case, $\delta_{max} = L/1500$, is much lower than that of the first two cases. From Figure 5–12, for slenderness ratios between 50 and 100, the column curve of $\alpha_b = -1$ is lying between $\gamma = 0.0$ and 0.3. From $\lambda_n \geq 100$ onwards, it is then matched to the results of $\gamma = 0.0$. For $\alpha_b = -0.5$, the figure shows that this column curve has the same value as the values of $\gamma = 0.5$ from OpenSEES. Considering the column curve of $\alpha_b = 0$, for $\lambda_n \leq 65$, the axial force ratios of this column curve are lower than the values of the studied initial residual ratios, γ. On the other hand, for $\lambda_n > 65$, the column curve is lying between $\gamma = 0.7$ and 0.9 but it is closer to $\gamma = 0.9$ than to 0.7. For $\alpha_b = 0.5$ and 1, no suitable initial residual stress ratios can be identified from the figure.

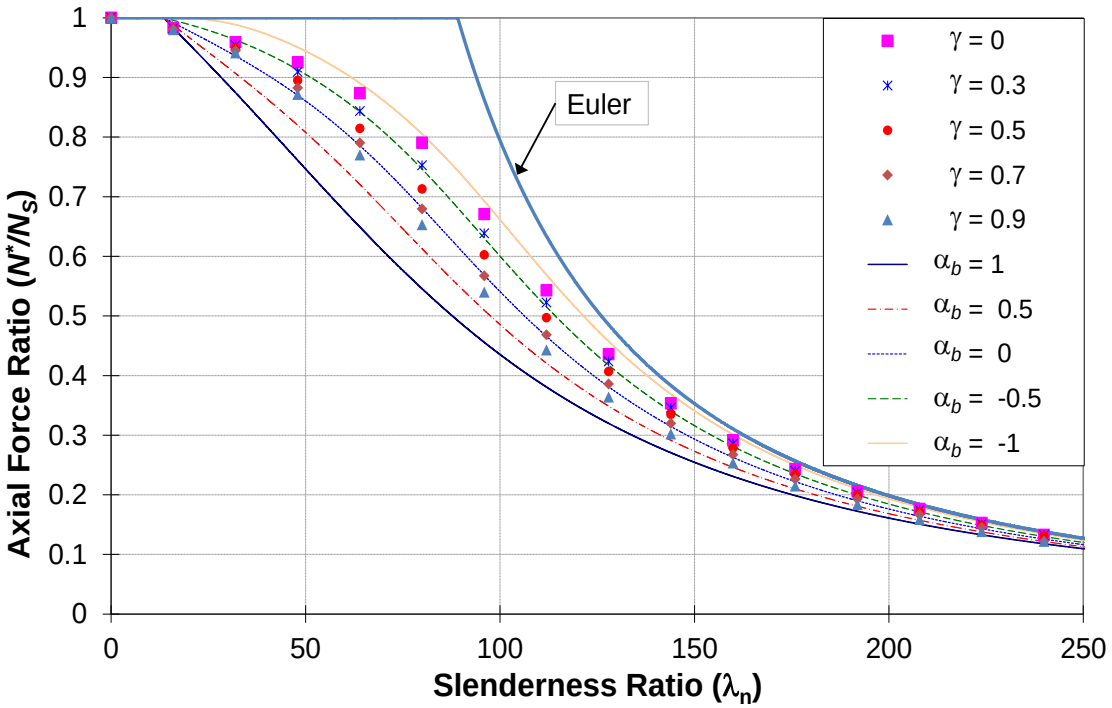

Figure 5–13: Column curves for linear *IRS*, $\delta_{max} = L/1000$

The axial force ratios for the last case, $\delta_{max} = L/1000$, are slightly lower than all the three previous three cases since the curves from OpenSEES are all bounded between the column curves of α_b = -1 and 1 as seen in Figure 5–13. The distributions of the results can be generally categorised into three sections which are $\lambda_n \leq 50$, $50 < \lambda_n \leq 175$ and $\lambda_n > 175$. For $\lambda_n \leq 50$, the results from OpenSEES for all initial residual stress ratios are mostly squeezed between the column curves of α_b = -0.5 and 0. For slenderness ratios between 50 and 175, the results are distributed over the first four column curves, α_b = -1 to 0.5. For the rest of the slenderness ratios, they are bounded between α_b = -1 and 1. From the figure, the closest initial residual stress ratios that would match the column curves of α_b = -1, -0.5 and 0 are γ = 0.0, 0.3 and 0.7 respectively. For α_b = 1, no clear ratio can be assigned to it unless a higher initial residual stress ratio is used.

5.4.4.2 Results from the constant *IRS* pattern

From Figure 5–14, all of the initial cases, i.e. $\lambda_n \leq 50$, are almost identical to the Euler curve. For $\gamma = 0.0$, the results are generally similar to the Euler curve. The only difference observed is for λ_n between 50 and 80. It is most likely due to the effect of the gradually yielding of the fibres. For all the other four cases, no general trend can be found. Also, the buckling forces of $\gamma = 0.5$ for $\lambda_n \approx 80$ is less than the buckling forces of $\gamma = 0.7$.

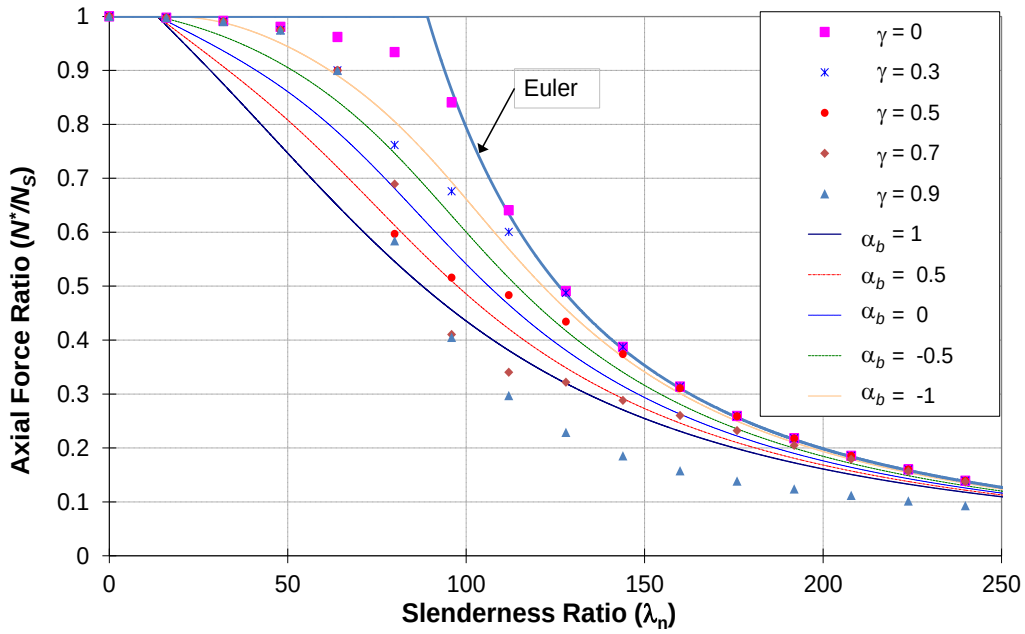

Figure 5–14: Column curves for constant *IRS*, $\delta_{max} = L/300000$

Figure 5–15 shows the results for $\delta_{max} = L/1500$. For this case, the $\gamma = 0.0$ case can be matched with the column curve of $\alpha_b = -1$. For $\gamma = 0.3$, it is initially matched to the $\alpha_b = -0.5$. However, for λ_n between 60 and 100, it is closer to $\alpha_b = 0$. For $\gamma = 0.5$, it is on the $\alpha_b = -0.5$ for $\lambda_n \leq 50$. It then moves to $\alpha_b = 0.5$ when λ_n is approximately between 75 and 125. For the rest of the $\gamma = 0.5$ ($\lambda_n > 125$), it lies between $\alpha_b = 0$ and 0.5. Both $\gamma = 0.7$ and 0.9 have very similar results up to $\lambda_n \approx 100$. After $\lambda_n = 100$, the curve of $\gamma = 0.7$ lies on $\alpha_b = 1$. However, $\gamma = 0.9$ gives lower strengths then the strengths of $\alpha_b = 1$.

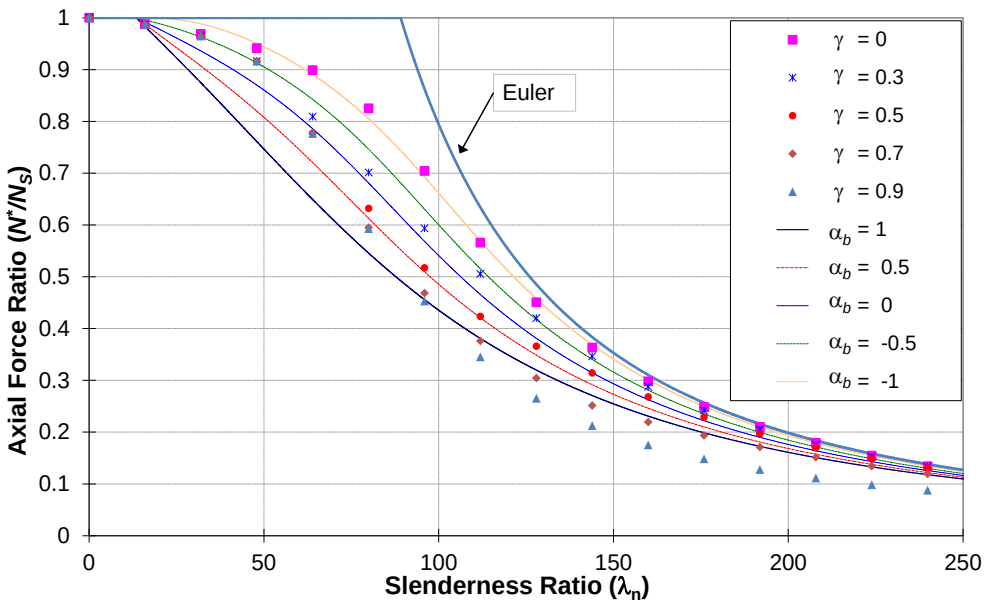

Figure 5–15: Column curves for constant *IRS*, $\delta_{max} = L/1500$

The results of $\delta_{max} = L/1000$, as given in Figure 5–16, are similar to $\delta_{max} = L/1500$. However, the strengths of this case are slightly lower than $\delta_{max} = L/1500$ for all five γ values since a larger initial out-of-straightness is used. For this case, $\gamma = 0.0$ lies between $\alpha_b = -1$ and -0.5 but it is close to $\alpha_b = -1$ when $\lambda_n \leq 100$. For $\gamma = 0.3$, it is on $\alpha_b = 0$ for λ_n is between 50 and 125 but close or on $\alpha_b = -0.5$ for the rest of the slenderness ratios. For $\gamma = 0.5$ and 0.7, they are mostly are on $\alpha_b = 0.5$ and 1 respectively.

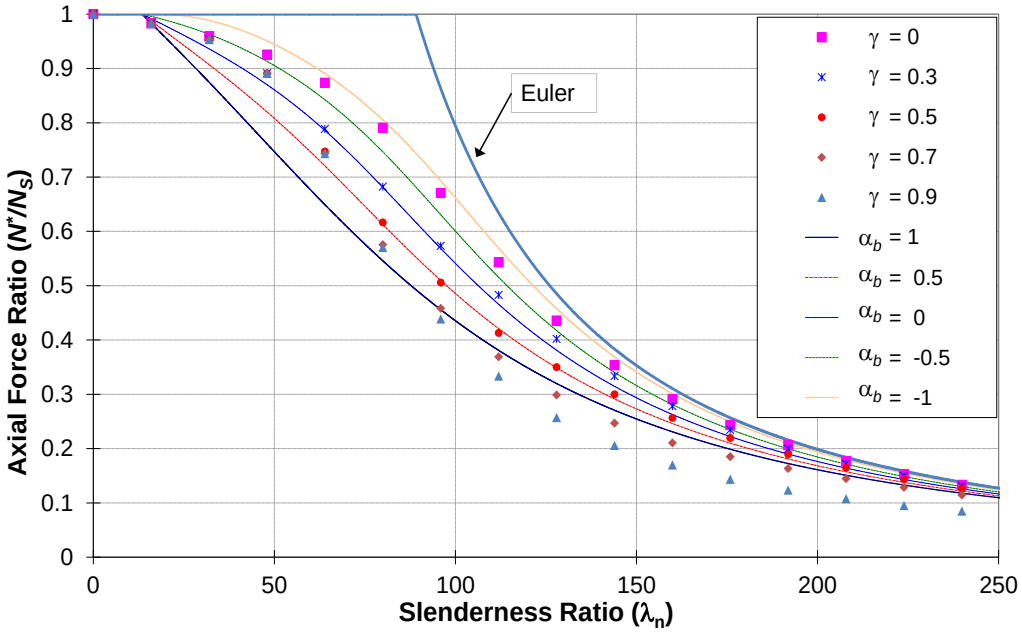

Figure 5–16: Column curves for constant *IRS*, $\delta_{max} = L/1000$

5.4.5 Discussions of initial residual stress (IRS) ratios and column curves

Table 5–11 and Table 5–12 relate the initial residual stress ratios to the column curves for both linear and constant *IRS* patterns for intermediate slenderness ratios between 50 and 200. Outside these ranges, the results may vary.

Table 5–11: Summary of *IRS* ratios to column curves (Linear)

α_b	**γ (Linear)**			
	$\delta_{max} = 0$	$\delta_{max} = L/300000$	$\delta_{max} = L/1500$	$\delta_{max} = L/1000$
-1	0.5	0.7	0.3	0.0
-0.5	0.75	0.9	0.5	0.3
0	0.9	-	0.9	0.7
0.5	-	-	-	0.9
1	-	-	-	-

From the results of the control case, linear pattern, it clearly shows that the results are unlikely to produce a complete matching of the column curves even though the maximum permissible initial out-of-straightness value, $\delta_{max} = L/1000$, was used. Some of the values appear to be unrealistic i.e. $\gamma = 0.0$ and 0.9. Here, $\gamma = 0.0$ corresponds to the section with zero initial stress. Therefore, it means the column response is affected by the second order effect with the out-of-straightness. Note that, $\gamma = 0.9$ is a very high value for a hot-rolled I-section with the linear initial residual stress distribution.

Table 5–12: Summary of *IRS* ratios to column curves (Constant)

α_b	**γ (Constant)**		
	$\delta_{max} = L/300000$	$\delta_{max} = L/1500$	$\delta_{max} = L/1000$
-1	Unable to define a proper value due to fluctuating results	0.0	0.0
-0.5		0.2/0.3	0.1
0		0.4	0.3
0.5		0.5/0.6	0.5
1		0.7	0.6/0.7

For the constant pattern, a set of approximated ratios can be found for $\delta_{max} = L/1500$ and $L/1000$. Nevertheless, for $\delta_{max} = L/30000$, there is no distinct values of the *IRS* ratios for each column curves due to the sudden reduction in forces. However, the results tend to be unrealistic or underestimated even though a complete set of values can be found from the

constant case. This is because it is unlikely for any kind of steel sections to have such a constant *IRS* distribution.

The linear distribution cannot represent the behaviour of the column with large positive α_b possibly due to the following reasons:

- The types of the initial residual stress distribution – The results obtained above were only considered with the distribution for the hot-rolled I-section. However, the column curves in the standard are for many different types of sections, manufacturing processes including welded, hollow sections, cold-form steel and etc. Hence, it means that each section would have its particular initial residual stress distribution [1,14]. For example, Figure 44 in Bjorhovde Ph.D thesis[22] illustrates a distribution for a welded wide flange shape used in developing the SSRC curve by the probabilistic method as given in Section 2.5.
- The forces obtained from OpenSEES were program terminations which occur as a result of zero stiffness. Several fibres may have yielded before this occurs. However, the Australian/New Zealand column curves were developed based on the multiple column concept and an assumption of the first yield of a geometrically imperfect member as described earlier in Section 2.5 [21]. This may be the reason why the results from OpenSEES are higher than those values from the column curves as shown in Figure 5–8 to Figure 5–13.
- The through-thickness initial residual stresses were neglected.
- The column section chosen may not be the most appropriate.

Based on the results, the true results are possibly between the values of both cases since the constant *IRS* distribution is an extreme pattern for a section. In general, for a linear distribution, initial residual stress ratios of 0.3 and 0.5 are generally used for hot-rolled sections as suggested by the ECCS *IRS* distribution [14, 23, 24].

5.5 SUMMARY OF INITIAL RESIDUAL STRESS RATIO

The results from the verification process and the sensitivity studies show that the configurations used in OpenSEES for this research are able to accurately consider the second order effects and to produce accurate results.

Based on the results of the simply supported column, a constant set of values of the initial residual stress ratios, matching with the five column curves, are unable to be obtained for all slenderness. To be able to continue this work, reasonable initial residual stress ratio values, i.e. 0.0 and 0.5, are going to be used in the latter tasks. This is consistent with previous studies and it roughly correspond to a column with an initial residual stress categories of α_b = -1 and 0.

6 DESCRIPTIONS OF THE MODEL CONFIGURATIONS

This chapter describes the configurations of the two models used in Chapter 7 and 8 to evaluate the effect of the initial residual stresses under the static and dynamic loadings. The dimension of the model, section size used, loading condition, mass and the period of the structures are clearly defined here.

6.1.1 A single cantilever column

Figure 6–1 shows a simple cantilever column subjected to an axial compression force, N^*, and a lateral force, H at top of the column. The height of the column is denoted by h in the figure. This simple model is considered as a single degree of freedom system and used as a benchmark model for evaluating the responses of the structure subjected to wind loads and for considering the effect of the initial residual stresses. The OpenSEES inputs are given in Appendix C4.

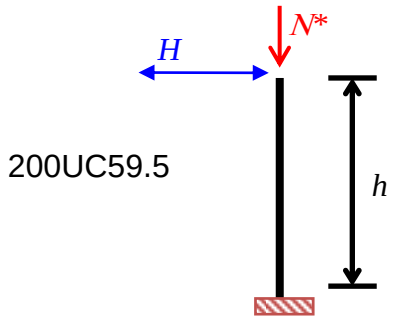

Figure 6–1: Single degree of freedom system structure

The I-section used for this model is 200UC59.5.The detailed section property is given in Table 6–1 in Section 6.1.2 later. It is a compact section which is able to reach its plastic flexural strength. The material yielded strength, f_y, is 300MPa and the material elastic modulus, E, is 200GPa. The detailed setting of the material for OpenSEES is given in section 5.1.3. The property of the section was obtained directly from OneSteel steel section catalogue [17]. The section axial compression capacity, N_s, is 2286kN according to the OneSteel table (A = 7620mm^2). This value may be higher than the value computed from the analysis programme because the area calculated in OpenSEE is based on the ideal rectangular dimensions of the flanges and the web (A = 7511mm^2). The cantilever column has 8 sub-elements for all the analyses performed in the later studies.

For the inelastic time-history analysis performed in Chapter 7, the mass of this cantilever column, as for a single degree of freedom system, is located on the top of the column. The value of the mass is 5099kg in the horizontal direction for all the initial residual stresses and the axial compressive force cases. This value is specifically used to make the structural period of the column to be 0.5s with the axial compressive force, $N^* = 0.355N_s$ and no initial residual stress, $\gamma = 0.0$ case. It should be noted that the structural period is calculated based on the column property after the gravity analysis has been performed.

For the initial residual stress (IRS) pattern, the linear *IRS* pattern as described in Section 5.1.2.1 is used for all the analyses performed in the later sections.

6.1.2 A low-rise three-story steel frame

Figure 6–2 shows a single-bay three storey steel moment-resisting frame. The frame has the storey height, *h*, of 3.05m and the width of 4.6m. Each column is subjected to an axial compressive force, N^*_c, of 450kN. A uniform distributed load (UDL) of 30kN/m is applied to each beam. However, because OpenSEES is unable to apply a *UDL* directly to model, the *UDL* is separated into a number of the point loads, N^*_b, applied at the nodes as shown in the figure. In this case, N^*_b is 9.2kN since there are 15 nodes along the clear length of the beam. The lateral force, *H*, is applied at left hand side of the frame at each level. For the roof, only half of the lateral force is applied. The OpenSEES inputs are given in Appendix C5.

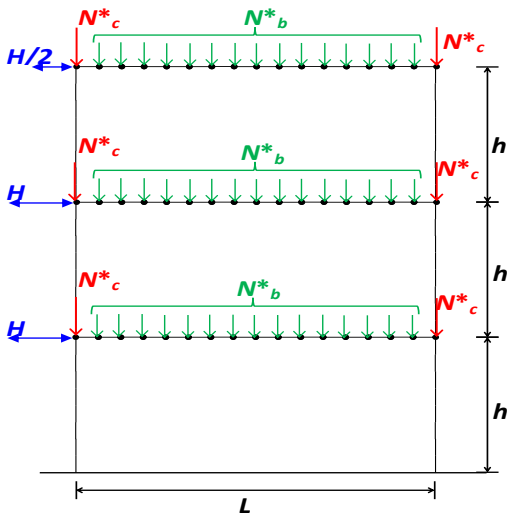

Figure 6–2: A low-rise three story steel moment-resisting frame

The sections used are 460UB67.1 and 200UC59.5 for the beams and columns respectively. Table 6–1 presents the section properties. It should be noted that the area, A_g, and the plastic section modulus, S_x, are the constant values and they are smaller than the values specified in the Onesteel catalogue[17]. Here, N_s is the sectional axial compressive capacity. Both sections are a compact so they can reach their plastic flexural strength. The material yielded strength, f_y, is 300MPa and the material elastic modulus, E, is 200GPa. For analysis accuracy, each column is divided into 8 sub-elements and each beam is divided into 16 sub-elements. For the initial residual stresses in the sections, for simplicity, both the columns and the beams have the same initial residual stress ratios. The setting of the material for OpenSEES is given in section 5.1.3. The linear *IRS* pattern as described in Section 5.1.2.1 is used for all the analyses performed in the later sections such as monotonic, push-pull and inelastic time-history analysis.

Table 6–1: Section properties for the three storey steel frame

Section	d (mm)	b_f (mm)	t_f (mm)	t_w (mm)	A_g (mm^2)	S_x (mm^3)	N_s (kN)
460UB67.1	454	190	12.7	8.5	8469.1	$1455.22e^3$	2540.73
200UC59.5	210	205	14.2	9.3	7511	$646.65e^3$	2253.3

For this low-rise steel frame, the mass of each floor is assumed to be concentrated on the top of the column at each storey. A full amount of the mass is applied to the columns at the first and second storey. For the roof level, only half of the full mass is used. The value of a full mass is 6747kg. Hence, the total mass of the frame is 33737kg. The structural period of the frame is 0.56s based on the case of $\gamma = 0.0$. As with the cantilever column model, this structural period is calculated with the structural property after the gravity analysis is conducted.

7 INITIAL RESIDUAL STRESS EFFECTS ON MONOTONIC AND CYCLIC BEHAVIOUR

The following chapter evaluates the effects of the initial residual stresses on the static responses of a single cantilever column and a single-bay three-storey frame. The pushover (monotonic loading) push-pull (cyclic) analyses were conducted for each model.

7.1 DESCRIPTIONS OF ANALYSIS METHODOLOGY

7.1.1 Pushover analysis (static monotonic loading)

The purpose of the pushover analysis is to observe the responses of the frames under the monotonic loading and obtain the maximum yielding displacements. This analysis consists of two parts, the gravity and the pushover analysis. The gravity analysis was firstly performed to take into account of the applied gravity force. It was followed by the pushover analysis to determine the lateral load capacity. The pushover analysis was carried out with the reduced sectional properties which were reduced by the gravity loadings. The OpenSEES codes are presented in Appendix C6.

Both analyses were conducted based on the load control integrator, using the incremental load ratio of 0.001. For the gravity analysis, there was 1000 load steps. For the pushover analysis, the analysis was terminated automatically when the maximum lateral strength was reached. The analysis configurations for both analyses are given in Table 5–3, which is same as the control case.

7.1.2 Push-Pull analysis (static cyclic loading)

Similar to the pushover analysis, the gravity force was performed before the cyclic loading was applied. The gravity analysis used the same configurations and settings as the control case given in Table 5–3. The OpenSEES codes are given in Appendix C7.

Unlike the gravity analysis, the push-pull analysis was performed with the displacement control integrator. The controlled displacement applied to the top node of the model or top left hand corner of a frame. The applied displacement, as illustrated in Figure 7–1, consists of two cycles of the maximum displacement, Δ_{max}, which was obtained from the pushover analysis that are given specifically later in Sections 7.2.1.1 (column) and 7.3.1

(frame). It was then followed by one cycle of each $1.25\Delta_{max}$, $1.5\Delta_{max}$ and $1.75\Delta_{max}$ and it was ended with two cycles of $2\Delta_{max}$.

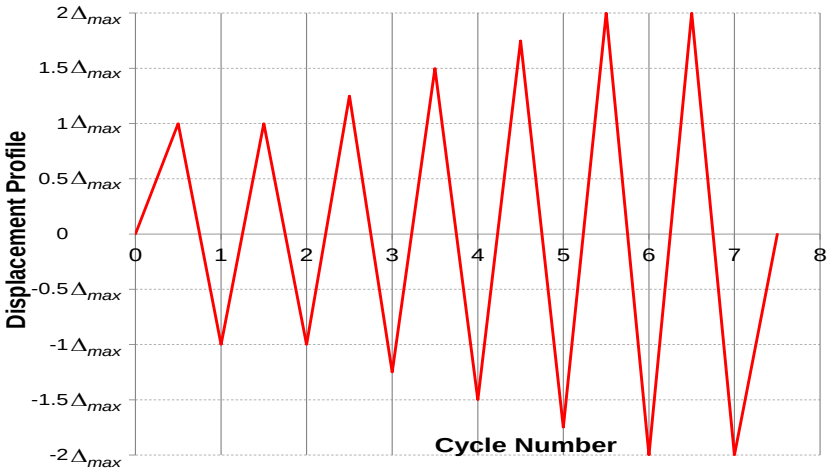

Figure 7–1: Applied displacement profile for push-pull analysis

7.2 RESPONSES OF A SINGLE CANTILEVER COLUMN

7.2.1 Responses of the column under monotonic loading

7.2.1.1 Benchmark case - Column height, h = 3.2m

Figure 7–2 to Figure 7–5 present the force-displacement relationship of the monotonic responses for the four compressive axial force cases, N^* = 0.0 (benchmark case), $0.355N_s$, $0.5N_s$ and $0.7N_s$. In each figure, two initial residual stresses (IRS) ratios, γ = 0.0 and 0.5, are compared. Here, the *IRS* pattern used for all the analysis, as indicated in Chapter 6, is the linear *IRS* pattern described in Section 5.1.1.1.

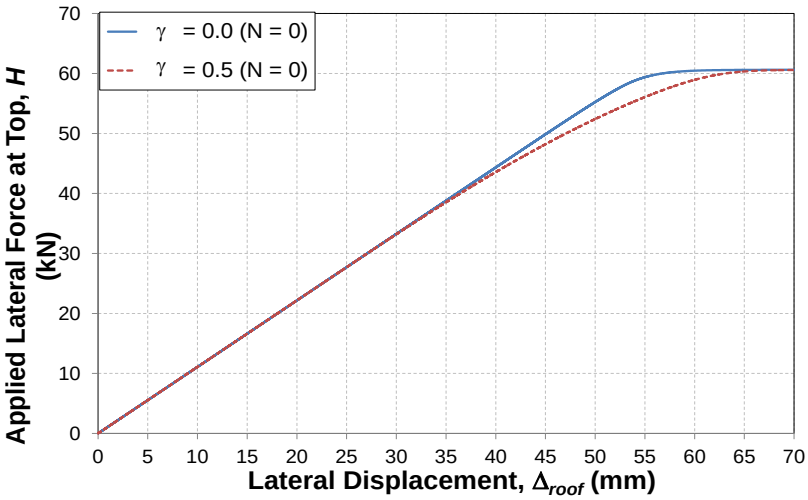

Figure 7–2: Response of the 3.2m cantilever column with N^*/N_s = 0

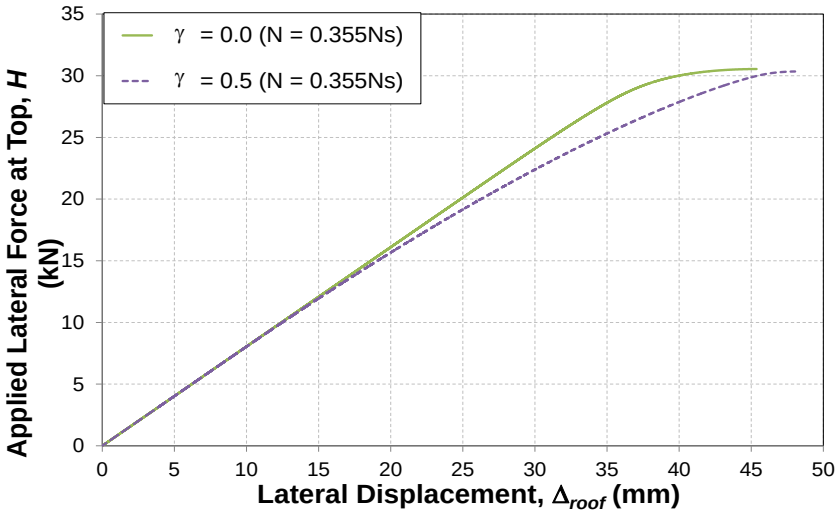

Figure 7–3: Response of the 3.2m cantilever column with $N^*/N_s = 0.355$

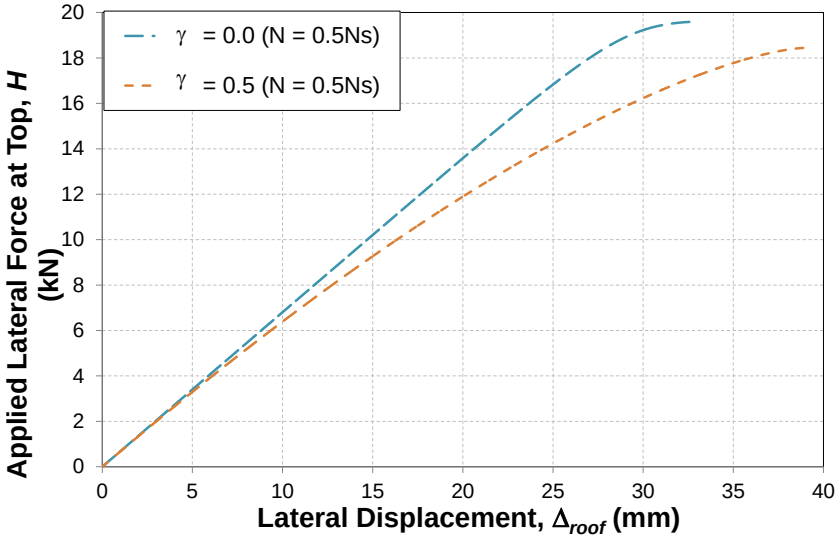

Figure 7–4: Response of the 3.2m cantilever column with $N^*/N_s = 0.5$

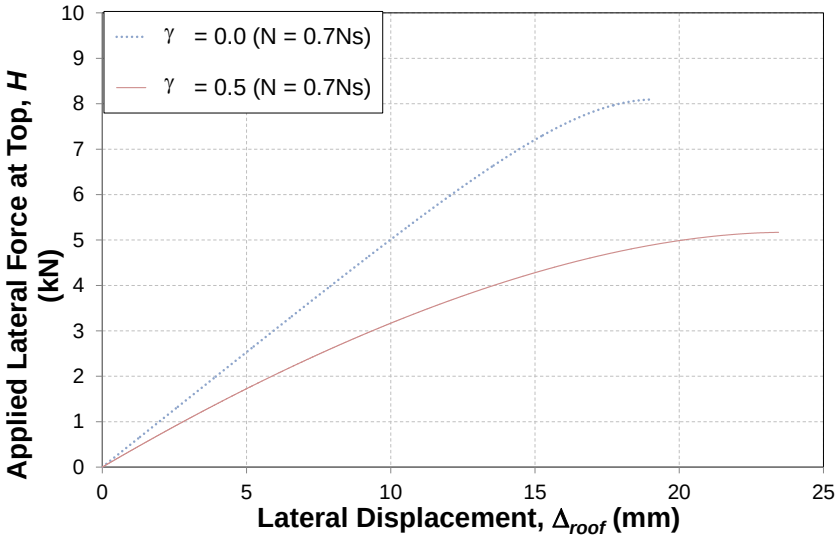

Figure 7–5: Response of the 3.2m cantilever column with $N^*/N_s = 0.7$

Table 7–1 gives summary of the maximum lateral applied force (H_{max}), corresponding lateral displacement (Δ_{max}) and the secant stiffness (K_s). Here, the structure stiffness, as computed by Eq. 7-1, is the secant stiffness measuring between the origin and the point equal to 90% of the maximum applied lateral force, H_{max}, and its corresponding displacement, $\delta_{0.9Hmax}$ as illustrated in Figure 7–6.

Table 7–1: Summary of the results of monotonic loading for a 3.2m cantilever column

	γ = 0.0				γ = 0.5			
N^*/N_s	0	0.355	0.5	0.7	0	0.355	0.5	0.7
H_{max} (kN)	60.7	30.6	19.6	8.10	60.7	30.4	18.5	5.17
Δ_{max} (mm)	160	45.4	33.1	19.1	162	48.0	39.1	23.4
K_s (kN/mm)	1.11	0.80	0.67	0.48	1.03	0.70	0.53	0.27

$$K_s = \frac{0.9H_{max}}{\Delta_{0.9H_{max}}} \qquad \text{Eq. 7 – 1}$$

where

H_{max} = Maximum applied lateral force

$\Delta_{0.9Hmax}$ = Corresponding displacement at $0.9H_{max}$

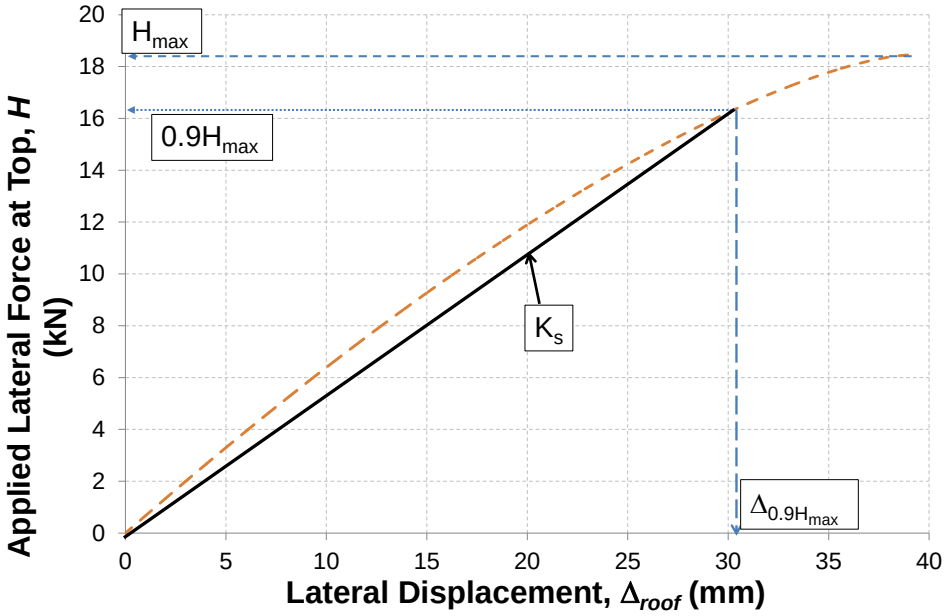

Figure 7–6: Illustration of computing of secant stiffness of structure

The maximum applied lateral force, H_{max}, does not change for γ = 0.0 and 0.5 when N^* = 0. The difference is 0.20kN (0.66% over the γ = 0.0 case) for $N^* = 0.355N_s$. For $N^* = 0.5N_s$ to $0.7N_s$, the differences increase to 1.52kN (7.73%) for $N^* = 0.5N_s$ and 2.93kN (36.2%) for $N^* = 0.7N_s$. Comparing the secant stiffness, K_s, of the structure, the *IRS* effect reduces the stiffness by 7.2%, 12.5%, 20.9% and 43.8% (over the γ = 0.0 case) for N^*/N_s = 0, 0.355, 0.5 and 0.7 respectively.

Based on the responses of the column presented in the above figures, the effect of the initial residual stress, in general, does not influence the responses of the column if $H/H_y < (1 - \gamma - N^*/N_s)$. H_y is the lateral applied force at first yield of fibre in a section, which is computed as the elastic moment strength over the height of the column. For example, the elastic moment of the column used in this study is 175.2kNm. Hence, the lateral applied force at first yield is 54.8kN. By applying the above relationship, the maximum lateral applied force that is unaffected by *IRS* is approximately 7.95kN. It can be confirmed by the overlapping of the two curves in Figure 7–3 when H < 7.95kN.

It can be summarised that the effect of the applied axial force is significant for the maximum lateral strength and the structural stiffness. For γ = 0.0, the maximum lateral force decreases by 50%, 68% and 87% as N^*/N_s changes from 0, 0.355, 0.5 and 0.7 respectively and the structural stiffness is reduced by 27%, 40% and 56%. For γ = 0.5, the reductions of both H_{max} and K_s are even greater because of the *IRS* effect. These reductions of force and stiffness are caused by *P*-delta effect.

Table 7–2 compares the values obtained above and the code method, the alternative and general method given in NZS3404:1997. The equations are given in Appendix D. Here, M_{code} is the maximum allowable member moment capacity by code methods and H_{code} is the lateral force capacity computed by Eq. 7-2. In Eq. 7-2, L is the length of the cantilever column. This method considers both the *P*-delta effect and the *IRS* effect explicitly. The corresponding α_b for the code column curves are -0.5 and 0 for γ = 0.0 and 0.5 respectively. They were estimated directly from Figure 5–13. Here, the positive difference means that the code value is higher than H_{max} given in Table 7–1. Both methods are unconservative and they slightly overestimate the lateral strength, H_{max}, for

moderate axial forces (i.e. N^*/N_s = 0.355 and 0.5) when no *IRS* is accounted for high axial force, the code methods are very conservative.

$$H_{code} = \frac{M_{code}}{L} \qquad \text{Eq. 7 – 2}$$

Table 7–2: Comparison of maximum applied forces by code methods (h = 3.2m) [1]

		γ = 0.0				γ = 0.5			
N^*/N_s		0	0.355	0.5	0.7	0	0.355	0.5	0.7
M (kNm)	Alternative	198	110	72.7	18.0	198	101	60.4	0
	General	194	102	64.2	12.3	194	93.3	52.1	0
H (kN)	Alternative	62.0	34.3	22.7	5.63	62.0	31.7	18.9	0
	General	60.6	31.8	20.1	3.84	60.6	29.2	16.3	0
	Actual	60.7	30.6	19.6	8.10	60.7	30.4	18.5	5.17
Diff (%)	Alternative	2.13	12.2	15.9	-30.5	2.13	4.28	2.05	-100
	General	-0.13	4.05	2.35	-52.6	-0.13	-4.08	-12.0	-100

7.2.1.2 Comparison case - Column height, h = 2.0m

The responses of the 2m column, as shown in Figure 7–7 to Figure 7–10 and summarised in Table 7–3, are very similar to the responses of the 3.2m long column. Here, the differences for H_{max} are 0.02%, 0.32%, 0.89% and 5% for N^* = 0.355N_s, 0.5N_s and 0.7N_s respectively. For K_s, the differences are 6.62%, 9.05%, 14.3% and 27.7% for N^* = 0.355N_s, 0.5N_s and 0.7N_s respectively. The reductions in both H_{max} and K_s between two *IRS* cases are smaller for this case. It is because the *P*-delta effect is less since the column is shorter. As a result, there is also a lower magnitude of the *IRS* effect.

Table 7–3: Summary of the results of monotonic loading for a 2m cantilever column

	γ = 0.0				γ = 0.5			
N^*/N_s	0	0.355	0.5	0.7	0	0.355	0.5	0.7
H_{max} (kN)	97.0	61.6	44.7	24.0	96.98	61.4	44.3	22.8
Δ_{max} (mm)	83.6	20.7	15.2	8.74	84.2	20.6	15.6	10.5
K_s (kN/mm)	4.53	3.98	3.77	3.39	4.23	3.62	3.23	2.45

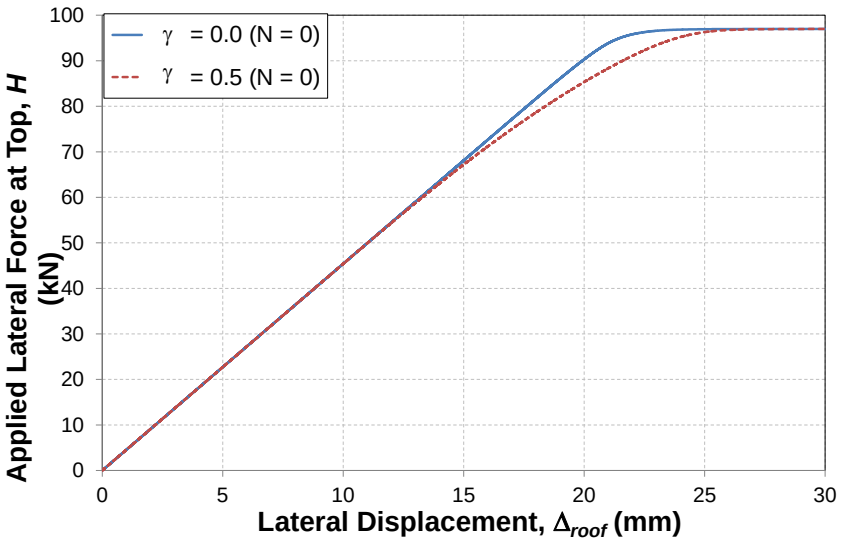

Figure 7–7: Response of the 2m cantilever column with $N^*/N_s = 0$

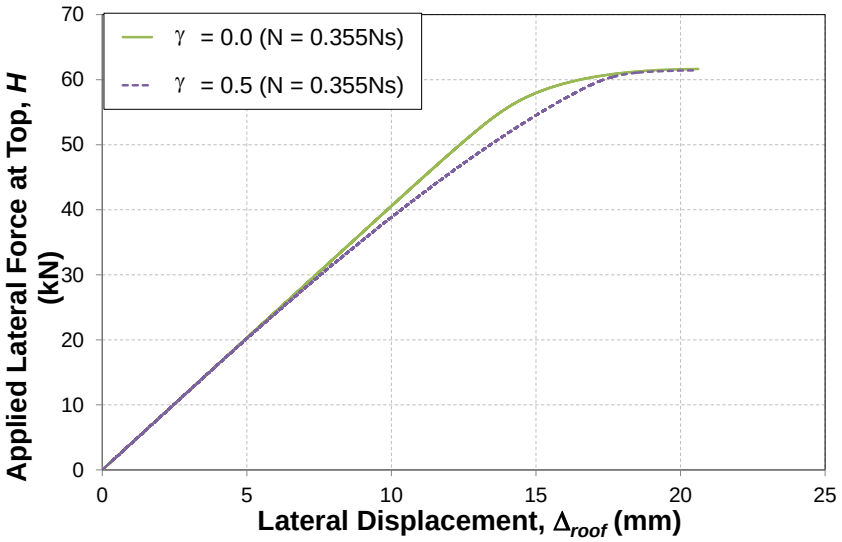

Figure 7–8: Response of the 2m cantilever column with $N^*/N_s = 0.355$

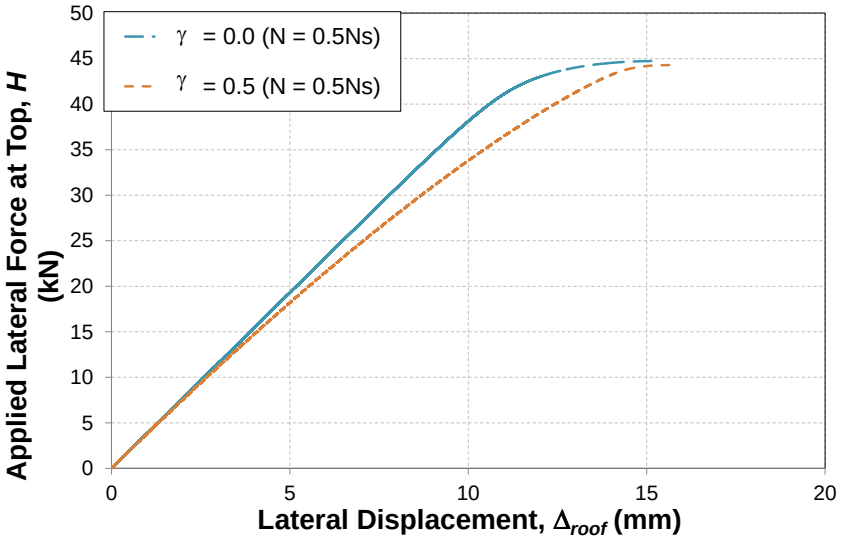

Figure 7–9: Response of the 2m cantilever column with $N^*/N_s = 0.5$

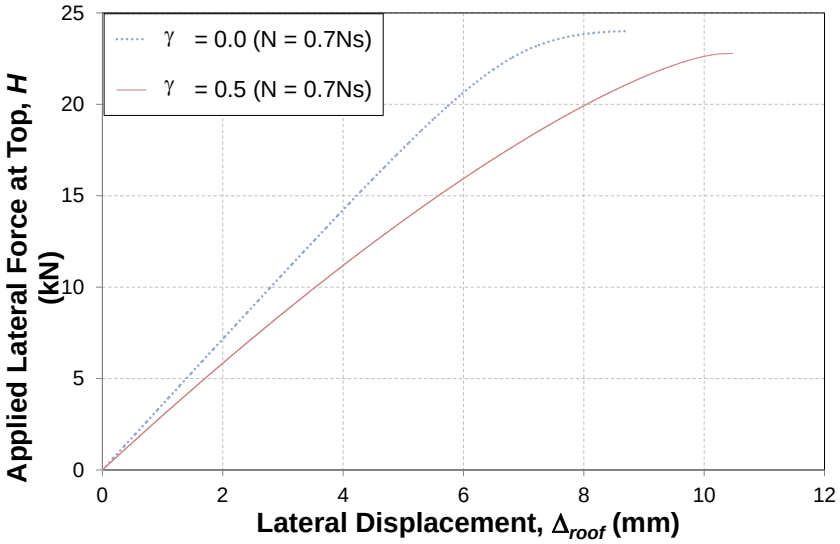

Figure 7–10: Response of the 2m cantilever column with $N^*/N_s = 0.7$

The comparisons, as shown in Table 7–4 between the analysis results and the code methods, alternative and general method, for this case also have the similar responses as the benchmark case, h = 3.2m. The alternative method, in general, overestimated the maximum applied lateral forces. On the contrary, the general method produces accurate results for $N^*/N_s = 0$ and conservative results for the rest of the cases. Here, the difference (Diff) in % is computed by the ratio between each code method and the actual value then minus 1. Here, the negative value means the analysis results are greater than the code methods.

Table 7–4: Comparison of maximum applied forces by code methods (h = 2.0m) [1]

		γ = 0.0				γ = 0.5			
N^*/N_s		0	0.355	0.5	0.7	0	0.355	0.5	0.7
M (kNm)	Alternative	198	124	94.1	50.6	198	121	88.7	42.7
	General	194	117	85.8	42.6	194	113	80.4	34.9
H (kN)	Alternative	99.2	62.4	47.1	25.3	99.2	60.5	44.4	21.3
	General	97.0	58.6	42.9	21.3	97.0	56.8	40.2	17.5
	Actual	97.0	61.6	44.7	24.0	96.98	61.4	44.3	22.8
Diff (%)	Alternative	2.25	1.30	5.28	5.50	2.27	-1.45	0.16	-6.40
	General	0.00	-4.87	-4.00	-11.3	0.02	-7.56	-9.28	-23.5

7.2.2 Response of columns subjected to cyclic loading

7.2.2.1 Sensitivity study for the displacement step size

The maximum displacements, Δ_{max}, used for the push-pull analysis were 45.4mm, 33.1mm and 19.1mm for $N^* = 0.355N_s$, $0.5N_s$ and $0.7N_s$ respectively. They were obtained from Table 7–1. For all of the axial force cases, the displacement step size was $\Delta_{max}/400$. Different to the pushover case, only the benchmark case, h = 3.2m, was considered.

Figure 7–11 a) and b) show the sensitivity study between the step sizes of $\Delta_{max}/400$ and $\Delta_{max}/800$ (half of the previous step size) for $N^* = 0.355N_s$ and $0.7N_s$ of $\gamma = 0.0$ case. The results show that the step size only affects the results between the elastic and the plastic transition for $1.25\Delta_{max}$ to $1.5\Delta_{max}$ and at the first failure point where there is a jump in the force-displacement response. However, the differences are generally small enough (< 5%) and can be neglected.

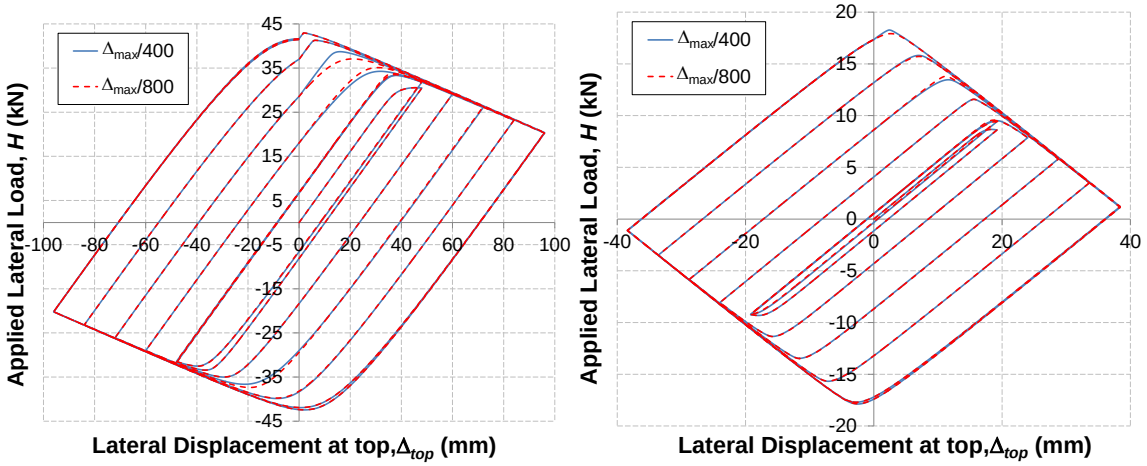

a) $N^* = 0.355N_s$ b) $N^* = 0.7N_s$

Figure 7–11: Sensitivity study for push-pull analysis for $\gamma = 0.0$ of Model 1

7.2.2.2 Effect of axial force and initial residual stresses

Figure 7–12 a) to c) present the results of the force-displacement response for all three axial force cases. The results generally show that the effect of the initial residual stress affects the loading response in the first cycle of loading and during the transitions of the elastic region to the post-yielded region. Moreover, the magnitudes of the effect decrease with an increasing number of displacement cycles or with a deflection of the column. This phenomenon can be seen even more clearly on the high compressive axial force

case i.e. $N^* = 0.7N_s$. The effects of the initial residual stresses are eliminated completely after 3 cycles. For all axial force cases, the response of the first cycle is almost the same as the response obtained in the pushover analysis.

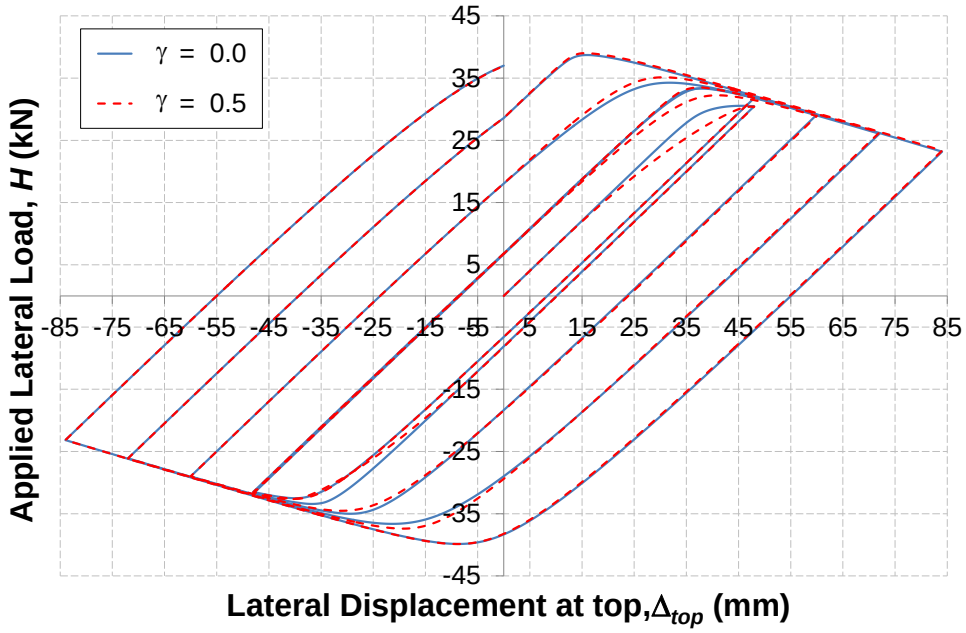

a) $N^* = 0.355N_s$

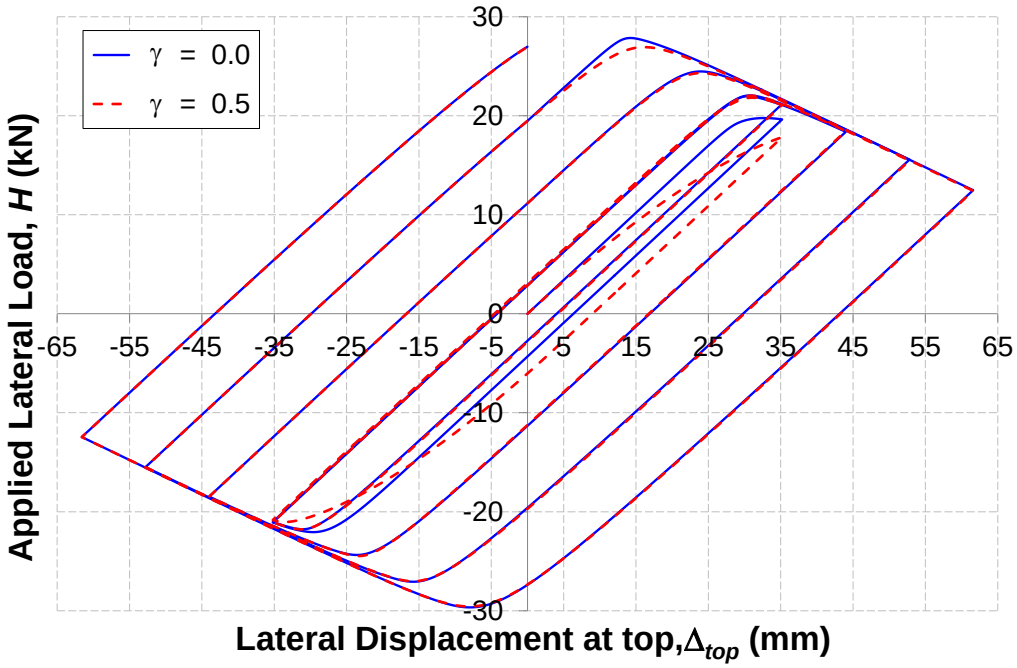

b) $N^* = 0.5N_s$

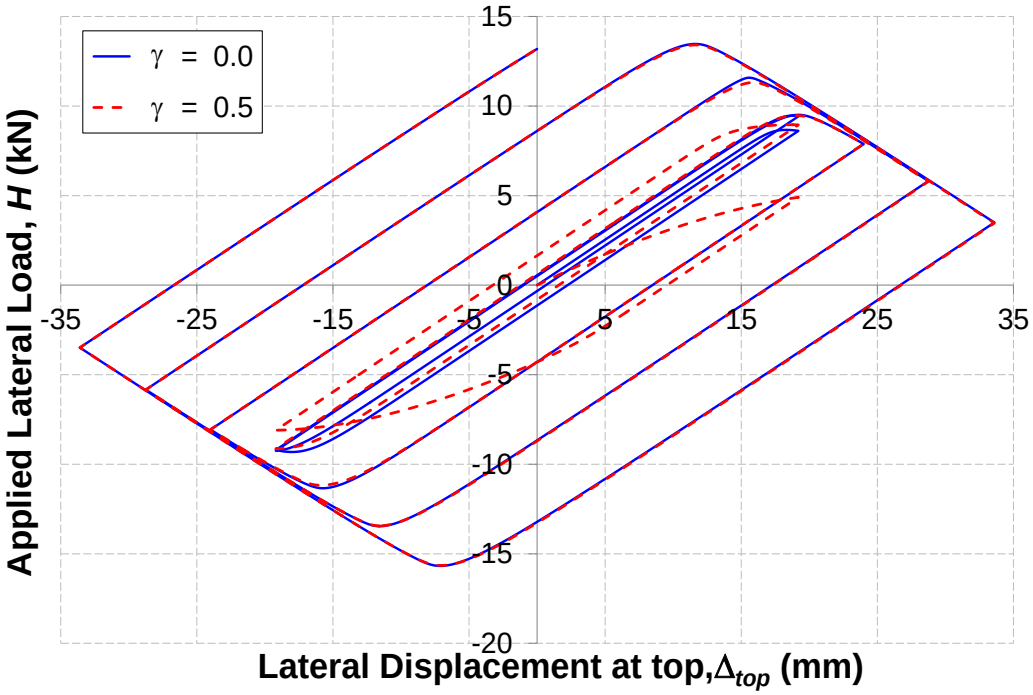

c) $N^* = 0.7N_s$

Figure 7–12: Response of the column subjected to static cyclic loadings

It can also be seen from the figure that the overall strength of the system decreases as the deflection increases as shown by the negative slope of the curves at the plastic ranges. This is due to the *P*-delta effects where the axial compressive force causes the system to deform further. The *P*-delta effect is also caused by the differences in the maximum lateral applied force between the positive and negative loadings.

Another behaviour that can be observed from all the axial force cases is that the maximum lateral forces of the negative/reverse loading are generally larger than the loading in the corresponding positive direction. This can be understood by imaging a bilinear loop (Gregory et al. 1993) which is loaded from a larger absolute displacement at zero force in the second half cycle than in the first half cycle. It is a consequence of the post-elastic stiffness as illustrated in Figure 7–13. The solid line in the figure shows how the negative bilinear stiffness increases the peak forces at each cycle.

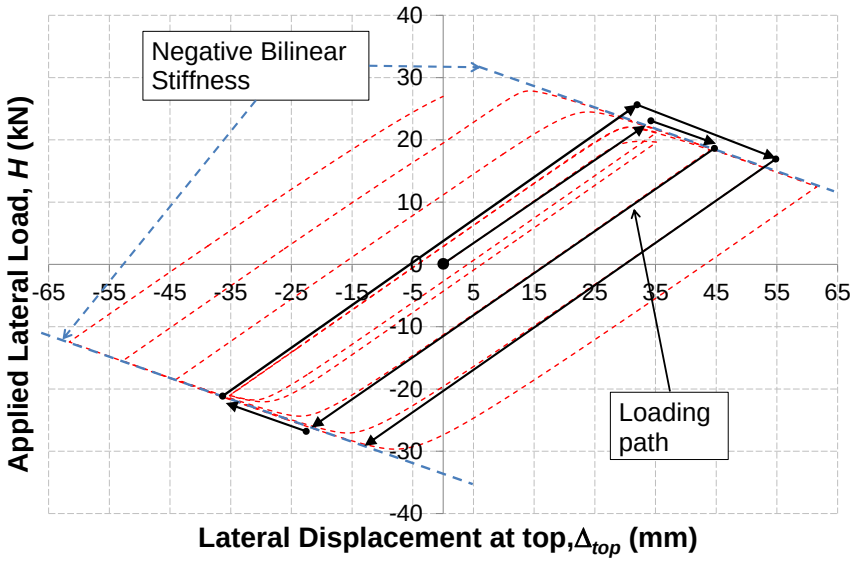

Figure 7–13: Illustration of effect of negative bilinear stiffness

7.3 THREE STOREY FRAME BEHAVIOUR

7.3.1 Responses of low-rise frame under monotonic loading

Figure 7–14 presents monotonic base shear force (V_{base}) versus roof lateral displacement (Δ_{roof}) for different initial residual stress (IRS) ratios for the frame described in Section 6.1.2. The full lateral force, *H*, is applied to both first and the second storey whereas half of the full applied force is applied to the roof level. The monotonic responses were obtained by using load control method as described in Section 7.1.1. Table 7–5 summarises the values of the maximum V_{base}, corresponding roof lateral displacement, and the secant structural stiffness (K_s) as calculated by Eq. 7-1.

It is found that the ultimate base shear force, V_{base}, decreases while the initial residual stress ratios increases. It also means that the lateral capacity of the frame is reduced due to *IRS* effects. However, the reduction of the lateral force capacity of the frame is insignificant because the difference between γ = 0.0 and 0.7 is only 3.5% which is considered to be small. On the contrary, the maximum roof deflection increases with increasing *IRS* ratio since the *IRS* reduces the frame stiffness. The rate of the increasing of the deflection is almost twice as faster as than the decreasing rate of the base shear force. From the results, there is an 8.7% increase in the roof deflection between the γ = 0.0 and 0.7 but there is only a 3.5% reduction in V_{base}. For the structural stiffness, the

results clearly indicate that K_s is significantly affected by *IRS* effects as the K_s is reduced by 3.5%, 9.1% and 14.8% between γ = 0.0 and γ = 0.3, 0.5 and 0.7 cases.

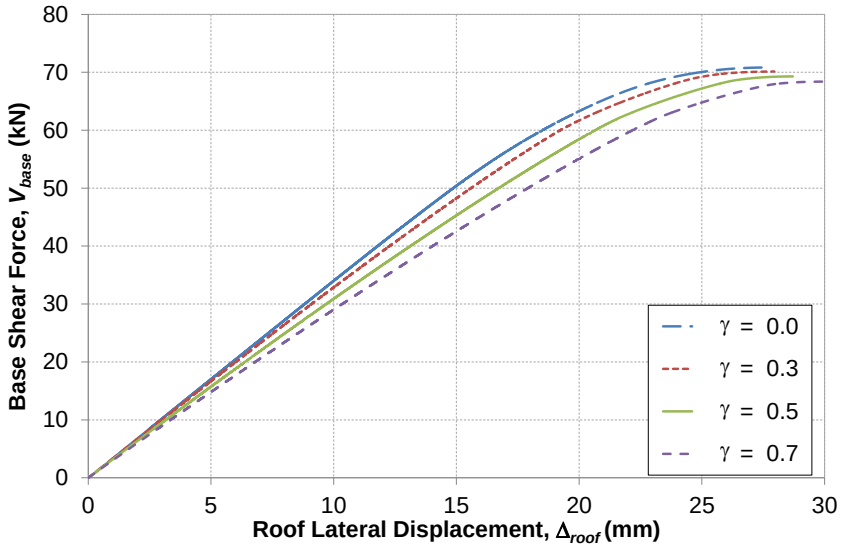

Figure 7–14: Monotonic response of three storey low-rise steel frame

Table 7–5: Summary of the results of the monotonic loading for the low-rise steel frame

IRS Ratio	V_{base}		Δ_{roof}		K_s	
	value	diff.	value	diff.	value	diff.
	(kN)	(%)	(mm)	(%)	(kN/mm)	(%)
γ = 0.0	70.82	-	27.51	-	3.15	-
γ = 0.3	70.15	0.95	27.95	1.60	3.04	3.46%
γ = 0.5	69.29	2.16	28.71	4.36	2.86	9.12%
γ = 0.7	68.39	3.43	29.92	8.76	2.68	14.8%

The analysis found that the first two hinges are formed at the bottom of the columns on the ground floor. The above maximum compressive axial forces (negative sign indicates that the force is acting in compression) for all the cases are found in the right hand column on the ground floor. The maximum bending moments are found in the bottom of the left hand column on the ground floor. From the results, the ultimate flexural capacities, M_{ult}, for the column are 75kNm and 62kNm for N^*_{col} = -1487kN and -1626kN respectively for the γ = 0.0 case. Here, the maximum axial compressive force in the column on the ground level is approximately 0.72 of the sectional compressive capacity, N_s. The other finding from the results is that the ultimate forces are not affect by the *IRS* effects. The full collapse mechanism of the frame for all cases are found to be column-

sway, as shown in Figure 2–4, where the hinges are formed at the top and the bottom of the columns on the ground floor.

7.3.2 Responses of the low-rise frame subjected to static cyclic loadings

The maximum roof displacement, Δ_{max}, used in the push-pull analysis, obtained from the static pushover analysis, is 27.51mm as shown in Table 7–5. The configuration and the displacement loading profile are given in Chapter 7.1.2. The displacement step is $\Delta_{max}/50$. Figure 7–15 shows the plots of the sensitivity study for the control displacement step, $\Delta_{max}/50$, and the half of its step, $\Delta_{max}/100$ for γ = 0.0 and 0.7. Both figures show that there are only minor differences (the maximum difference is less than 1%) between these two cases during the third and fifth cycles. Since the differences are small enough to be negligible, $\Delta_{max}/50$, therefore, is sufficient to produce satisfactory results.

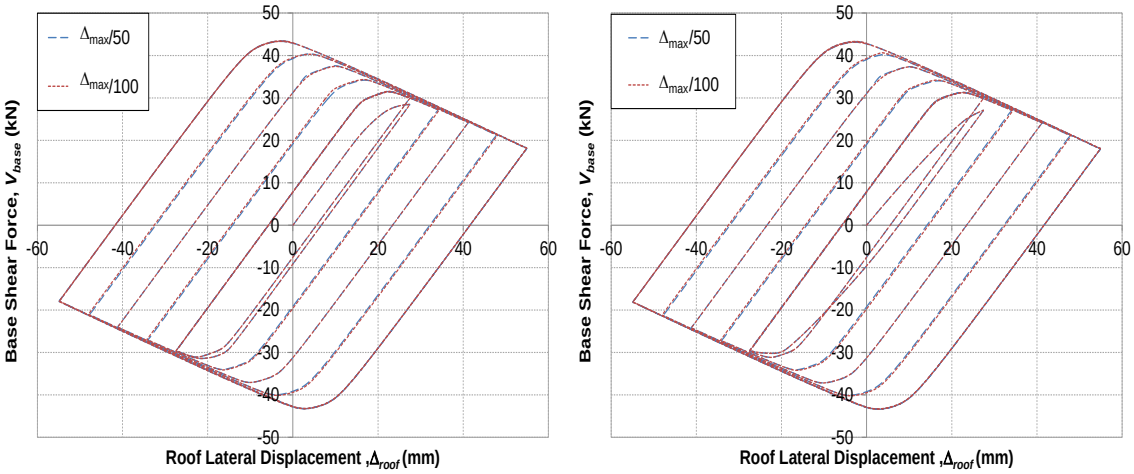

a) γ = 0.0 b) γ = 0.7

Figure 7–15: Comparison of the displacement step sizes

Figure 7–16 presents the results of the base shear force and the lateral displacement at the roof for the four *IRS* cases, γ = 0.0, 0.3, 0.5 and 0.7. The responses of the frame under the static push-pull analysis are similar to the response of the cantilever cases. From the figures, the following responses can be clearly seen:

1) The initial residual stress only affects the response during the first cycle of the loading;

2) Due to the *P*-delta effect, the post-yielded structural stiffness has a negative value. It is indicated by the decrease of the base shear force while the deflections at the roof level increase.

3) Loading in the reverse direction (negative loading in the figure) is generally larger than the loadings of the corresponding positive direction especially in the initial cycle to each displacement level as shown in Figure 7–1. Table 7–6 presents the differences between the initial (positive) and the reverse (negative) directions. Note that the negative differences indicate that the loadings in the positive direction are less than in the negative direction. This is due to the negative bilinear hysteresis loop as illustrated in Figure 7–13. However, the differences become smaller once the deflection becomes larger. This response is also caused by the P-delta effect.

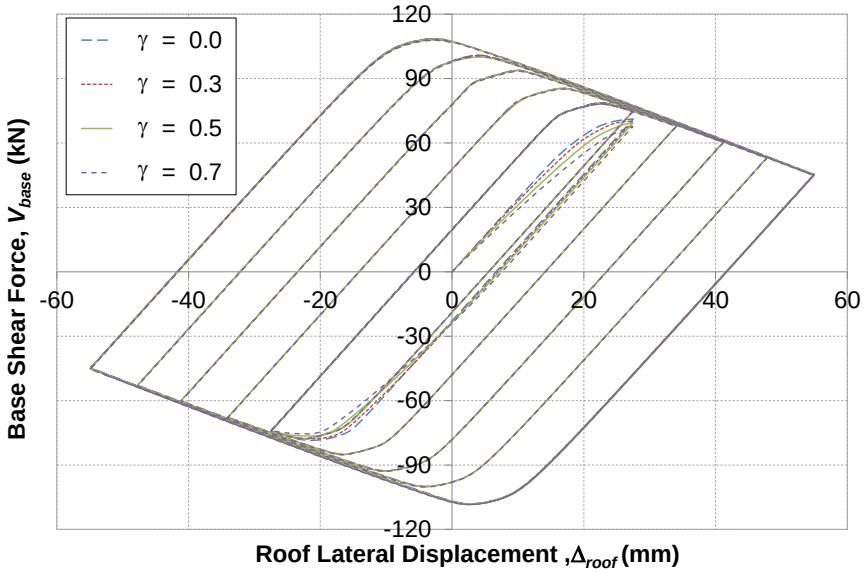

Figure 7–16: Response of the low-rise frame subjected to cyclic loadings

Table 7–6: Differences in maximum base shear force between push and pull directions

IRS Ratio	Number of loading cycle						
	1st (%) $\pm\Delta_{max}$	2nd (%) $\pm\Delta_{max}$	3rd (%) $\pm1.25\Delta_{max}$	4th (%) $\pm1.5\Delta_{max}$	5th (%) $\pm1.75\Delta_{max}$	6th (%) $\pm2\Delta_{max}$	7th (%) $\pm2\Delta_{max}$
γ = 0.0	-10.459	+1.295	-7.953	-8.350	-1.796	+0.264	0.419
γ = 0.3	-10.802	+0.914	-8.378	-8.600	-2.058	+0.045	0.226
γ = 0.5	-10.446	+0.407	-8.606	-8.562	-2.319	-0.136	0.061
γ = 0.7	-11.558	+0.273	-8.840	-9.152	-2.710	-0.516	-0.252

7.4 SUMMARY OF STATIC LOADINGS

For monotonic loading under load control:

- The effect of the initial residual stress does not affect the structural responses before the yielding occurs i.e. $H/H_y < (1 - \gamma - N^*/N_s)$.
- From the monotonic analysis of the 3.2m tall cantilever column, it was found that:
  - An increase in initial residual stresses from $\gamma = 0.0$ to 0.5, caused a decrease in maximum lateral strength of 0% for $N^*/N_s = 0$ but 36% for $N^*/N_s = 0.7$. An *IRS* change from 0 to 0.5 caused a secant stiffness decrease of 7.2% and 44% for $N^*/N_s = 0$ and 0.7 respectively.
  - An increase in axial compressive force from $N^*/N_s = 0$ to 0.7 resulted in a decrease in the maximum lateral strength of 86% for $\gamma = 0.0$ and 91% for $\gamma = 0.5$ and in the secant stiffness of the column of 57% for $\gamma = 0.0$ and 73% for $\gamma = 0.5$.
- The combined effect of the initial residual stress and the axial compressive force affects the strength and stiffness more significantly than either of those effects alone.
- The behavior of the three storey frame shows that the secant stiffness of the frame decreased by 9% from $\gamma = 0.0$ to 0.5 and it is also shows a 2% decrease in the maximum lateral strength. This was much less significant than for the column alone when columns are subjected to similar axial compressive force.
- The *P*-delta effect due to the magnitudes of the axial compressive force affects the peak strength more significantly than the effect of the initial residual stresses.

For the cyclic loading under the displacement control:

- Under the column cyclic loadings, the strength of the structure under first cycles to the specified small displacements, where yielding occurred, was reduced by the initial residual stresses.
- The effect of the initial residual stress disappeared after several cycles of loading.

8 RESPONSE UNDER SEISMIC EXCITATIONS

8.1 SUMMARY OF THE EARTHQUAKES RECORDS

The 20 SAC earthquake records developed for the Los Angles, with probabilities of exceedance of 10% in 50 years, were used to perform the time-history analysis [26]. Table 8–1 summarised the major details of each record including the values of the un-scaled spectral acceleration at first mode of the structure, $S_{a(T1,5\%)}$, for the two models described in Chapter 6.

Table 8–1: Information of 20 SAC earthquake records used

Record Name	Total Duration (s)	Record Time Step (s)	$S_{a(T1,5\%)}$ (g)	
			T_1 = 0.5s	T_1 = 0.56s
la1	53.48	0.02	1.465	1.434
la2	53.48	0.02	1.561	1.696
la3	39.39	0.01	0.816	0.705
la4	39.39	0.01	0.878	0.600
la5	39.09	0.01	0.588	0.672
la6	39.09	0.01	0.434	0.431
la7	80	0.02	0.941	0.872
la8	80	0.02	0.570	0.542
la9	80	0.02	1.220	1.110
la10	80	0.02	0.932	0.693
la11	40	0.02	1.380	1.212
la12	40	0.02	1.829	1.325
la13	60	0.02	1.551	1.857
la14	60	0.02	1.446	1.480
la15	14.95	0.005	1.136	1.064
la16	14.95	0.005	1.142	1.210
la17	60	0.02	0.994	1.052
la18	60	0.02	2.241	1.600
la19	60	0.02	1.633	1.243
la20	60	0.02	1.331	1.478

The spectral acceleration given in the above table were based on the dynamic response spectrum for single degree-of-freedom elastic systems. It was computed by Sadashiva, 2011[27] using step-by-step Central Difference numerical method. Those values are based on a 5% damping ratio with time step size of 0.001s.

8.2 ANALYSIS METHODOLGY AND PROCEDURE

Incremental dynamic analysis (IDA) method, proposed by Vamvatsikos and Cornell (2002) [28, 29], is used to evaluate the effect of the initial residual stresses (IRS) on the structures subjected to the seismic loading. It involves performing a series of inelastic time-history analyses (ITHA) with several levels of intensity, from the elastic range to the global dynamic instability, to all earthquake records for every model. Hence, it is able to provide a better understanding of the changes in the structural response as the intensity of the ground motion increase and to estimate the dynamic capacity of the global structural system.

The results, in general, were presented in forms of *IDA* curves of the Intensity Measure (IM) to represent the seismic intensity versus the Engineering Demand Parameter (EDP) to measure the structural response. For this research, the target spectral acceleration with 5% damping ratio at the first mode of the structure was chosen to be the Intensity Measure and the maximum interstorey drift ratio, θ_{max}, to be the *EDP*. The interstory drift ratio, θ_{max}, is defined as the ratio of the relative displacement between any two adjacent storeys over the height of the storey.

For each analysis case, the sample means ($y_{50\%,IM}$), 16% ($y_{16\%,IM}$) and 84% ($y_{84\%,IM}$) confidence levels of the *EDP* at a given *IM* value are computed by using Eq. 8-1 to Eq. 8-4. This statistical numerical method was used generally to summarise a set of *IDA* curves to take account into of the randomness among the results.

$$y_{50\%,IM} = \sqrt[n]{\prod_{i=1}^{n} y_i} \qquad \text{Eq. 8 –1}$$

$$y_{16\%,IM} = y_{50\%} \exp^{-\sigma_{\ln,IM}} \qquad \text{Eq. 8 –2}$$

$$y_{85\%,IM} = y_{50\%} \exp^{\sigma_{\ln,IM}} \qquad \text{Eq. 8 –3}$$

$$\sigma^2_{ln,IM} = \sum_{i=1}^{n} \left(ln \left[\frac{y_i}{y_{50\%,IM}} \right]^{1/\sqrt{n}} \right)^2 \qquad \text{Eq. 8 –4}$$

where

n = Total number of *EQ* records considered,

$\sigma_{ln,IM}$ = Standard deviation of the logarithms at a given *IM*,

y_i = *EDP* value due to i^{th} *EQ* record at a given *IM*.

Figure 8–1 presents the general analysis procedure for a structure that is subjected to specified gravity loads using an incremental dynamic analysis for one earthquake (EQ) record. This procedure is repeated for each of the 20 *EQ* records given in Section 8.1. In this procedure, the values of γ in Step 1 and $S_{a,target}$ in second step were defined by the user. The Scale Factor (SF) in Step 3 was calculated by Eq. 8-5. OpenSEES was used to perform the inelastic time history analysis (ITHA) where the configurations of *ITHA* were described in Section 8.3. The codes of OpenSEES were given in Appendix C8. Step 5 was to obtain θ_{max} for the specified $S_{a,target}$. For Step 6, if the maximum interstorey drift ratio (θ_{max}) is less than the interstorey drift ratio at collapse ($\theta_{collapse}$) as specified by the user (a 5% is used in this study), the next step was to increase $S_{a,target}$ and repeat Steps 3 to 6 until $\theta_{max} > \theta_{collapse}$.

$$ScaleFactor, SF = \frac{S_{a,target}}{S_{a,i(T1,5\%)}} \qquad \text{Eq. } 8-5$$

where

$S_{a,target}$ = Target(scaled) spectral acceleration

$S_{a,i(T1,5\%)}$ = Un-scaled 5%-damped spectral acceleration of i^{th} record at 1st mode, T_1.

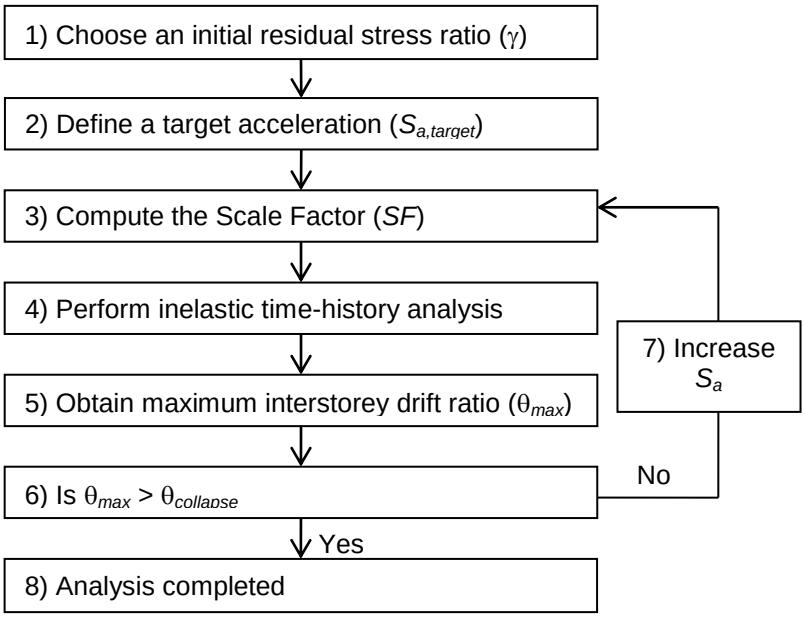

Figure 8–1: Overview of the analysis algorithm for *IDA*

8.3 ANALYSIS CONFIGURATIONS AND CASES CONSIDERED

8.3.1 Analysis configurations for inelastic time-history analysis

A complete inelastic time-history analysis, similar to the pushover and push-pull analysis, consists of a gravity load analysis, to take into account of gravity forces, followed by applying the *EQ* records. The configurations for the gravity load are given in Table 5–3 and for the inelastic time-history analysis (ITHA) is summarised in Table 8–2.

Table 8–2: Configurations for inelastic time-history analysis

Command	Method
Geometric Transformation	Corotational
Constraints	Transformation
Numberer	RCM
System	Band General
Test	NormDispIncr 1.0e-8 30 0
Algorithm	ModifiedNewton
Analysis	Transient

The commands, used in *ITHA* that are different to static analysis, are:

- Transient for Analysis[13,30] – it is used to solve time-dependent analysis where the time step is constant. For the transient analysis, it requires to specify the mass and the damping values.
- Newmark for Integrator[13,30] – it is one of specified integrator command for the transient analysis. Here, the average acceleration method is used with the two parameters, γ and β, to be 0.5 and 0.25.
- UniformExcitation for Load pattern[13,30] – this load pattern is applied to implement the *EQ* records into *ITHA*. It is used in conjunction with timeSeries command. For both models used in this study, the acceleration is applied to the horizontal direction (1st degree-of-freedom) of the supports.
- Series for timeSeries[13] – the inputs for Series command are the time steps of the input data, the loading history and the scale factor. For this study, the time step of each *EQ* records is given in Table 8–1. Moreover, because the unit of the *EQ* records is in cm/s/s, the scale factor needs to be multiplied by 10 to mm/s/s to ensure that the unit is consistent with others.

The damping model used in *ITHA* is the Initial Stiffness Rayleigh Damping (ISRD) [30,31] where the damping matrix is to be constant throughout the analysis. In OpenSEES, the general damping matrix, *D*, for OpenSEES is given by Eq. 8-5. The users need to define the values for these four factors.

$$D = \alpha_m M + \beta_{current} K_{current} + \beta_{initial} K_{initial} + \beta_{last} K_{last} \quad \text{[13,30]} \qquad \text{Eq. 8 – 5}$$

where

M = Mass matrix used to compute Damping;

α_m = Factor applied to mass matrix;

$K_{current}$, $K_{initial}$ & K_{last} = Stiffness matrix at current, initial and last-committee state determination used to calculate Damping.

$\beta_{current}$, $\beta_{initial}$ & β_{last} = Factors applied to current, initial and last-committee stiffness matrix respectively.

In this study, since *ISRD* is applied and it uses only the initial stiffness to compute the damping, it needs only to define α_m and $\beta_{initial}$ whereas the $\beta_{current}$ and β_{last} are zero. The α_m and $\beta_{initial}$ are functions of the damping ratio and the natural frequencies of structures as given in Eq. 8-6 and Eq. 8-7. Here, for the first model, the cantilever column, since only one structural period for this model, the 1st-mode natural frequency is used for both ω_i and ω_j. For the low-rise three storey frame, the factors are computed by using the 1st and the 3rd mode natural frequency following the recommendation of Carr (Ruaumoko Manual). A 5% damping ratio is used for both models.

$$\alpha_m = \zeta\left(\left(2\omega_i\omega_j\right)/\left(\omega_i + \omega_j\right)\right) \qquad \text{Eq. 8 – 6}$$

$$\beta_{initial} = 2\zeta/\left(\omega_i + \omega_j\right) \qquad \text{Eq. 8 – 7}$$

where

ζ = Damping ratio;

ω_i , ω_j = Natural frequencies of i^{th}, j^{th} mode.

The analysis time step is 0.001s for most of the records. The only exceptions are for *EQ* records of La15 and La16 where an analysis time step of 0.0005s is used since the time step of the records is 0.005s.

8.3.2 Performed analysis cases

Two axial compressive force ratios, N^*/N_s = 0.355 and 0.5, are applied to the cantilever column model in Section 6.1.1. The initial residual stress (IRS) ratios considered are γ = 0.0 and 0.5 for each axial force ratio and a linear distribution of *IRS* was used. For the low-rise frame, the evaluation of *IRS* effect is also based on the results from the two *IRS* ratios, γ = 0.0 and 0.5. However, unlike the first model, only one gravity loading condition is considered. This is specified in Section 6.1.2 previously. For each of the analysis case, it comprises 20 cases, one for each earthquake (EQ) record.

8.4 A SINGLE CANTILEVER COLUMN (Model 1)

Figure 8–2 and Figure 8–3 present the Incremental Dynamic Analysis (IDA) curves of all 20 SAC *EQ* records of γ = 0.0 (a) and 0.5 (b) for N^*/N_s = 0.355 and 0.5 respectively. The curves in these graphs are approximately linear until $S_a \approx$ 0.7g and 0.6g for γ = 0.0 and 0.5 respectively with N^*/N_s = 0.355 and $S_a \approx$ 0.4g for both γ values with N^*/N_s = 0.5. For the responses beyond these points, it is hard to define a clear trend among the 20 *IDA* curves since each of the records has its own characteristics and hence results in different response.

Each *IDA* curve can be categorized into one of these types which are softening, hardening or weaving, according to its response (Vamvatsikos et al., 2002 [28]) as presented in Table 8–3. In general, most of *IDA* cases have the softening behaviour where a gradual increase in θ_{max} with an increase in S_a. In general, those records that give softening responses result in lower maximum spectral acceleration, $S_{a,max}$, ($S_{a,max} \approx$ 1.2g for N^*/N_s = 0.355 and 0.7g for N^*/N_s = 0.5) values compared to with those from hardening ($S_{a,max} \approx$ 1.4g for N^*/N_s = 0.355 and 1.0g for N^*/N_s = 0.5) and weaving ($S_{a,max} \approx$ 1.8g for N^*/N_s = 0.355 and 0.9g for N^*/N_s = 0.5) cases.

Table 8–3: Summary of individual *IDA* curves for cantilever column

N*/Ns	0.355		0.5	
γ	0.0	0.5	0.0	0.5
Softening	la3-la5, la13, la15-la18			
	la6, la7, la9	la8	la7,la8, la12	La7-la12
Hardening	la10			la6, la14, la19
	la8	la8, la12	la9, la11	
Weaving	la1, la2,la14, la19, la20			la1,la2,la20
	la11	la7, la11	la6	

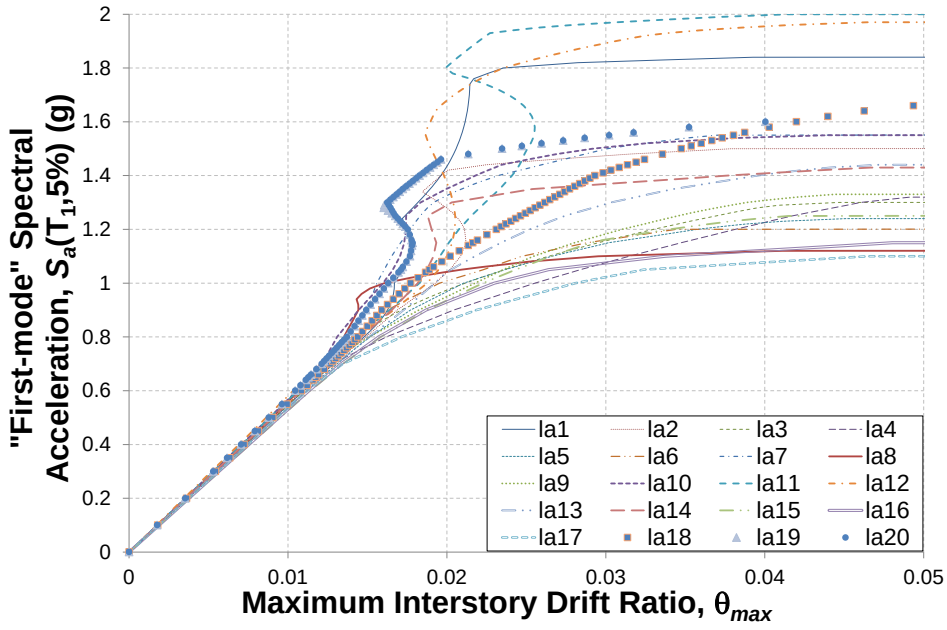

a) γ = 0.0

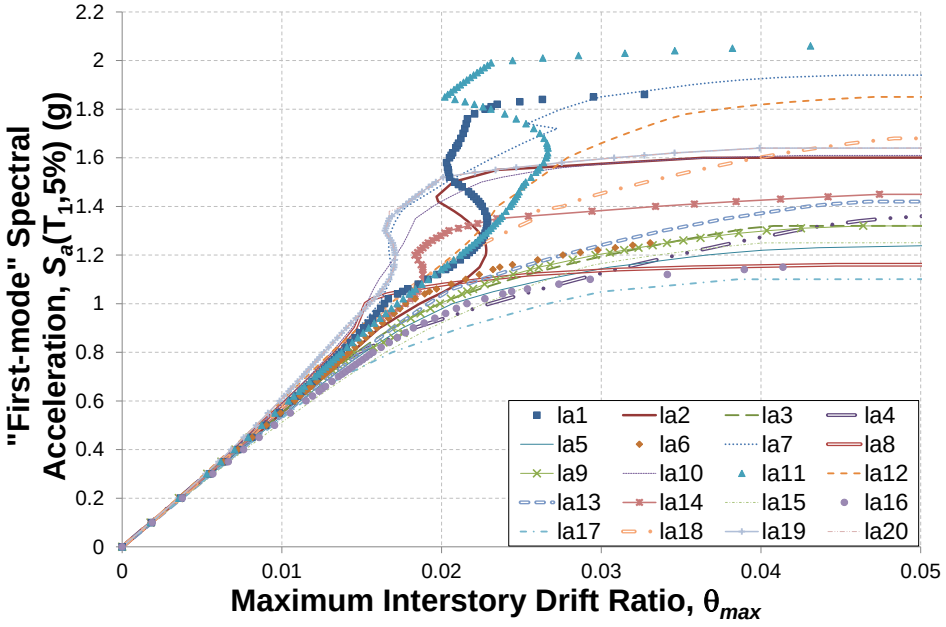

b) γ = 0.5

Figure 8–2: 20 *IDA* curves for N^*/N_s = 0.355 of model 1

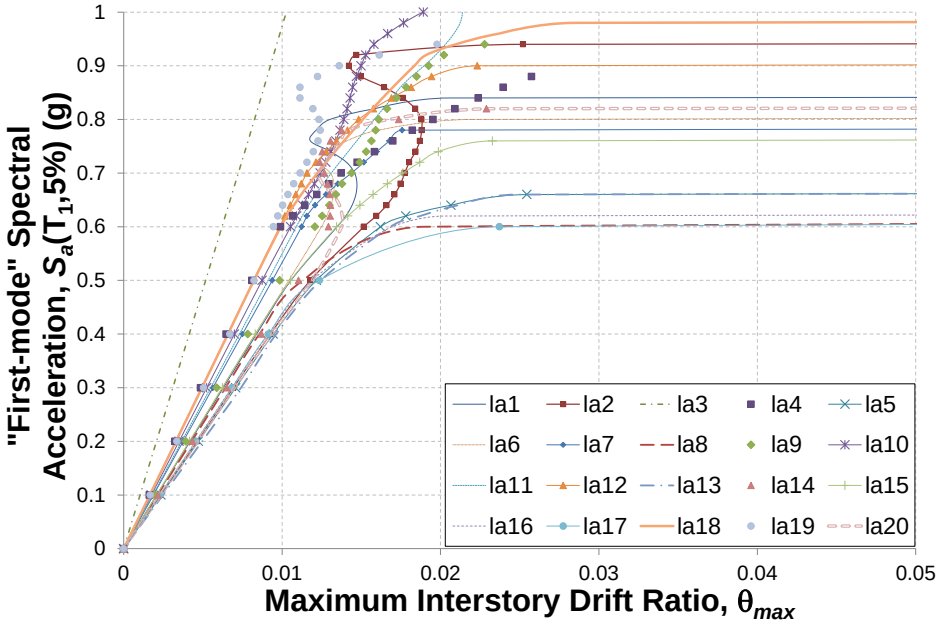

a) γ = 0.0

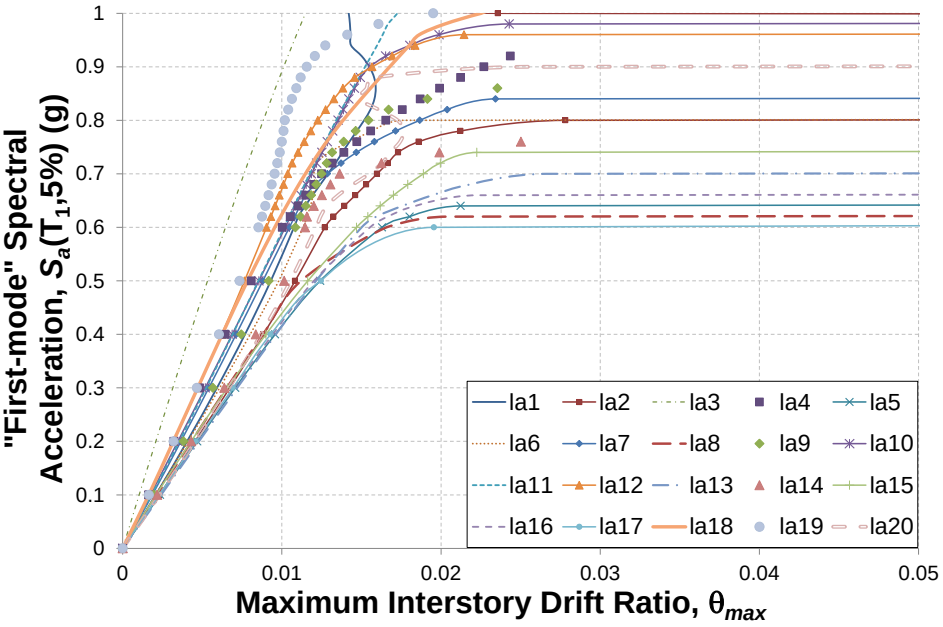

b) γ = 0.5

Figure 8–3: 20 *IDA* curves for N^*/N_s = 0.5 of model 1

Figure 8–4 a) and b) present the comparison between the two initial residual stress (IRS) values for N^*/N_s = 0.355 and 0.5 respectively. The 20 *IDA* curves, as shown in Figure 8–2 and Figure 8–3, were summarised into 16%, 50% and 84% confidence levels (C.L.). For N^*/N_s = 0.355, the responses for γ = 0.5 always result in slightly lower drifts than for the γ = 0.0 case for all three confidence levels. For structures where drift is related to damage, this means that a structure with initial residual stresses is likely to have less damage

under the same level of shaking for these cases. For $N^*/N_s = 0.5$, the drifts of $\gamma = 0.5$ are also generally lower than for the $\gamma = 0.0$ case except for response of 50% confidence level when $S_a > 0.70$g. This is the opposite of what would be predicated by a secant stiffness and equivalent damping approach but it is consistent with the ideas of dynamic stability.

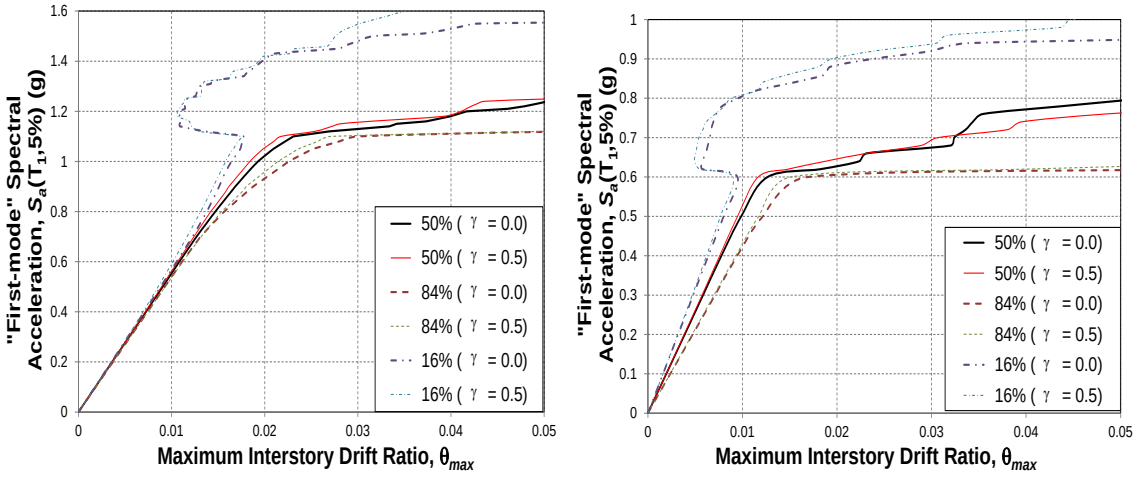

a) $N^*/N_s = 0.355$ b) $N^*/N_s = 0.5$

Figure 8–4: Comparison between $\gamma = 0.0$ and 0.5 for model 1

At $\theta_{max} = 0.05$, the differences in maximum spectral acceleration between the two *IRS* cases are given in Table 8–4. According to the 50% confidence level, the strength of the column is either unaffected ($N^*/N_s = 0.355$) or reduced up to 2.5% ($N^*/N_s = 0.5$) when the *IRS* effect is considered. On the contrary, both 16% and 84% confidence levels indicate that the *IRS* effect tends to increase the column strength by up to 1.61% for this case. In general, the opposite would be expected as initial residual stresses decrease the structural stiffness and this could reverse the effective period and the peak displacement.

Table 8–4: Comparisons of *IRS* effect on maximum spectral acceleration (Model 1)

Confidence Level	Maximum Spectral Acceleration at θ_{max} = 5% (g)					
	$N^*/N_s = 0.355$			$N^*/N_s = 0.5$		
	γ=0.0	γ=0.5	Diff (%)	γ=0.0	γ=0.5	Diff (%)
16%	1.56	1.62	3.85	0.96	1.02	6.25
50%	1.22	1.22	0.0	0.8	0.78	-2.5
84%	1.1	1.1	0.0	0.62	0.63	1.61

Figure 8–5 a) and b) compare the effect of the axial compressive force. It is found that increasing the axial force can lead to significant reduction in maximum 1st mode spectral acceleration at θ_{max} = 5%. For the column, by increasing N^*/N_s = 0.355 to 0.5, the maximum spectral acceleration for γ = 0.0 decreased by 38%, 34% and 43% for 16%, 50% and 84% confidence levels respectively. For γ = 0.5, the values were 37%, 36% and 42%.

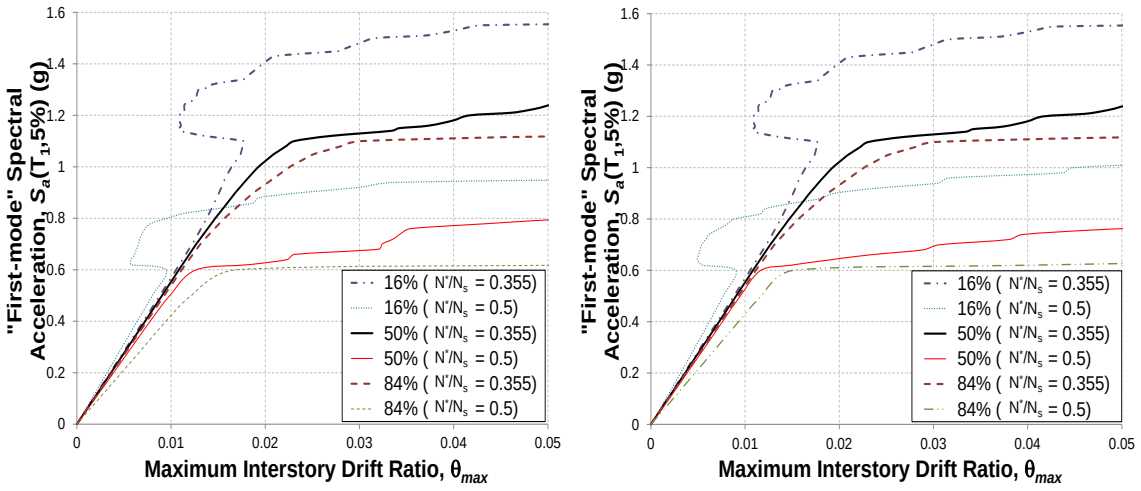

a) γ = 0.0 b) γ = 0.5

Figure 8–5: Comparison between N^*/N_s = 0.355 and 0.5 for model 1

Considering the structural period of 1st mode after applying the gravity loads, there is no difference between two *IRS* cases for both axial compressive force ratios. On the contrary, an increase in axial force ratio, from 0.355 to 0.5, resulted in increasing the structural period from 0.5s to 0.544s. Here, an increase in structural period can lead to increase in the spectral displacement as illustrated in Figure 8–6. The red solid line in the figure is the median values of spectral displacement from the 20 SAC earthquake records.

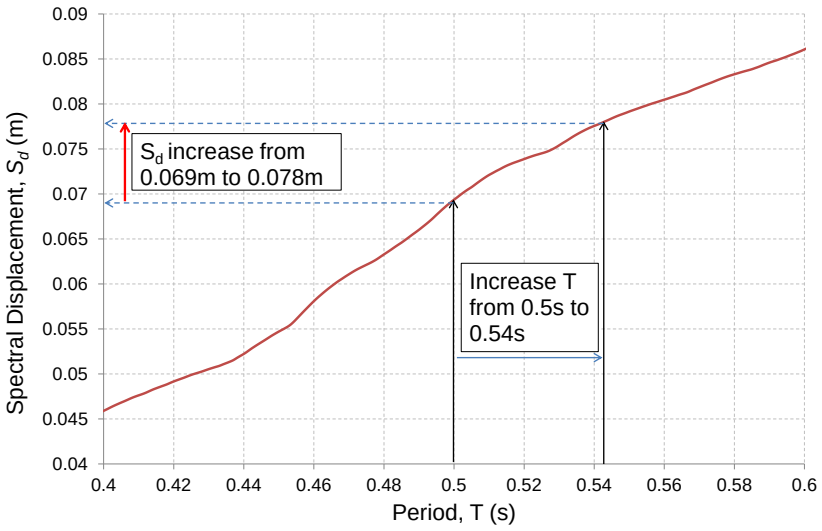

Figure 8–6: Illustration of effect of increasing structural period

The differences which have approximately a 40% sudden increase in θ_{max} as shown in Figure 8–5 may be due to the following factors:

a) Change in elastic period

– The fundamental response period including axial force effect, T_p, can be found by Eq. 8-8 (Andrews, 1977) [32]. T_o is the fundamental response period when N^* = 0. Here, T_o is 0. 426s. Hence, T_p at N^* = 811.18kN (0.355N_s) is 0.485s and at N^* = 1143kN (0.5N_s) is 0.517s. The computed periods by using Eq. 8-8 are less than the values computed from OpenSEES which are 0.5s and 0.544s for N^*/N_s = 0.355 and 0.5 respectively. The periods computed using Eq. 8-8 are less than 5% different from the OpenSEES values. This is most likely due to the change in member local stiffness due to axial force, which is not considered in Eq. 8-8. As can be seen from Figure 8–6, the increase in elastic displacement from the change in period is 12%.

$$T_o/\sqrt{(1-\theta)} \qquad \text{Eq. 8 – 8}$$

where

θ = N^*/K_oL

N^* = Applied axial compressive force;

K_o = Initial elastic stiffness (for model 1 is 1108.4kN/m)

L = Height of the column (= 3.2m).

b) Change in secant period at yield

– This includes the nonlinearity associated with initial residual stresses and yielding. In section 7.2.1.1, it was shown that the stiffness of the member at 90% of the full applied load were 0.8 and 0.67 for N^*/N_s = 0.355 and 0.5 respectively when γ = 0.0; hence, the effective periods, based on the secant stiffness, are 0.502s and 0.548s for for N^*/N_s = 0.355 and 0.5 respectively. These periods are slightly longer than those from the elastic analysis. This causes the changes in displacement, from Figure 8–6, from N^*/N_s = 0.355 to 0.5 is 13%.

c) The effect of the change in strength

– For long period structures, the equal displacement method is often used. This implies that strength is not important. For a period of 0.5s or so, the average effect of strength is not likely to be significant.

d) The effect of the decrease in post-elastic stiffness

– It is due to *P*-delta effects, as shown in Figure 7–13. This tends to exacerbate inelastic deformation in one direction alone. It is likely to be the most significant effect.

8.5 A LOW-RISE THREE STOREY FRAME (Model 2)

The seismic responses for the three-storey frame from the 20 SAC records are summarised into 16%, 50% and 84% fractile curves, as shown in Figure 8–7, using Eq. 8-1 to 8-4 described in Section 8.2. Here, the maximum interstorey drift ratio, θ_{max}, is determined based on the displacements of the nodes of the left hand side of the frames. As described in Section 6.1.2, both beams and columns have the same initial residual stress ratio. The overall behaviours between two initial residual stress (IRS) ratios are similar. For both ratios, the 16% confidence level shows a weaving response, softening for the 50% and slightly hardening behaviour for the 84% confidence level.

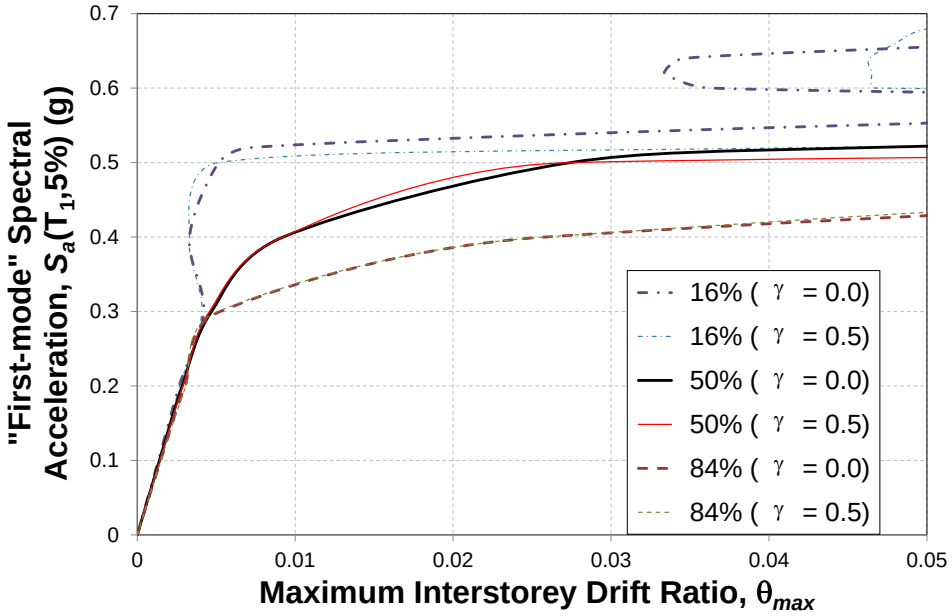

Figure 8–7: Comparison between γ = 0.0 and 0.5 for model 2

Table 8–5 presents the summary of the maximum spectral accelerations of the three confidence levels for all *IRS* ratios. The positive number in diff indicates γ = 0.0 is greater than γ = 0.5. The maximum axial compressive force under the gravity loading is 1419kN which is about $0.62N_s$. During the seismic excitations, the maximum axial compressive force increased to as much as 1670kN (≈ $0.77N_s$). For 16% confidence level, due to the weaving behavior, there are three S_a when θ_{max} = 0.05. However, only the lowest S_a values are to be considered which are given in Table 8–5.

Considering the 50% percentile, for $\theta_{max} \leq 0.01$, the behaviors between both *IRS* ratios are almost matched to each other. From 0.01 to 0.027, 50% of the records agree that the response of γ = 0.5 is slightly stronger than the γ = 0.0 case. However, the spectral acceleration of γ = 0.0, when $\theta_{max} \geq 0.027$, becomes greater than γ = 0.5. At θ_{max} = 0.05 for 50%, $S_{a,(T1,5\%)}$ = 0.522g for γ = 0.0 and 0.507g for γ = 0.5 which is about 2.87% reduction. For the 84% fractile curve, the maximum spectral accelerations for γ = 0.0 and 0.5, based on θ_{max} = 0.05, are 0.429g and 0.432g. As the difference is less than 1%, the effect of *IRS*, with 84% of the EQ records, is unaffected to the seismic responses of the frame.

Table 8–5: Summary of the maximum spectral acceleration (Model 2)

Confidence Level	Maximum Spectral Acceleration at θ_{max} = 5% (g)		
	γ=0.0	γ=0.5	Diff (%)
16%	0.553	0.522	5.61
50%	0.522	0.507	2.87
84%	0.429	0.432	-0.70

By including the *IRS* into the sections for both columns and beams, the fundamental mode of the structural period has only been raised slightly by 0.018% (from 0.56s to 0.5601s for γ = 0.0 to 0.5). The increasing of the structural period is because of the reduction of the global stiffness of the frame caused by initial residual stress. The structural period was computed after the gravity loading had been applied.

8.6 SUMMARY OF SEISMIC RESPONSES

It is found that by increasing the initial residual stress ratios from 0 to 0.5, the spectral accelerations were sometimes greater and sometimes smaller for specific values of maximum interstorey drift ratio, θ_{max}. At θ_{max} = 5% of the spectral acceleration of the column remained the same for N^*/N_s = 0.355 and decreased by about 2.5% for N^*/N_s = 0.5. This means that the column's capacity to resist strong earthquake is reduced by 2.5%. For the three-storey frame which had column gravity axial force of $0.62N_s$ and total compressive force of up to $0.77N_s$, the median spectral acceleration decreased by approximately 2.1% at θ_{max} = 5%.

The response of the cantilever column shows that the seismic performances are not significantly affected by a linear distribution of the initial residual stresses up to $0.5f_y$. For the frame, the effect is not significant with compressive axial forces even up to about $0.75N_s$. For this reason, it is justifiable to ignore the effects of the initial residual stresses in realistic frames.

9 CONCLUSIONS AND RECOMMENDATIONS

The aim of this thesis is to consider the effect of frame strength on the likely frame monotonic behaviour, and the effects of initial residual stresses on the seismic behaviour of the steel structures. These two effects were considered in this research by: 1) performing monotonic analysis of structures with different strengths, and 2) performing static cyclic and 3) seismic analyses of structure considering different levels of axial force.

9.1 CONCLUSIONS

The major findings are described in relation to the questions given in Section 1.2. These are:

i) Can the consideration of member overstrength, rather than member dependable strength, result in significantly different element demands or a weaker overall structure strength?

The effect of overstrength, based on the frame studied in Chapter 4, is likely to increase the demands in the member. Hence, it can also have impacts on connection and foundation design. It is also found that the likely minimum frame lateral strength does not always occur when the steel structure has the minimum material/section strengths. The structural configuration studied in this research gives a reduction of up to 6% in the lateral structural capacity of the overstrength case comparing with a frame using the dependable section capacity.

ii) How likely is the response of steel frames with initial residual stresses affected by cyclic loadings, such as may occur from wind?

In the first half cycle of loading, the behaviour is identical to monotonic loading. Thereafter, the effect of initial residual stresses decreased and it disappeared after several displacement cycles since subsequent cycles to the same displacement resulted in increased maximum strength, rather than deterioration. The behaviour under cyclic loading was not considered to critically affect the behaviour under wind loading.

The post-yielded structural behaviour, which influences the seismic responses, is significantly affected by the *P*-delta effect. This was influenced by the magnitude of the axial compressive force more significantly than the effect of the initial residual stresses.

The effect of member initial residual stresses (IRS) was much less significant in a frame structure when beam yielding occurred than in a column structure.

iii) Is the seismic response of steel frames likely to be detrimentally affected by member initial residual stresses?

The results of *IDA* shows that by increasing column initial residual stress of $0.5f_y$, for specified levels of earthquake shaking, the displacement demands were similar to those with no initial residual stresses for compressive axial forces up to $0.5N_s$. For the frames, the displacement demands were decreased similarly with compressive axial load of more than $0.75N_s$.

iv) Based on the answers to the questions above, how should steel frames need to be analysed/designed?

- Since the member demands may differ significantly when the member overstrength, rather than the dependable strength, is used, and also because it can cause the frame to be weaker, that analysis for design be conducted considering both (i) the member dependable strength and (ii) the member overstrength. This recommendation is consistent with that for inelastic dynamic time history analysis of structures in severe seismic regions to obtain critical demands.
- Based on the findings from cyclic push-pull analysis and seismic incremental dynamic analysis on single cantilever columns and low-rise steel frames, it seems that member initial residual stresses do not significantly affect the responses for the majority of structures which have compressive axial stress level of less than $0.75f_y$ and initial residual stress of less than $0.5\ f_y$. Therefore, it is not necessary to change the current design methods and the initial residual stresses by using current method where *IRS* is considered explicitly.

9.2 LIMITATIONS AND FUTURE RESEARCH RECOMMENDATIONS

- The modelling conducted in this project, for both overstrength and initial residual stress effects, were performed in two dimensions (i.e. a 2-D model was subject to in-plane demands) However, in the reality, both the loading and the behaviour of structures are three-dimensional. As loading can come from all directions and structures can deform in all directions and can exhibit out-of-plane movement, the inelastic effects may be load-path dependent. Therefore, it is required to conduct further research on the effects of 3-D models.

- The findings from this research are based on limited and simple structural configurations only. A wider range of the structural configurations including unsymmetrical, portal or braced framed structures can also be considered.

- The effects of initial residual stresses for structure subjected to cyclic loadings (both static and dynamic) and overstrength were considered individually in this study. Also, in current design practice, these two effects are taken into account explicitly. Therefore, there is a need to examine in the combined effects of overstrength and initial residual stresses.

- This study considered a limited number of initial residual stress (IRS) ratios, *IRS* distributions and the axial force ratios. This could be extended to determine more precisely when the behaviour differed significantly from the case of when there is no initial residual stress.

- The inelastic time history analysis in Chapter 8 considered only the seismic excitation in the horizontal direction. Therefore, in the further research, it is recommended to consider the effect of vertical ground motion shaking on the seismic response.

10 REFERENCES

1. New Zealand Standard, NZS3404:1997, Steel Structure Standard. Standard New Zealand
2. Lu A. Y. C, *"Effect of Residual Stresses on the Design of Columns In Steel Frames"*, Undergraduate Research Report, Department of Civil Engineering, University of Canterbury, Christchurch, 2008.
3. Lu A. Y. C., MacRae G. A., Ziemian R. D., Hann C., Peng B. H. H. and Clifton G. C., *"Extended Direct Analysis of Steel Frames"*, NZ society of Structural Engineering (SESOC) Journal, Vol. 22 No.2, 2009.
4. American Institution of Steel Construction Inc (2007). *"Steel Construction Manual 13th edition."* First printing in 2005.
5. Australia/New Zealand Standard, AS/NZS1170.0:2002, Structural Design Actions – Part 0: General Principles. Joint Technical Committee BD-006.
6. Okazaki T., Parkolap M. and Fahnestock L. A., *"Interface of the Direct Analysis Method and Seismic Design."* Proceeding of 2009 Structure Congress, 2009
7. Okazaki T., Fahnestock L. A. and Parkolap M., *"On the Interface of Stability and Seismic Design Requirements for Steel Buildings."*
8. Gupta A. and Krawinkler H., *"Prediction of Seismic Demands for SMRFs. With Ductile Connections and Elements."* SAC background Document, Report No. SAC-BS-99/06, 1999.
9. Galambos T. V. and Ketter R. L., *"Columns under Combined Bending and Thrust."* Journal of the Engineering Mechanics Division, ASCE, 85(EM2), 1959, pp. 135 -152.
10. Computer and Structures Inc. (CSI), *Basic Analysis Reference Manual*, 2007.
11. McGuire W., Gallaghear R. H. and Ziemian R. D., *"Matrix Structural Analysis, 2nd Edition."* John Wiley & Sons Inc. 1999.
12. Martines-Garcia J. M. *"Benchmark Studies to Evaluate New Provisions for Frame Stability Using Second-Order Analysis."* [MS Thesis], Bucknell University, Pennsylvania, 2002, Chapter 2.
13. Mazzoni S., Mckenna F., Scott M. H., and Fenves G. L., "*Open System for Earthquake Engineering Simulation User Command Language Manual."* Pacific Earthquake Engineering Research Centre, University of California, Berkeley, 2006.
14. Technical committee 8 – Structural Stability Technical Working Group 8.2 - System, *Ultimate Limit State Calculation of Sway Frames with Rigid Joints."* Publication No. 33 European Convention for Constructional Steelwork, 1984.

15. Filippou F. C., Popov E. P., Bertero V. V.,*"Effects of Bond Deterioration on Hysteretic Behaviour of Reinforeced Concrete Joints."* Earthquake Engineering Research Center, University of California, Berkeley. Report EERC 83-19, 1983.
16. Lamarch C. P. and Tremblay R., *"Accounting for Residual Stresses in the Seismic Stability of Nonlinear Beam-Column Elements with Cross-section Fiber Discretization."* Proceedings of the 2008 Annual Stability Conference, Structural Stability Research Council, April 2-5, 2008, Nashville, Tennessee, pp.59-77.
17. OneSteel Market mills, *"Hot Rolled and Structural Steel Products, Third Edition."* OneSteel, 2003.
18. Scott M. H., *"Numerical Integration Options for the Force-Based Beam-Column Element in OpseSees."* OpenSees Wiki, 2011.
19. De Souza R. M., *"Force-Based Finite Element for Large Displacement Inelastic Analysis of Frames."* Ph.D thesis, University of California, Berkeley, California, 2000.
20. Ziemian D. Ronald, *"Guide to Stability Design Criteria for Metal Structures."* Sixth Edition, John Wiley and Sons Ltd, 2010.
21. Trahair N. S. and Bradford M. A., *"The Behaviour and Design of Steel Structures to AS 4100."* Third Edition – Australian, E & FN Spon, 1998.
22. Bjorhovde R., *"Deterministic and Probabilistic Approaches to the Strength of Steel Columns."* Ph. D thesis, University of Lehigh, Bethlehem, Pennsylvania, 1972.
23. Taras A. and Greiner R., *"Development of Consistent Buckling Curves for Torsional and Lateral-Torsional Buckling."* Steel Construction – Design and Research 1, issue 1, 2008, pp 42-50.
24. Greiner R. and Taras A., *"New Design Curves for LT and TF Buckling with Consistent Derivation and Code-Conform Formulation."* Steel Construction – Design and Research 3, No. 3, 2010, pp 176-186.
25. Key P. W., Hasan S. W. and Hancock G. J., *"Column Behaviour of Cold-Formed Hollow Sections."* Journal of Structural Engineering, ASCE, Vol. 114, No. 2, 1988, pp. 390-407.
26. Suites of Earthquake Ground Motions for Analysis of Steel Moment Frame Structures. http://nisee.berkeley.edu/data/strong_motion/sacsteel/ground_motions.html
27. Sadashiva V. K., *"Appendix D – Quantifying Structural Irregularity Effects for Simple Seismic Design."* Ph. D thesis, University of Canterbury, Christchurch, New Zealand, 2011.
28. Vamvatsikos D. and Cornell C. A., *"Incremental Dynamic Analysis."* Earthquake Engineering and Structural Dynamic, Vol. 31, 2002, pp. 491-514.

29. Vamvatsikos D. and Cornell C. A., *"Applied Incremental Dynamic Analysis."* Earthquake spectra, Earthquake Engineering Research Institute, Vol. 20, No. 2, 2004, pp. 823-533.
30. Welcome to the OpenSeesWiki, http://opensees.berkeley.edu/wiki/index.php/Main_Page
31. Charney F. A., *"Unitended Consequences of Modeling Damping in Structures."* Journal of Structural Engineering, ASCE, Vol. 134, No. 4, 2008, pp. 581-592.
32. Andrews A. L., *"Slenderness Effects in Earthquake Resisting Frames."* Bull. NZSEE, 10(3), 1977, pp. 154-158

11 APPENDICES

Appendix A: Commentary of Clause C7.3 in ANSI/AISC 360-05 (2005)

Computational software accounting for geometric and material nonlinearity is used. Modelling of second-order effects should satisfy ANSI/AISC 360-05, 2005 Clause C7.3. That is, for the benchmark structures shown in ANSI/AISC 360-05, 2005 Figure C-A-7.2 as given in Figure AA–1, when M_{max}/M_o and y_{max}/y_o are greater than 2.5, the computational results should agree within 3% of the theoretical solutions.

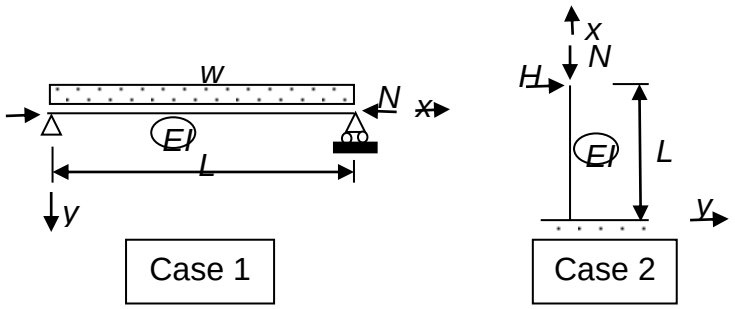

Figure AA–1: Cases for evaluation of accuracy of geometric nonlinearity

For Case 1, the closed form solution for a simply supported flexural member subjected to axial force, as shown in Figure AA–1, is:

$$M_{\max}\left(@\,x=\frac{L}{2}\right)=M_o\left[\frac{2(\sec u-1)}{u^2}\right] \qquad u=\sqrt{\frac{NL^2}{4EI}}, M_o=\frac{wL^2}{8} \qquad \text{Eq. AA1-1}$$

$$y_{\max}\left(@\,x=\frac{L}{2}\right)=y_o\left[\frac{12(2\sec u-u^2-2)}{5u^4}\right] \qquad y_o=\frac{5wL^4}{384EI} \qquad \text{Eq. AA1-2}$$

For Case 2, the closed form solution for a flexural cantilever member is:

$$M_{\max}(@\,x=0)=M_o\left[\frac{\tan\alpha}{\alpha}\right] \qquad \alpha=\sqrt{\frac{NL^2}{EI}}, M_o=HL \qquad \text{Eq. AA1-3}$$

$$y_{\max}(@\,x=L)=y_o\left[\frac{3(\tan\alpha-\alpha)}{\alpha^3}\right] \qquad y_o=\frac{HL^3}{3EI} \qquad \text{Eq. AA1-4}$$

Appendix B: Effects of different analysis options

1) Model Configurations

The first benchmark model is a vertical cantilever column which is free at top but fixed at bottom as shown in Figure AB–1. A lateral force, *H*, of 120kN and a compression axial force, *N*, of 3000kN are applied at top of the column. The column length, *L*, is 3m. The column section is 310UC137.

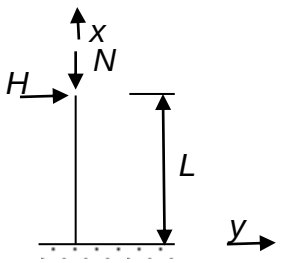

Figure AB–1: Cantilever Column with Fixed Based

2) Descriptions of analysis case

Table AB–1: Summary of analysis options for each case

Case Name	Geometric Transformation	System Equation	Constraints	Algorithm
Control case	Corotational	BandGeneral	Transformation	ModifiedNewton
1	Corotational	BandGeneral	Plain	Linear
2	Corotational	BandGeneral	Plain	Newton
3	Corotational	BandGeneral	Plain	ModifiedNewton
4	Corotational	BandGeneral	Transformation	Linear
5	Corotational	BandGeneral	Transformation	Newton
6	Corotational	BandSPD	Plain	Linear
7	Corotational	BandSPD	Plain	Newton
8	Corotational	BandSPD	Plain	ModifiedNewton
9	Corotational	BandSPD	Transformation	Linear
10	Corotational	BandSPD	Transformation	Newton
11	Corotational	BandSPD	Transformation	ModifiedNewton
12	Corotational	UmfPack	Plain	Linear
13	Corotational	UmfPack	Plain	Newton
14	Corotational	UmfPack	Plain	ModifiedNewton
15	Corotational	UmfPack	Transformation	Linear

16	Corotational	UmfPack	Transformation	Newton
17	Corotational	UmfPack	Transformation	ModifiedNewton

3) Descriptions of analysis case

Table AB–2: Results for each analysis case

Case	Top Node Displacement (mm)	Difference to Control case (%)	Base Moment (kNm)	Difference to Control case (%)
Control Case	7.76322	-	165.439	-
1	7.76321	-0.00013	165.437	-0.00121
2	7.76332	0.0013	165.439	0.00000
3	7.76322	0.0000	165.439	0.00000
4	7.76321	-0.00013	165.437	-0.00121
5	7.76332	0.0013	165.439	0.00000
6	7.76321	-0.00013	165.437	-0.00121
7	7.76332	0.0013	165.439	0.00000
8	7.76322	0.0000	165.439	0.00000
9	7.76321	-0.00013	165.437.	-0.00121
10	7.76332	0.0013	165.439	0.00000
11	7.76322	0.0000	165.439	0.00000
12	7.76321	-0.00013	165.437	-0.00121
13	7.76332	0.0013	165.439	0.00000
14	7.76322	0.0000	165.439	0.00000
15	7.76321	-0.00013	165.437	-0.00121
16	7.76332	0.0013	165.439	0.00000
17	7.76322	0	165.439	0.00000

Appendix C: OpenSEES inputs Codes

C1: Codes for linear initial residual stress distribution

```
proc UCsection { secID fy d bf tf tw rs}
#####################################################################
      # UCsection  $secID $fy $d $bf $tf $tw $rs
      #
#####################################################################
      # create a standard UC/UB section given the nominal section
properties
      # written: Arthur Lu
      # date: 21/01/10
      # input parameters
      # secID - section ID number
      # fy = steel yielding strength
      # d  = nominal depth
      # tw = web thickness
      # bf = flange width
      # tf = flange thickness
      # rs = maximum residual stress value
# General information
set resc [expr -($rs*$fy)] # negative residual stress at tip flange and
central of web
set rest [expr $rs*$fy] # postive residual stress at flange centre and
tip of web
set resab [expr (-$resc)+$rest] # absolute value between negative and
positive
set fl 8 # number of flange discretization
set w [expr ($bf-$tw)/($fl*2)]
set s [expr ($d-2*$tf)/($fl*2+1)]
set nfe 5 # number of fibers in element
set E 200000.000
set r 20.000
set b 0.000
# Coordinations for setting sections
set tt [expr $d/2]
set tb [expr $d/2-$tf]
set bt [expr -($d/2-$tf)]
set bb [expr -($d/2)]
set ll [expr -($tw/2)]
set rr [expr $tw/2]
set gf [expr $resab/($bf/2)]
set gw [expr $resab/(($d-$tf)/2)]
# Material definition $Type $Hloop $Tag $fy $E $b $r0 $cR1 $cR2
$hardening 4 parameters $Residualstress
for {set matf 1 } {$matf <= $fl} {incr matf 1 } {
uniaxialMaterial Steel02 [expr $matf+$secID*100] $fy $E $b $r 0.925
0.15 0.0 1.0 0.0 1.0 [expr -($gf*($tw/2+($fl-$matf+0.5)*$w)-$rest)]
}# Flange Materials
for {set matw 0} {$matw <= [expr $fl-1]} {incr matw 1} {
uniaxialMaterial Steel02 [expr $matw+$fl+2+$secID*100] $fy $E $b $r
0.925 0.15 0.0 1.0 0.0 1.0 [expr (($gw*($fl-$matw)*$s)-$rest)]
```

```
}# Web Materials
uniaxialMaterial Steel02 [expr $fl+1+$secID*100] $fy $E $b $r 0.925
0.15 0.0 1.0 0.0 1.0 $rest # web and flange joint
uniaxialMaterial Steel02 [expr $fl*2+2+$secID*100] $fy $E $b $r 0.925
0.15 0.0 1.0 0.0 1.0 $resc # centre of web
section Fiber $secID {
# Section definition $Material $nfIJ $nfJK $yI $zI $yJ $zJ $yK $zK $yL
$zL
for {set ee 0} {$ee <= [expr $fl-2]} {incr ee 1} {
patch quadr [expr $ee+1+$secID*100] $nfe $nfe $bb [expr $bf/2-
($ee+1)*$w] $bt [expr $bf/2-($ee+1)*$w] $bt [expr $bf/2-$ee*$w] $bb
[expr $bf/2-$ee*$w] # Upper left flange
patch quadr [expr $ee+1+$secID*100] $nfe $nfe $bb [expr -($bf/2-
$ee*$w)] $bt [expr -($bf/2-$ee*$w)] $bt [expr -($bf/2-($ee+1)*$w)] $bb
[expr -($bf/2-($ee+1)*$w)] # lower left flange
patch quadr [expr $ee+1+$secID*100] $nfe $nfe $tb [expr $bf/2-
($ee+1)*$w] $tt [expr $bf/2-($ee+1)*$w] $tt [expr $bf/2-$ee*$w] $tb
[expr $bf/2-$ee*$w] # upper right flange
patch quadr [expr $ee+1+$secID*100] $nfe $nfe $tb [expr -($bf/2-
$ee*$w)] $tt [expr -($bf/2-$ee*$w)] $tt [expr -($bf/2-($ee+1)*$w)] $tb
[expr -($bf/2-($ee+1)*$w)] # lower right flange}
patch quadr [expr $ee+1+$secID*100] $nfe $nfe $bb $rr $bt $rr $bt [expr
$bf/2-($ee)*$w] $bb [expr $bf/2-($ee)*$w] # Upper left flange
patch quadr [expr $ee+1+$secID*100] $nfe $nfe $bb [expr -($bf/2-
($ee)*$w)] $bt [expr -($bf/2-($ee)*$w)] $bt $ll $bb $ll# lower left
flange
# upper right flange
patch quadr [expr $ee+1+$secID*100] $nfe $nfe $tb $rr $tt $rr $tt [expr
$bf/2-($ee)*$w] $tb [expr $bf/2-($ee)*$w]
# lower right flange
patch quadr [expr $ee+1+$secID*100] $nfe $nfe $tb [expr -($bf/2-
($ee)*$w)] $tt [expr -($bf/2-($ee)*$w)] $tt $ll $tb $ll
patch quadr [expr $fl+1+$secID*100] $nfe $nfe $bb $ll $bt $ll $bt $rr
$bb $rr
# web
for {set ww 0} {$ww <= [expr $fl-1]} {incr ww 1} {
patch quadr [expr $ww+$fl+2+$secID*100] $nfe $nfe [expr $bt+$ww*$s] $ll
[expr $bt+($ww+1)*$s] $ll [expr $bt+($ww+1)*$s] $rr [expr $bt+$ww*$s]
$rr
patch quadr [expr $ww+$fl+2+$secID*100] $nfe $nfe [expr $tb-($ww+1)*$s]
$ll [expr $tb-$ww*$s] $ll [expr $tb-$ww*$s] $rr [expr $tb-($ww+1)*$s]
$rr
}
patch quadr [expr $fl*2+2+$secID*100] $nfe $nfe [expr $bt+$fl*$s] $ll
[expr $tb-$fl*$s] $ll [expr $tb-$fl*$s] $rr [expr $bt+$fl*$s] $rr
# Flange web joints
patch quadr [expr $fl+1+$secID*100] $nfe $nfe $tb $ll $tt $ll $tt $rr
$tb $rr
}
```

C2: Codes for constant initial residual stress distribution

```
proc UCsection2 { secID fy d bf tf tw rs} {
#####################################################################
      # UCsection  $secID $fy $d $bf $tf $tw $rs
      #
#####################################################################
      # create a standard UC/UB section given the nominal section
properties
      # written: Arthur Lu
      # date: 21/01/10
      # input parameters
      # secID - section ID number
      # fy = steel yielding strength
      # d  = nominal depth
      # tw = web thickness
      # bf = flange width
      # tf = flange thickness
      # rs = maximum residual stress value
# General information
set resc [expr -($rs*$fy)] # negative residual stress at tip flange and
central of web
set rest [expr $rs*$fy] # postive residual stress at flange centre and
tip of web
set resab [expr (-$resc)+$rest] # absolute value between negative and
positive
set fl 8 # number of flange discretization
set w [expr ($bf-$tw)/($fl*2)]
set s [expr ($d-2*$tf)/($fl*2+1)]
set nfe 5 # number of fibers in element
set E 200000.000
set r 20.000
set b 0.000
# Coordinations for setting sections
set tt [expr $d/2]
set tb [expr $d/2-$tf]
set bt [expr -($d/2-$tf)]
set bb [expr -($d/2)]
set ll [expr -($tw/2)]
set rr [expr $tw/2]
set gf [expr $resab/($bf/2)]
set gw [expr $resab/(($d-$tf)/2)]

# Material definition $Type $Hloop $Tag $fy $E $b $r0 $cR1 $cR2
$hardening 4 parameters $Residualstress
 # Flange Materials
uniaxialMaterial Steel02 101 $fy $E $b $r 0.925 0.15 0.0 1.0 0.0 1.0
$rest
uniaxialMaterial Steel02 102 $fy $E $b $r 0.925 0.15 0.0 1.0 0.0 1.0
$resc

section Fiber $secID {
# Section definition $Material $nfIJ $nfJK $yI $zI $yJ $zJ $yK $zK
$yL $zL
```

```
# Upper left flange Compression
for {set ee 0} {$ee <= 3} {incr ee 1} {
patch quadr 102 $nfe $nfe $bb [expr $bf/2-($ee+1)*$w] $bt [expr
$bf/2-($ee+1)*$w] $bt [expr $bf/2-$ee*$w] $bb [expr $bf/2-$ee*$w]
# Upper left flange tension
patch quadr 101 $nfe $nfe $bb [expr $bf/2-($ee+5)*$w] $bt [expr
$bf/2-($ee+5)*$w] $bt [expr $bf/2-($ee+4)*$w] $bb [expr $bf/2-
($ee+4)*$w]

# lower left flange Compression
patch quadr 102 $nfe $nfe $bb [expr -($bf/2-$ee*$w)] $bt [expr -
($bf/2-$ee*$w)] $bt [expr -($bf/2-($ee+1)*$w)] $bb [expr -($bf/2-
($ee+1)*$w)]

# lower left flange tension
patch quadr 101 $nfe $nfe $bb [expr -($bf/2-($ee+4)*$w)] $bt [expr -
($bf/2-($ee+4)*$w)] $bt [expr -($bf/2-($ee+5)*$w)] $bb [expr -
($bf/2-($ee+5)*$w)]

# upper right flange compression
patch quadr 102 $nfe $nfe $tb [expr $bf/2-($ee+1)*$w] $tt [expr
$bf/2-($ee+1)*$w] $tt [expr $bf/2-($ee)*$w] $tb [expr $bf/2-
($ee)*$w]

# upper right flange tension
patch quadr 101 $nfe $nfe $tb [expr $bf/2-($ee+5)*$w] $tt [expr
$bf/2-($ee+5)*$w] $tt [expr $bf/2-($ee+4)*$w] $tb [expr $bf/2-
($ee+4)*$w]

# lower right flange compression
patch quadr 102 $nfe $nfe $tb [expr -($bf/2-$ee*$w)] $tt [expr -
($bf/2-$ee*$w)] $tt [expr -($bf/2-($ee+1)*$w)] $tb [expr -($bf/2-
($ee+1)*$w)]

# lower right flange tension
patch quadr 101 $nfe $nfe $tb [expr -($bf/2-($ee+4)*$w)] $tt [expr -
($bf/2-($ee+4)*$w)] $tt [expr -($bf/2-($ee+5)*$w)] $tb [expr -
($bf/2-($ee+5)*$w)]
}
# web
for {set ww 0} {$ww <= 3} {incr ww 1} {
# Left
patch quadr 102 $nfe $nfe [expr $bt+$ww*$s] $ll [expr
$bt+($ww+1)*$s] $ll [expr $bt+($ww+1)*$s] $rr [expr $bt+$ww*$s] $rr
patch quadr 101 $nfe $nfe [expr $bt+($ww+4)*$s] $ll [expr
$bt+($ww+5)*$s] $ll [expr $bt+($ww+5)*$s] $rr [expr $bt+($ww+4)*$s]
$rr
# Right
patch quadr 102 $nfe $nfe [expr $tb-($ww+1)*$s] $ll [expr $tb-
$ww*$s] $ll [expr $tb-$ww*$s] $rr [expr $tb-($ww+1)*$s] $rr
patch quadr 101 $nfe $nfe [expr $tb-($ww+5)*$s] $ll [expr $tb-
($ww+4)*$s] $ll [expr $tb-($ww+4)*$s] $rr [expr $tb-($ww+5)*$s] $rr
}
}
}
```

C3: Code for model used in Column curves matching

```
# OpenSees
# code for IRS matching
# Model Descriptions:
# A column with pinned base and roller at top
# subjected to an axial compression force at top
# with initial delfection at mid of the column
# Units: N, mm, s
# -------------------------
# Start of model generation
# -------------------------
# Create ModelBuider (with two-dimensions and 2 DOF/nods)
for {set m 2} {$m <= 30} {incr m 2} {
wipe
model BasicBuilder -ndm 2 -ndf 3
source UCsection.tcl
# Create nodes & add to Domain -  Command: node nodeID xCrd yCrd
set l [expr $m*1000.000]
puts $l
set sg 8
set sl [expr $l/$sg]
set ios [expr $l/1000.000]
set pi 3.141592654
for {set n 0} {$n <= [expr $sg-1]} {incr n 1 } {
node $n [expr $ios*sin($sl*$n/$l*$pi)] [expr $sl*$n]
}
node $sg 0.0 $l
# Set the boundary conditions - command: fix nodeID xResrnt?
yResrnt?
fix 0 1 1 0
fix $sg 1 0 0
# Define Geometric Transformation $TransTag
      geomTransf Corotational 1

# Define materials for truss elements
#-------------------------------
set coln 1
# Define Section using 310UC137
set d 321.0000
set bf 309.0000
set tf 21.7000
set tw 13.8000
set fy 300.0000
# Define residual stress ratio, gamma
set rs 0.7000
UCsection $coln $fy $d $bf $tf $tw $rs
# Define elements
#---------------------
# Create nonlinear elements - command: element NBC <ID node1 node2
Intpoint sectag $TransTag>
for {set q 1} {$q <= $sg} {incr q 1 } {
element nonlinearBeamColumn $q [expr $q-1] $q 5 1 1
}
#-------------------------
# Start of recorder generation
#-------------------------
#--------Recording file-----------------
```

```
recorder Node -file rect0$l.out -time -node 0 -dof 1 2 3 reaction
recorder Node -file disp0$l.out -time -node 5 -dof 1 2 3 disp

# Define loads
#-----------------------
# Create a Plain load pattern with a linear TimeSeries
pattern Plain 1 Linear {

#Create the load - command: load nodeID xForce(N) yForce(N)
load $sg 0.0 -1000.000 0.0
}

#-------------------------------------
# End of model generation
#-------------------------------------
# Start of analysis generation
#-------------------------------------
#----------system-----------------------
      system BandGeneral
#--------DOF numberer-------------------
      numberer RCM
#--------Constraints--------------------
      constraints Transformation
#--------Convergence test---------------
      test NormDispIncr 1.0e-6 30 0
#--------Integrator---------------------
      integrator LoadControl 1
#--------Algorithm----------------------
      algorithm ModifiedNewton

#--------Analysis scheme----------------
# Perform the analysis
analysis Static
analyze 6000

puts "End of Analysis"
#-------------------------
# End of analysis
#-------------------------
}
```

C4: Model 1: Single cantilever column with gravity load analysis

```
# Model 1
# Single Member Behaviour
# |
# |    3.2m
# |
# fix support
#
# Units: N, mm, s
# -------------------------
# Start of model generation
# -------------------------
# Create ModelBuider (with two-dimensions and 2 DOF/nods)
wipe

model BasicBuilder -ndm 2 -ndf 3
source UCsectionhm.tcl

# Create nodes & add to Domain -  Command: node nodeID xCrd yCrd
set sl [expr 3200.000/8.000]

#LH Col
node 1 0.000 0.000
node 2 0.000 [expr $sl*1.000]
node 3 0.000 [expr $sl*2.000]
node 4 0.000 [expr $sl*3.000]
node 5 0.000 [expr $sl*4.000]
node 6 0.000 [expr $sl*5.000]
node 7 0.000 [expr $sl*6.000]
node 8 0.000 [expr $sl*7.000]
node 9 0.000 [expr $sl*8.000]

# Set the boundary conditions - command: fix nodeID xResrnt?
yResrnt?
fix 1 1 1 1

# Define Geometric Transformation $TransTag
#geomTransf Linear 1
#geomTransf PDelta 1
geomTransf Corotational 1

# Define materials for truss elements
#------------------------------
# General Property (Yield stress and Residual stress)
set rs 0.000
set fy 300.000

# Define Section for Column (200UC59.5)
set d1 210.000
set bf1 205.000
set tf1 14.200
set tw1 9.300
UCsectionhm 1 $fy $d1 $bf1 $tf1 $tw1 $rs

# Define elements
#---------------------
```

```
#Create nonlinear elements - command: element NBC <ID node1 node2
Intpoint sectag $TransTag>
element nonlinearBeamColumn 1 1 2 5 1 1
element nonlinearBeamColumn 2 2 3 5 1 1
element nonlinearBeamColumn 3 3 4 5 1 1
element nonlinearBeamColumn 4 4 5 5 1 1
element nonlinearBeamColumn 5 5 6 5 1 1
element nonlinearBeamColumn 6 6 7 5 1 1
element nonlinearBeamColumn 7 7 8 5 1 1
element nonlinearBeamColumn 8 8 9 5 1 1

# Define loads
#------------------------
# Create a Plain load pattern with a linear TimeSeries
pattern Plain 1 "Linear" {

#Create the load - command: load nodeID xForce(N) yForce(N)
load 9 0.000 0.000 0.000
}

#-------------------------------------
# End of model generation
#-------------------------------------
# Start of analysis generation
#-------------------------------------
#----------system-----------------------
      system BandGeneral
#--------DOF numberer-------------------
      numberer RCM
#--------Constraints--------------------
      constraints Transformation
#--------Convergence test---------------
      test NormDispIncr 1.0e-8 30 0
#--------Integrator---------------------
      integrator LoadControl 0.001
#--------Algorithm----------------------
      algorithm ModifiedNewton
#--------Analysis scheme----------------
# Perform the analysis
analysis Static
analyze 1000

puts "End of Gravity Analysis"
#--------------------------
# End of analysis
#--------------------------
loadConst -time 0.0

#--------------------------
# Start of recorder generation
#--------------------------
#--------Recording file-----------------
recorder Node -file dispr0n0.out -time -node 9 -dof 1 disp
recorder Node -file resr0n0.out -time -node 1 -dof 1 2 3 reaction
```

C5: Model 2: Three-story single-bay frame with gravity load analysis

```
# Model 2
# 3-storey single-bay structure
# Width: 4.6m
# Storey height: 3.05m
# Units: N, mm, s
# -------------------------
# Start of model generation
# -------------------------
# Create ModelBuider (with two-dimensions and 2 DOF/nods)
wipe
model BasicBuilder -ndm 2 -ndf 3
source UCsection.tcl
# Create nodes & add to Domain -  Command: node nodeID xCrd yCrd
set slc [expr 3050.000/8.000]
set slb [expr 4600.000/16.000]
set res 0.000
#LH Col - Level 1
node 1 0.000 0.000
node 3 0.0 [expr $slc*1.000]
node 5 0.0 [expr $slc*2.000]
node 7 0.0 [expr $slc*3.000]
node 9 0.0 [expr $slc*4.000]
node 11 0.0 [expr $slc*5.000]
node 13 0.0 [expr $slc*6.000]
node 15 0.0 [expr $slc*7.000]
node 17 0.0 [expr $slc*8.000]
#LH Col - Level 2
node 34 0.0 [expr $slc*9.000]
node 36 0.0 [expr $slc*10.000]
node 38 0.0 [expr $slc*11.000]
node 40 0.0 [expr $slc*12.000]
node 42 0.0 [expr $slc*13.000]
node 44 0.0 [expr $slc*14.000]
node 46 0.0 [expr $slc*15.000]
node 48 0.0 [expr $slc*16.000]
#LH Col - Level 3
node 65 0.0 [expr $slc*17.000]
node 67 0.0 [expr $slc*18.000]
node 69 0.0 [expr $slc*19.000]
node 71 0.0 [expr $slc*20.000]
node 73 0.0 [expr $slc*21.000]
node 75 0.0 [expr $slc*22.000]
node 77 0.0 [expr $slc*23.000]
node 79 0.0 [expr $slc*24.000]
#Beam - Level 1
node 18 [expr $slb*1.000] 3050.000
node 19 [expr $slb*2.000] 3050.000
node 20 [expr $slb*3.000] 3050.000
node 21 [expr $slb*4.000] 3050.000
node 22 [expr $slb*5.000] 3050.000
node 23 [expr $slb*6.000] 3050.000
node 24 [expr $slb*7.000] 3050.000
node 25 [expr $slb*8.000] 3050.000
node 26 [expr $slb*9.000] 3050.000
node 27 [expr $slb*10.000] 3050.000
node 28 [expr $slb*11.000] 3050.000
```

```
node 29 [expr $slb*12.000] 3050.000
node 30 [expr $slb*13.000] 3050.000
node 31 [expr $slb*14.000] 3050.000
node 32 [expr $slb*15.000] 3050.000
#Beam - Level 2
node 49 [expr $slb*1.000] 6100.000
node 50 [expr $slb*2.000] 6100.000
node 51 [expr $slb*3.000] 6100.000
node 52 [expr $slb*4.000] 6100.000
node 53 [expr $slb*5.000] 6100.000
node 54 [expr $slb*6.000] 6100.000
node 55 [expr $slb*7.000] 6100.000
node 56 [expr $slb*8.000] 6100.000
node 57 [expr $slb*9.000] 6100.000
node 58 [expr $slb*10.000] 6100.000
node 59 [expr $slb*11.000] 6100.000
node 60 [expr $slb*12.000] 6100.000
node 61 [expr $slb*13.000] 6100.000
node 62 [expr $slb*14.000] 6100.000
node 63 [expr $slb*15.000] 6100.000
#Beam LHS - Level 3
node 80 [expr $slb*1.000] 9150.000
node 81 [expr $slb*2.000] 9150.000
node 82 [expr $slb*3.000] 9150.000
node 83 [expr $slb*4.000] 9150.000
node 84 [expr $slb*5.000] 9150.000
node 85 [expr $slb*6.000] 9150.000
node 86 [expr $slb*7.000] 9150.000
node 87 [expr $slb*8.000] 9150.000
node 88 [expr $slb*9.000] 9150.000
node 89 [expr $slb*10.000] 9150.000
node 90 [expr $slb*11.000] 9150.000
node 91 [expr $slb*12.000] 9150.000
node 92 [expr $slb*13.000] 9150.000
node 93 [expr $slb*14.000] 9150.000
node 94 [expr $slb*15.000] 9150.000
#RH Col - Level 1
node 2 4600.000 0.000
node 4 4600.000 [expr $slc*1.000]
node 6 4600.000 [expr $slc*2.000]
node 8 4600.000 [expr $slc*3.000]
node 10 4600.000 [expr $slc*4.000]
node 12 4600.000 [expr $slc*5.000]
node 14 4600.000 [expr $slc*6.000]
node 16 4600.000 [expr $slc*7.000]
node 33 4600.000 [expr $slc*8.000]
#RH Col - Level 2
node 35 4600.000 [expr $slc*9.000]
node 37 4600.000 [expr $slc*10.000]
node 39 4600.000 [expr $slc*11.000]
node 41 4600.000 [expr $slc*12.000]
node 43 4600.000 [expr $slc*13.000]
node 45 4600.000 [expr $slc*14.000]
node 47 4600.000 [expr $slc*15.000]
node 64 4600.000 [expr $slc*16.000]
#RH Col - Level 3
node 66 4600.000 [expr $slc*17.000]
```

```
node 68 4600.000 [expr $slc*18.000]
node 70 4600.000 [expr $slc*19.000]
node 72 4600.000 [expr $slc*20.000]
node 74 4600.000 [expr $slc*21.000]
node 76 4600.000 [expr $slc*22.000]
node 78 4600.000 [expr $slc*23.000]
node 95 4600.000 [expr $slc*24.000]
# Set the boundary conditions - command: fix nodeID xResrnt?
yResrnt?
fix 1 1 1 1
fix 2 1 1 1
# Define Geometric Transformation $TransTag
geomTransf Corotational 1
# Define materials for truss elements
#-------------------------------
# Beam Property (460UB67.1)
set brs $res
set bfy 300.000
set bd 454.000
set bbf 190.000
set btf 12.700
set btw 8.500
UCsectionhm 1 $bfy $bd $bbf $btf $btw $brs
# Column Property (200UC59.5)
set crs $res
set cfy 300.00
set cd 210.00
set cbf 205.00
set ctf 14.20
set ctw 9.30
UCsectionhm 2 $cfy $cd $cbf $ctf $ctw $crs
# Define elements
#---------------------
#Create nonlinear elements - command: element NBC <ID node1 node2
Intpoint sectag $TransTag>
#LH Col - Level 1
element nonlinearBeamColumn 1 1 3 5 2 1
element nonlinearBeamColumn 2 3 5 5 2 1
element nonlinearBeamColumn 3 5 7 5 2 1
element nonlinearBeamColumn 4 7 9 5 2 1
element nonlinearBeamColumn 5 9 11 5 2 1
element nonlinearBeamColumn 6 11 13 5 2 1
element nonlinearBeamColumn 7 13 15 5 2 1
element nonlinearBeamColumn 8 13 17 5 2 1
#LH Col - Level 2
element nonlinearBeamColumn 9 17 34 5 2 1
element nonlinearBeamColumn 10 34 36 5 2 1
element nonlinearBeamColumn 11 36 38 5 2 1
element nonlinearBeamColumn 12 38 40 5 2 1
element nonlinearBeamColumn 13 40 42 5 2 1
element nonlinearBeamColumn 14 42 44 5 2 1
element nonlinearBeamColumn 15 44 46 5 2 1
element nonlinearBeamColumn 16 46 48 5 2 1
#LH Col - Level 3
element nonlinearBeamColumn 17 48 65 5 2 1
element nonlinearBeamColumn 18 65 67 5 2 1
element nonlinearBeamColumn 19 67 69 5 2 1
```

```
element nonlinearBeamColumn 20 69 71 5 2 1
element nonlinearBeamColumn 21 71 73 5 2 1
element nonlinearBeamColumn 22 73 75 5 2 1
element nonlinearBeamColumn 23 75 77 5 2 1
element nonlinearBeamColumn 24 77 79 5 2 1
#RH Col - Level 1
element nonlinearBeamColumn 25 2 4 5 2 1
element nonlinearBeamColumn 26 4 6 5 2 1
element nonlinearBeamColumn 27 6 8 5 2 1
element nonlinearBeamColumn 28 8 10 5 2 1
element nonlinearBeamColumn 29 10 12 5 2 1
element nonlinearBeamColumn 30 12 14 5 2 1
element nonlinearBeamColumn 31 14 16 5 2 1
element nonlinearBeamColumn 32 16 33 5 2 1
#RH Col - Level 2
element nonlinearBeamColumn 33 33 35 5 2 1
element nonlinearBeamColumn 34 35 37 5 2 1
element nonlinearBeamColumn 35 37 39 5 2 1
element nonlinearBeamColumn 36 39 41 5 2 1
element nonlinearBeamColumn 37 41 43 5 2 1
element nonlinearBeamColumn 38 43 45 5 2 1
element nonlinearBeamColumn 39 45 47 5 2 1
element nonlinearBeamColumn 40 47 64 5 2 1
#RH Col - Level 3
element nonlinearBeamColumn 41 64 66 5 2 1
element nonlinearBeamColumn 42 66 68 5 2 1
element nonlinearBeamColumn 43 68 70 5 2 1
element nonlinearBeamColumn 44 70 72 5 2 1
element nonlinearBeamColumn 45 72 74 5 2 1
element nonlinearBeamColumn 46 74 76 5 2 1
element nonlinearBeamColumn 47 76 78 5 2 1
element nonlinearBeamColumn 48 78 95 5 2 1
#Beam - Level 1
element nonlinearBeamColumn 49 17 18 5 1 1
element nonlinearBeamColumn 50 18 19 5 1 1
element nonlinearBeamColumn 51 19 20 5 1 1
element nonlinearBeamColumn 52 20 21 5 1 1
element nonlinearBeamColumn 53 21 22 5 1 1
element nonlinearBeamColumn 54 22 23 5 1 1
element nonlinearBeamColumn 55 23 24 5 1 1
element nonlinearBeamColumn 56 24 25 5 1 1
element nonlinearBeamColumn 57 25 26 5 1 1
element nonlinearBeamColumn 58 26 27 5 1 1
element nonlinearBeamColumn 59 27 28 5 1 1
element nonlinearBeamColumn 60 28 29 5 1 1
element nonlinearBeamColumn 61 29 30 5 1 1
element nonlinearBeamColumn 62 30 31 5 1 1
element nonlinearBeamColumn 63 31 32 5 1 1
element nonlinearBeamColumn 64 32 33 5 1 1
#Beam - Level 2
element nonlinearBeamColumn 65 48 49 5 1 1
element nonlinearBeamColumn 66 49 50 5 1 1
element nonlinearBeamColumn 67 50 51 5 1 1
element nonlinearBeamColumn 68 51 52 5 1 1
element nonlinearBeamColumn 69 52 53 5 1 1
element nonlinearBeamColumn 70 53 54 5 1 1
element nonlinearBeamColumn 71 54 55 5 1 1
```

```
element nonlinearBeamColumn 72 55 56 5 1 1
element nonlinearBeamColumn 73 56 57 5 1 1
element nonlinearBeamColumn 74 57 58 5 1 1
element nonlinearBeamColumn 75 58 59 5 1 1
element nonlinearBeamColumn 76 59 60 5 1 1
element nonlinearBeamColumn 77 60 61 5 1 1
element nonlinearBeamColumn 78 61 62 5 1 1
element nonlinearBeamColumn 79 62 63 5 1 1
element nonlinearBeamColumn 80 63 64 5 1 1
#Beam - Level 3
element nonlinearBeamColumn 81 79 80 5 1 1
element nonlinearBeamColumn 82 80 81 5 1 1
element nonlinearBeamColumn 83 81 82 5 1 1
element nonlinearBeamColumn 84 82 83 5 1 1
element nonlinearBeamColumn 85 83 84 5 1 1
element nonlinearBeamColumn 86 84 85 5 1 1
element nonlinearBeamColumn 87 85 86 5 1 1
element nonlinearBeamColumn 88 86 87 5 1 1
element nonlinearBeamColumn 89 87 88 5 1 1
element nonlinearBeamColumn 90 88 89 5 1 1
element nonlinearBeamColumn 91 89 90 5 1 1
element nonlinearBeamColumn 92 90 91 5 1 1
element nonlinearBeamColumn 93 91 92 5 1 1
element nonlinearBeamColumn 94 92 93 5 1 1
element nonlinearBeamColumn 95 93 94 5 1 1
element nonlinearBeamColumn 96 94 95 5 1 1
# Define loads
#-----------------------
# Create a Plain load pattern with a linear TimeSeries
pattern Plain 1 "Linear" {
#Create the load - command: load nodeID xForce(N) yForce(N)
load 17 0.00 -450000.000 0.000
load 33 0.00 -450000.000 0.000
load 48 0.00 -450000.000 0.000
load 64 0.00 -450000.000 0.000
load 79 0.00 -450000.000 0.000
load 95 0.00 -450000.000 0.000
for {set na 18} {$na <= 32} {incr na 1} {
load $na 0.000 -9200.000 0.000
}
for {set nb 49} {$nb <= 63} {incr nb 1} {
load $nb 0.000 -9200.000 0.000
}
for {set nc 80} {$nc <= 94} {incr nc 1} {
load $nc 0.000 -9200.000 0.000
}
}
system BandGeneral
numberer RCM
constraints Transformation
test NormDispIncr 1.0e-8 30 0
integrator LoadControl 0.001
algorithm ModifiedNewton
analysis Static
analyze 1000
remove recorders
loadConst -time 0.0
```

C6: Code for performing pushover analysis

```
#For model1:
pattern Plain 2 Linear {;               # define load pattern
load 9 1000.00 0.000 0.000
};         # end load pattern
```

```
 For Model 2
 # -- STATIC PUSHOVER/CYCLIC ANALYSIS
 set h 1000.000
 set hr 500.000
 # create load pattern for lateral pushover load coefficient when
 using linear load pattern
 pattern Plain 2 Linear {;              # define load pattern
 load 17 $h 0.000 0.000
 load 48 $h 0.000 0.000
 load 79 $hr 0.000 0.000
 };
#-------------------------------------
# Start of analysis generation
#-------------------------------------
#----------system-----------------------
      system BandGeneral
#--------DOF numberer-------------------
      numberer RCM
#--------Constraints--------------------
      constraints Transformation
#--------Convergence test---------------
      test NormDispIncr 1.0e-8 30 0
#--------Integrator---------------------
      integrator LoadControl 0.001
#--------Algorithm----------------------
      algorithm ModifiedNewton
#--------Analysis scheme----------------
# Perform the analysis
analysis Static
analyze 70000

puts "End of left to right Analysis"
```

C7: Code for performing push-pull analysis

Main File: Run all

```
source Model1.tcl   <= this is the model file given in B4 or B5
source Displcontrolcyc.tcl
```

Sub-file 1: Displcontrolcyc.tcl

```
# ------------------------------------------------------------------
--------------------------------
# Example 5. 2D Frame --  Static Reversed Cyclic Analysis
#     by    Silvia Mazzoni & Frank McKenna, 2006 # source in
procedures
source GeneratePeaks.tcl;
set iDmax "0.011 0.011 0.01375 0.0165 0.01925 0.022 0.022";    #
vector of displacement-cycle peaks, in terms of storey drift ratio
set Fact [expr $sl*8.000];              # scale drift ratio by
storey height for displacement cycles
set Dincr [expr 0.011*$sl/50.000];# displacement increment for
pushover. you want this to be very small, but not too small to slow
analysis
set CycleType Full;                # you can do Full / Push / Half
cycles with the proc
set Ncycles 1;                # specify the number of cycles at each
peak
# -- STATIC PUSHOVER/CYCLIC ANALYSIS
# create load pattern for lateral pushover load coefficient when
using linear load pattern
pattern Plain 2 "Linear" {
#Create the load - command: load nodeID xForce(N) yForce(N)
load 9 1000.00 0.000 0.000
}
# ----------- set up analysis parameters
source LibAnalysisStaticParameters.tcl; #
set fmt1 "%s Cyclic analysis: CtrlNode %.3i, dof %.1i, Disp=%.4f";

# format for screen/file output of DONE/PROBLEM analysis
foreach Dmax $iDmax {
      set iDstep [GeneratePeaks $Dmax $Dincr $CycleType $Fact];
# this proc is defined above
      for {set i 1} {$i <= $Ncycles} {incr i 1} {
            set zeroD 0
            set D0 0.0
            foreach Dstep $iDstep {
                  set D1 $Dstep
                  set Dincr [expr $D1 - $D0]
                  integrator DisplacementControl  $IDctrlNode
$IDctrlDOF $Dincr
                  analysis Static
# -------------------first analyze command-----------------------
                  set ok [analyze 1]
# ----------------if convergence failure-----------------------
if {$ok != 0} {
                        if {$ok != 0} {
                              puts "Trying Newton with Initial
Tangent .."
                              test NormDispIncr   1.00e-8 2000 0
                              algorithm Newton -initial
```

```
                              set ok [analyze 1]
                              test $testTypeStatic $TolStatic
$maxNumIterStatic    0
                              algorithm $algorithmTypeStatic
                        }
                        if {$ok != 0} {
                              puts "Trying Broyden .."
                              algorithm Broyden 8
                              set ok [analyze 1 ]
                              algorithm $algorithmTypeStatic
                        }
                        if {$ok != 0} {
                              puts "Trying NewtonWithLineSearch .."
                              algorithm NewtonLineSearch 0.8
                              set ok [analyze 1]
                              algorithm $algorithmTypeStatic
                        }
                        if {$ok != 0} {
                              set putout [format $fmt1 "PROBLEM"
$IDctrlNode $IDctrlDOF [nodeDisp $IDctrlNode $IDctrlDOF]]
                              puts $putout
                              return -1
                        }; # end if
                  }; # end if
                  # -------------------------------------------------
--------------------------------------------------
                  set D0 $D1;
# move to next step
            }; # end Dstep
      };          # end i
};    # end of iDmaxCycl
# ------------------------------------------------------------------
----------------------------------
if {$ok != 0 } {
      puts [format $fmt1 "PROBLEM" $IDctrlNode $IDctrlDOF [nodeDisp
$IDctrlNode $IDctrlDOF]]
} else {
      puts [format $fmt1 "DONE"  $IDctrlNode $IDctrlDOF [nodeDisp
$IDctrlNode $IDctrlDOF]]
}
```

Sub-file 2: GeneratePeaks.tcl

```
proc GeneratePeaks {Dmax {DincrStatic 0.01} {CycleType "Full"} {Fact
1} } {;
# by Silvia Mazzoni, 2006
      file mkdir data
      set outFileID [open data/tmpDsteps.tcl w]
      set Disp 0.
      puts $outFileID "set iDstep { ";puts $outFileID $Disp;puts
$outFileID $Disp;# open vector definition and some 0
      set Dmax [expr $Dmax*$Fact]; # scale value
      if {$Dmax<0} {;  # avoid the divide by zero
            set dx [expr -$DincrStatic]
      } else {
            set dx $DincrStatic;
      }
      set NstepsPeak [expr int(abs($Dmax)/$DincrStatic)]
```

```
      for {set i 1} {$i <= $NstepsPeak} {incr i 1} {;           #
zero to one
            set Disp [expr $Disp + $dx]
            puts $outFileID $Disp;              # write to file
      }
      if {$CycleType !="Push"} {
            for {set i 1} {$i <= $NstepsPeak} {incr i 1} {;
      # one to zero
                  set Disp [expr $Disp - $dx]
                  puts $outFileID $Disp;              # write to file
            }
            if {$CycleType !="HalfCycle"} {
                  for {set i 1} {$i <= $NstepsPeak} {incr i 1} {;
            # zero to minus one
                        set Disp [expr $Disp - $dx]
                        puts $outFileID $Disp;              # write to
file
                  }
                  for {set i 1} {$i <= $NstepsPeak} {incr i 1} {;
            # minus one to zero
                        set Disp [expr $Disp + $dx]
                        puts $outFileID $Disp; # write to file
                  }
            }
      }
      puts $outFileID " }";         # close vector definition
      close $outFileID
      source data/tmpDsteps.tcl;          # source tcl file to define
entire vector
      return $iDstep
```

Sub-file 3: LibAnalysisStaticParameters.tcl

```
#  by  Silvia Mazzoni & Frank McKenna, 2006
constraints Transformation

set numbererTypeStatic RCM
numberer $numbererTypeStatic

set systemTypeStatic BandGeneral;         # try UmfPack for large
model
system $systemTypeStatic

variable TolStatic 1.e-8;                           # Convergence Test:
tolerance
variable maxNumIterStatic 30;                  # Convergence Test:
test $testTypeStatic $TolStatic $maxNumIterStatic $printFlagStatic;
# for improved-convergence procedure:
      variable maxNumIterConvergeStatic 2000;
      variable printFlagConvergeStatic 0;

variable algorithmTypeStatic Newton
algorithm $algorithmTypeStatic;
integrator DisplacementControl  $IDctrlNode   $IDctrlDOF $Dincr
set analysisTypeStatic Static
analysis $analysisTypeStatic
```

C8: Codes for perform inelastic time history analysis

Main File: RunAll

```
puts "---------Aanalysis Start Model or 2-----------"
set sam [expr 2.24135272388486*100.00000] #un-scaled Sa
for {set res 0} {$res <= 5} {incr res 5} { #residual stress ratios
for {set sat 105} {$sat <= 140} {incr sat 5} { # target Sa
puts "-------Start Sat = $sat & Res = $res --------"
set sf [expr $sat/$sam] # scale factor
puts $sf
source m11a18.tcl # Model file + subfile 1: Inelastic time history
analysis
puts "-------Finsih Sat = $sat --------"
}
puts "-----Done res = $res-----"
}
puts "-----Finished------"
```

Sub-file 3: Setting for inelastic time history analysis

```
#Eigen Values:          #Displays 4 fundamental periods
set Lambda [eigen -fullGenLapack 3]
puts "Lambda            Omega                   Period"
foreach Lambda $Lambda {
if {$Lambda > 0.0} {
set Omega [expr pow($Lambda,0.5)]
set Period [expr (2*3.141592654)/$Omega]
puts "$Lambda $Omega $Period"}}
set xDamp 0.05;               # 5% damping ratio
set nEigenI 1;    # mode 1
set nEigenJ 1;    # mode 3
set lambdaN [eigen [expr $nEigenJ]];# eigenvalue analysis for
nEigenJ modes
set lambdaI [lindex $lambdaN [expr $nEigenI-1]]; # eigenvalue mode i
set lambdaJ [lindex $lambdaN [expr $nEigenJ-1]]; # eigenvalue mode j
set omegaI [expr pow($lambdaI,0.5)];
set omegaJ [expr pow($lambdaJ,0.5)];
set alphaM [expr $xDamp*((2.*$omegaI*$omegaJ)/($omegaI+$omegaJ))];
# K-prop. damping parameter;   +betaKcomm*KlastCommitt
set betaK [expr 2.*$xDamp/($omegaI+$omegaJ)];       # K-prop.
damping parameter;   +betaKcomm*KlastCommitt
puts "alphaM = $alphaM"
puts "betaK = $betaK"
set sfs [expr $sf*10.000]
puts $sfs
# DYNAMIC ground-motion analysis -------------------------------
-------------------------
# create load pattern
set accelSeries "Series -dt 0.02 -filePath la18.eqf -factor $sfs";#
define acceleration vector from file (dt=0.01 is associated with the
input file gm)
pattern  UniformExcitation 2 1 -accel $accelSeries; # define where
and how (pattern tag, dof) acceleration is applied
rayleigh $alphaM 0.00 $betaK 0.00;# set damping based on first eigen
mode
# create the analysis
wipeAnalysis;     # clear previously-define analysis parameters
constraints Transformation; # how it handles boundary conditions
```

```
numberer RCM;# renumber dof's to minimize band-width (optimization),
if you want to
system BandGeneral;# how to store and solve the system of equations
in the analysis
test NormDispIncr 1.0e-8 30 0; # determine if convergence has been
achieved at the end of an iteration step
algorithm ModifiedNewton;# use Newton's solution algorithm: updates
tangent stiffness at every iteration
integrator Newmark 0.5 0.25; # determine the next time step for an
analysis
analysis Transient;# define type of analysis: time-dependent
analyze 65000 0.001; # apply 90000 0.001-sec time steps in analysis
puts "Done!"
```

Appendix D: Equations for Alternative and General Method

1): Summary of equations for both methods

CAPACITY OF MEMBERS UNDER COMPRESSION & BIAXIAL BENDING

Comparison of NZS3404 General and Alternative Methods

GENERAL	**ALTERNATIVE** NZS3404 – I Sections Complying with §8.1.5 with Under Compression and Biaxial Bending
Section Considerations: (§8.3.4.1)	***Section Considerations:*** (§8.3.4.2)
$\frac{N^*}{\phi N_s} + \frac{M^*_x}{\phi M_{sx}} + \frac{M^*_y}{\phi M_{sy}} \le 1$ $N_s = k_e A_n f_y$ (Eq. 6.2.1) $M_s = Z_e f_y$ (Eq. 5.2.1)	$\left(\frac{M^*_x}{\phi M_{rx}}\right)^{\gamma} + \left(\frac{M^*_y}{\phi M_{ry}}\right)^{\gamma} \le 1 \qquad \gamma = 1.4 + \left(\frac{N^*}{\phi N_s}\right) \le 2.0$ $N_s = k_e A_n f_y$ (Eq. 6.2.1) $M_s = Z_e f_y$ (Eq. 5.2.1) $M_{rx} = 1.18 M_{sx}\left(1 - \frac{N^*}{\phi N_s}\right) \le M_{sx}$ $M_{ry} = 1.19 M_{sy}\left[1 - \left(\frac{N^*}{\phi N_s}\right)^2\right] \le M_{sy}$
Member Considerations: (§8.4)	***Member Considerations:*** (§8.4) (Member slenderness check is additional - §8.4.2)
$\left(\frac{M^*_x}{\phi M_{cx}}\right)^{1.4} + \left(\frac{M^*_y}{\phi M_{iy}}\right)^{1.4} \le 1$	$\left(\frac{M^*_x}{\phi M_{cx}}\right)^{1.4} + \left(\frac{M^*_y}{\phi M_{iy}}\right)^{1.4} \le 1$
$M_{cx} = min\{M_{ix}, M_{ox}\}$	$M_{cx} = min\{M_{ix}, M_{ox}\}$
$M_{ox} = M_{bx}\left(1 - \frac{N^*}{\phi N_{cy}}\right)$	$M_{ox} = \alpha_{bc} M_{bxo}\sqrt{\left(1 - \frac{N^*}{\phi N_{cy}}\right)\left(1 - \frac{N^*}{\phi N_{oz}}\right)}$
$N_c = \alpha_c N_s$ with α_c from Table 6.3.3(2) using $k = 1.0$. M_{bx} is from §5.6 using appropriate α_m.	$N_c = \alpha_c N_s$ with α_c from Table 6.3.3(2) using $k = 1.0$ $N_{oz} = \frac{(GJ + \pi^2 EI_w / L_{eT}^2)}{(I_x + I_y)/A}$ $\frac{1}{\alpha_{bc}} = \frac{1 - \beta_{mx,y}}{2} + \left(\frac{1 + \beta_{mx,y}}{2}\right)^3\left(0.4 - 0.23\frac{N^*}{\phi N_{cy}}\right)$ $\beta_{mx,y}$ is the x moment ratio between lateral restraints M_{bxo} is from §5.6 using $\alpha_m = 1$.
To compute M_i use N_c about same bending axis. $M_i = M_s\left(1 - \frac{N^*}{\phi N_c}\right)$	To compute M_i use N_c and β_m about same bending axis $M_i = M_s\left\{\left[1 - \left(\frac{1 + \beta_m}{2}\right)^3\right]\left(1 - \frac{N^*}{\phi N_c}\right) + 1.18\left(\frac{1 + \beta_m}{2}\right)^3\sqrt{\left(1 - \frac{N^*}{\phi N_c}\right)}\right\}$

Figure AD–1: Equations for both General and Alternative method

2) Example of Spreadsheet used for performing the calculation for both methods

Table AD–1: Example of spreadsheet for both methods

Alternative Method According NZS3404					
Input					
Length of the beam Column		**L**	**5**	m	
			x axis		
Effective buckling Length		**Le**	**5**		
Strength Reduction Factor			**0.9**		
Design Moment		**M***	308.80	kNm	
Design Axial Force		**N***	110	kN	
Check 1a - Major Principal Axis In-Plane Member Capacity					
Plate element Slenderness			Yield slenderness	Plasticity slenderness limit	
a)Flange	7.51		9		
b)Web	22.72		45		Compact
kf	**1**				
Nominal Section Moment Capacity		Msx	344.40	kNm	
Section Moment Capacity		phi Msx	309.96	kNm	
Nominal Section Strength		Nsx	3192	kN	
	Section Strength	phi Nsx	2872.8	kN	
Calculate buckling factor					
Alpha b	**0.5**				
Modified slenderness ratio		47.25			
alpha a		19.91			
lambda		57.20			
Eta		0.14			
Zeta		1.91			
Alpha c		0.824			
Nominal Ideal member strength		Ncx	2630.31		
Ideal member strength		phi Ncx	2367.28		
End Moment ratio		βm	**1**		
Nominal Member Moment Capacity		Mix	396.84		
Member Moment Capacity		phi Mix	357.15		
Check for Major In-Plane Member Capacity (Mx* < phi Mix)					
Results		**Major in-plane member capacity is Satisfied**			
Check 1b - Major Principal Axis In-Plane Section Capacity					
Nominal Section Moment Capacity		**Mrx**	344.40		
Section Moment Capacity		**phi Mrx**	309.96		
Check for Major In-PlaneSection Capacity (Mx* < phi Mrx)					
Results		**Major in-plane section capacity is Satisfied**			